SANDIA REPORT

SAND96–2062 • UC–905
Unlimited Release
Printed August 1996

Molecular Dynamics of Gases and Vapors in Nanoporous Solids – Final LDRD Project Report

Phillip I. Pohl

Prepared by
Sandia National Laboratories
Albuquerque, New Mexico 87185 and Livermore, California 94550
for the United States Department of Energy
under Contract DE-AC04-94AL85000

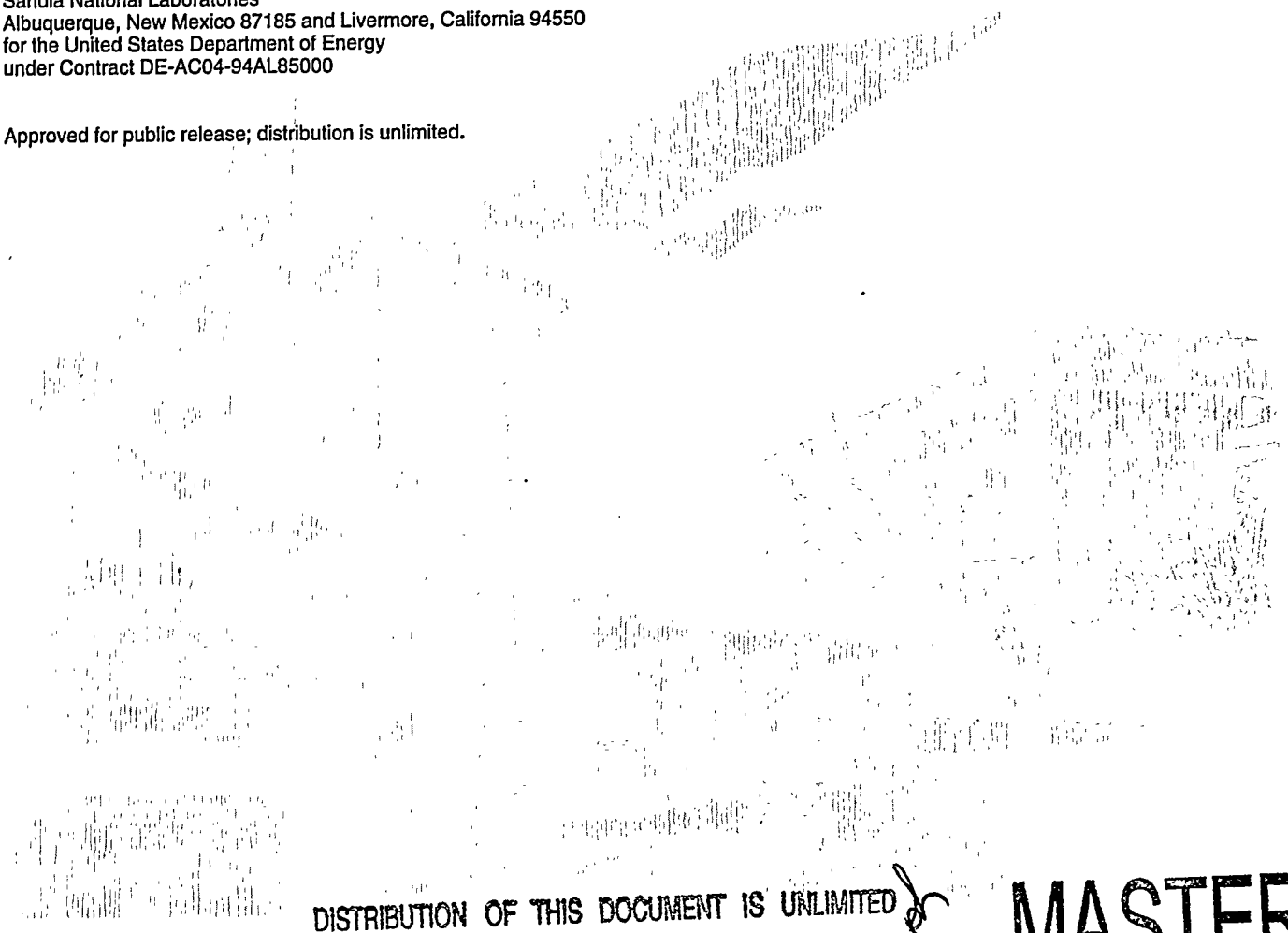

Issued by Sandia National Laboratories, operated for the United States Department of Energy by Sandia Corporation.

Available to DOE and DOE contractors from
Office of Scientific and Technical Information
PO Box 62
Oak Ridge, TN 37831

Prices available from (615) 576-8401, FTS 626-8401

Available to the public from
National Technical Information Service
US Department of Commerce
5285 Port Royal Rd
Springfield, VA 22161

NTIS price codes
Printed copy: A03
Microfiche copy: A01

SAND96-2062
Unlimited Release
Printed August 1996

Distribution
Category UC-905

Molecular Dynamics of Gases and Vapors in Nanoporous Solids - Final LDRD Project Report

Phillip I. Pohl
Energy & Environment Division
Sandia National Laboratories
Albuquerque, NM 87185

Abstract

This report provides a study of gases in microporous solids using molecular modeling. The theory of gas transport in porous materials as well as the molecular modeling literature is briefly reviewed. Work completed is described and analyzed with regard to the prevailing theory. The work covers two simple subjects, construction of porous solid models and diffusion of He, H_2, Ar and CH_4 down a pressure gradient across the material models as in typical membrane permeation experiments. The broader objective is to enhance our capability to efficiently and accurately develop, produce and apply microporous materials.

Executive Summary

The permeation of gases through silica molecular sieving membranes is a very slow process from a molecular modeling point of view. Massively Parallel supercomputers were used for studying these phenomena so that we could study larger models. A disadvantage in the study of these processes with strictly an MD approach, however, is that one still requires a long simulation to get adequate sampling of gas molecules passing through the membrane model. That is, for a permeability of 100 Barrer, a model membrane of size 20nmx20nmx20nm (containing 100,000 wall atoms - a very large calculation) the number of gas molecules passing from the 20 atm pressure side to the 2 atm pressure side is ~10/ns. To get reliable values of the permeability in this case would take about 30 million time steps which at 3 steps per cpu second will require 3 months of nonstop simulation. Some of the results reported below approach this extreme while others are quite the opposite. For determining the permeability of CH_4 through silicalite, reliable values can be obtained in around 10 hours of simulation time. To get around this, several researchers have used a lattice method for simulating diffusion through zeolites, which would be difficult but not impossible for amorphous materials. This is one item that may be pursued in future work. The major impacts in the field of molecular modeling from this work were:

- Building molecular models of imogolite and porous silica.
- Simulating steady-state gas permeation through porous solids.
- The size of the calculations were some of the largest ever enabling an engineering parameter, the permeability, to be evaluated.

In addition to these, the simulation results added to the understanding of gas interactions with porous solids by suggesting or supporting that:

- Stronger adsorbing molecules will retard the flow of smaller molecules in porous membranes.
- The solution diffusion concept is quite relevant for molecular sieving membranes.
- Molecular Sieving membranes require thin skins to be economically viable.
- A seven member SiO ring should provide a significant separating window for N_2/O_2.
- Isolating small pore imogolite and making composite membranes would improve separation factors for the species looked at.
-

Results show that a silica matrix with mean pore diameter of 4.5Å and 1.5 g/cc bulk density is necessary to strongly discriminate between the gases. The future of computing is going to expand, so the work described here should be of great use for materials researchers pursuing molecular scale control in the future. The future prospects of inorganic membranes, however, lies in making thin membranes with more abundant molecular sieving pores.

Acknowledgements

Over the long time it took to finish this work, there have been many individuals who helped immensely in terms of moral support or technical contributions. The management at Sandia include Charles Massey, Margaret Chu, and Joan Woodard. The membrane research group at the Advanced Materials Laboratory was instrumental in providing a motivating set of experimental results to compare to. Finally, the systems administrators at Sandia's Massively Parallel Computing Research Laboratory, most importantly Grant Heffelfinger and Jean-loup Faulon.

This work was supported by the U.S Department of Energy through Sandia's Laboratory Directed Research and Development program.

TABLE OF CONTENTS

EXECUTIVE SUMMARY II

ACKNOWLEDGEMENTS III

CHAPTER 1 - INTRODUCTION: WHY SIMULATE POROUS MEMBRANES 1

CHAPTER 2 - THEORY: TRANSPORT IN POROUS MATERIALS 3

Adsorption 3

Surface Diffusion 5

Transport in Zeolites 6

Membrane Transport 9

CHAPTER 3 - THEORY: MOLECULAR MODELING 14

Statistical & Molecular Mechanics 14

Molecular Dynamics 16
MD in Zeolites 17
Activated Diffusion 20
Non Equilibrium Molecular Dynamics 22

Monte Carlo Methods 24

Modeling Silica and Glass 26

CHAPTER 4 - RESULTS: POROUS MATERIAL MODELS 30

Zeolites 32

Imogolite 32

Microporous Silica 37

Mesoporous Silica 39

CHAPTER 5 - RESULTS: GASES IN POROUS MODELS 43

Gas Interactions With Porous Solids 43

Self Diffusivity from Molecular Dynamics 45

Permeability by Grand Canonical Molecular Dynamics 46
Silicalite Membranes 49
Zeolite A Membranes 51
Silica Membranes 54

Discussion 56

CHAPTER 6 - CONCLUSIONS AND RECOMMENDATIONS 59

Microporous Silica Molecular Models 59

Gas Dynamics in Porous Silica Models 60

Discussion 60

Recommendations 61

NOMENCLATURE 64

REFERENCES 66

APPENDIX - LDRD PROJECT INFORMATION 73

LIST OF FIGURES

Figure 1 Membrane Conceptual Model 1

Figure 2 Growth of Computing Power 2

Figure 3 Concentration Profiles Across Membranes 3

Figure 4 Concentration Dependence of Surface Diffusion 5

Figure 5 Zeolite Building Blocks and Structures 6

Figure 6 Permeability-Selectivity Relationships for Membrane Gas Separation 7

Figure 7 Energy Profile for Porous Crystal Membrane including Interfacial Processes 8

Figure 8 Transition from Knudsen to Configurational Diffusion in Zeolites 9

Figure 9 Temperature Dependence of Carbon Membrane Permeability 11

Figure 10 Activation Energy Dependence on Kinetic Diameter of Gas 12

Figure 11 Potential Function Used in Molecular Mechanics 15

Figure 12 Relation Between Force for MD and Potential Energy from MM 16

Figure 13 Trajectory of Methane Molecules in ZSM-5 at 300K 18

Figure 14 Variation of Pore Diameter in Zeolite A at 360K 19

Figure 15 Surface Mediated and Centralized Flow 22

Figure 16 Dual Control Volume Grand Canonical Molecular Dynamics System 24

Figure 17 Cylindrical Pore Meniscus Formation 25

Figure 18 Silica Gel Model with Adsorbing Methane 27

Figure 19 Model Pore Structure Characterization 31

Figure 20 Imogolite Pore Structure from Pore Program 31

Figure 21 Zeolite A (top) and Silicalite Pore Shapes (He and CH_4 Spheres) 33

Figure 22 Imogolite Atomic Structure (end view) 33

Figure 23 N_2 Adsorbed in Imogolite at 77K and 1 atm. 37

Figure 24 Microporous Silica Models from Cluster Aggregation 38

Figure 25 Surface Area of Microsphere Models 40

Figure 26 Expanded Mesoporous Glass Model Pore Sizes 41

Figure 27 Energy Profile for Gas Diffusion (Kcal/mol) 43

Figure 28 Adsorption Isotherms for Imogolite from Simulation and Experiment 44

Figure 29 GCMC Adsorption Isotherms in Silicalite and Silica ____45
Figure 30 Interaction Potentials for He, H_2 and CH_4 with Hydroxyl groups ____45
Figure 31 Simulated Density Gradients Using GCMD in a Cylindrical Pore____47
Figure 32 Schematic of Silicalite DCV-GCMD Membrane Simulation System ____49
Figure 33 Axial Density Profiles in Silicalite Membrane____50
Figure 34 Schematic of ZK4 DCV-GCMD Pore System____52
Figure 35 Single Gas Profiles: He across ZK4, single gas (dashed), mixed gas (solid)__53
Figure 36 Mixed Gas Density Profiles in ZK4 Membrane, He (solid), H_2 (dashed) ____53
Figure 37 Gas Profiles in ZK4 Membrane H_2 (300K) solid, H_2 (450K) dashed ____53
Figure 38 Silica Model Pore Size Distribution____55
Figure 39 Axial Density Profiles in Silica Model Membrane, H_2, He, CH_4____56
Figure 40 Pure He and Mixed (CH4) He Gas Density Profiles in Silica Model ____56
Figure 41 Pure CH_4 and Mixed CH_4 (with He) Gas Density Profiles in Silica Model___57

LIST OF TABLES

Table 1 Molecular Sieving Dimensions of Probe Gases____4
Table 2 Simulations of Glass Systems ____29
Table 3 Micropore Surface Area and Pore Volumes for Imogolite ____36
Table 4. Fluxes and Permeabilities (Barrers) for Silicalite____51
Table 5 Fluxes and Permeabilities for ZK4 from GCMD ____52
Table 6 Model Permeabilities (Barrers) in 1.5 g/cc Silica Model____55
Table 7 Gas Permeation (Barrers) in Silicate Model Membranes ____59

CHAPTER 1 - INTRODUCTION: WHY SIMULATE POROUS MEMBRANES

Engineered porous materials are important because they have a wide and growing range of applications (Schaefer, 1994, and Chen, 1994). Removal of contaminant gases and particulates from offgas streams by using porous ceramic membranes and adsorbents is a fast growing option, since inorganics can operate at elevated temperatures and under highly corrosive conditions (Pohl, 1993). Generally, porous solids can be used as catalysts, sensors, insulation and in separation processes such as pervaporation or pressure swing adsorption. Successful development of these materials, however, requires a detailed understanding of gas flow within the confined geometries.

Figure 1 Membrane Conceptual Model

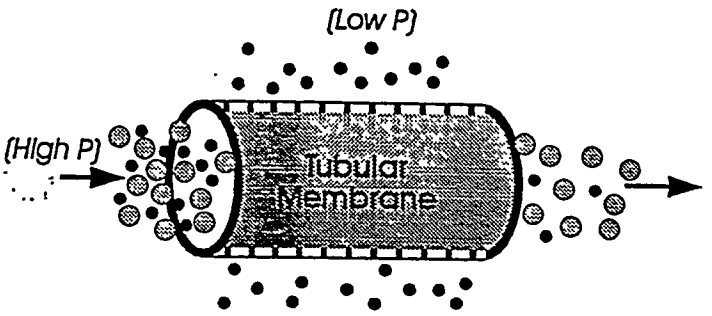

Membrane processes rely on differences in adsorption and diffusion as the way of separation. In the molecular sieving process, the diffusion of certain gases is greatly retarded because of their molecular size (Bhave 1991, Figure 1). Molecular sieving materials have pore sizes that allow certain molecules to pass, but not other larger molecules. The objective of many research programs around the world is to develop inorganic membranes exhibiting high selectivity and high flux for gas separations under extreme thermal, chemical and mechanical conditions (Burggraaf, 1995; Koros, 1995). Since the pores are so small, the applications of these membranes are almost exclusively restricted to gas phase processes. Significant progress has recently been made on these materials (Brinker et al., 1995, 1993; de Lange et al., 1995a,b; Yan et al., 1995a,b; and Vroon, 1995). Permeation through porous materials is calculated as the molar flow rate, N, through a sample of cross sectional area A, given a pressure gradient dp/dl,

$$N = -PA\,dp/dl \qquad (1)$$

The gas permeability, P, has units of mol m/(m^2 s Pa) and as a function of mean pore radius, r, is,

$$P = C_p r^2 p + C_k r + \frac{C_s}{r} \qquad (2)$$

where C_k, C_p and C_s are derived from the governing equations for Knudsen diffusion, Poiseuille flow and surface diffusion respectively, p is the mean pressure, and r is the mean pore radius (Keizer et al., 1988). Surface diffusion increases and Knudsen diffusion and laminar flow decrease by reducing r. At ambient pressures Knudsen diffusion predominates for pore sizes less than 1μm, and surface diffusion contributes significantly only for pores less than 10nm. Below 1nm, however, this equation becomes suspect, making design predictions unacceptable. As

discussed below, a proper conceptual model of micropore diffusion includes gas and surface components and an activated diffusion term.

Computer simulations in materials science has evolved steadily over the past decade with advances in hardware and software. Simulations can yield information that is difficult or impossible to extract from experimental data alone. For atomistic calculations, however, the size and complexity of the model is currently limited by the available computer memory. One area that is actively studied by molecular modeling is the interactions of gases with microporous solids. Micropores have diameters or widths less than 2 nm (Rouquerol et al., 1994), hence, the models required are around a thousand atoms. The objective here is to understand the materials' structural properties which control their applications such as diffusion, adsorption and catalysis.

The power of computers has risen steadily over the last 50 years but, recently, with the advent of parallel computing, has experienced an increased rate of improvement over previous computers as shown in Figure 2. This figure shows an astounding growth in computing power over the last 10 years and should continue to grow at least for the next 5 years as the U.S. Department of Energy is committing funds to develop teraFLOP speed computing capability.

Computer simulations were applied in the present work to investigate diffusion of gases in microporous solids. The first two chapters of this report review pertinent literature. Next, the results are given which include building and characterizing porous material model, and gas dynamics in these models. In this way several popular theories for gas diffusion through micropores can be tested. The final chapter evaluates theses theories and recommends future work which can improve the prospects of developing improved understanding of molecular sieving membranes and other advanced porous materials. Developing an ability to simulate silica from sol-gel methods (Brinker and Scherer, 1990) would also be a very useful effort.

Figure 2 Growth of Computing Power

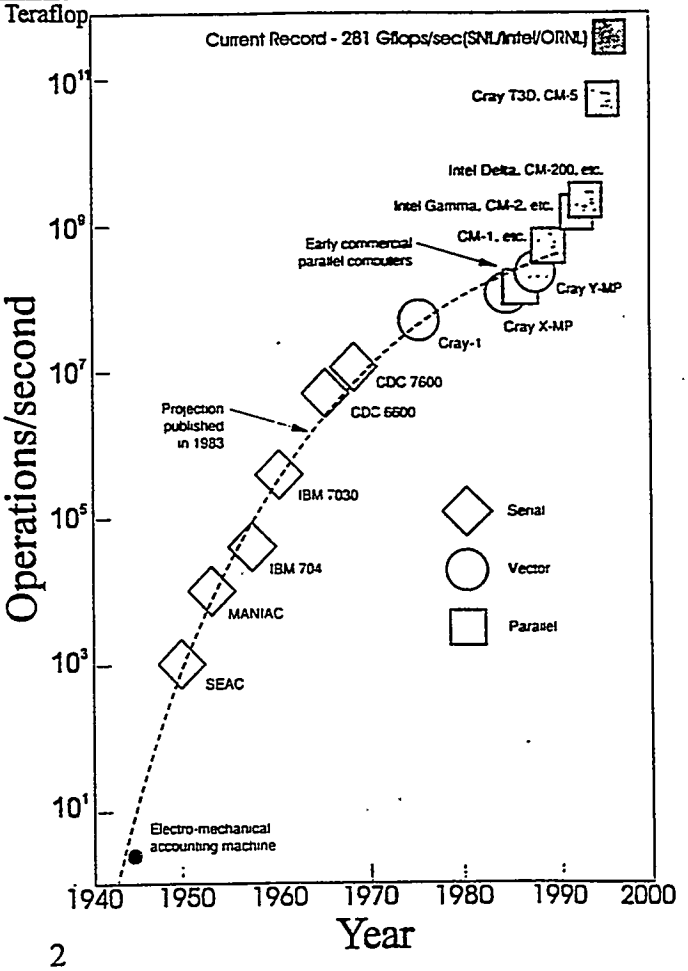

CHAPTER 2 - THEORY: TRANSPORT IN POROUS MATERIALS

A description of gas theory, such as by Chapman and Cowling (1970) centers on viscosity, thermal conduction and diffusion and relates these to kinetic theory and statistical mechanics. These phenomena in non-uniform gases represent the tendencies towards uniformity of mass-velocity, temperature and composition. The elementary theories of these quantities all depend on the mean free-path of the gas. This breaks down, however, for diffusion in micropores since the mean free path is now much larger than the pores. One way around this dilemma is by realizing that the chemical potential gradient is the driving force for diffusion as Cussler (1984) pointed out. In Figure 3, different scenarios for diffusion through membranes are considered where C is a concentration and μ is the chemical potential. In (a) the solute is more soluble in membrane than in adjacent solution; in (b) it is less so; both cases correspond to a chemical potential gradient like that in (c). The chemical potential is difficult to measure in the lab, but, as shown below, is easily accessible through computer simulations. While this was probably developed with organic polymeric membranes in mind, the same concept holds true for porous membranes where adsorption or intrapore gas concentration is analogous to solubility. The models described further below all take this concept into account. In this chapter, adsorption is introduced as it controls the concentration of gas in the solid. Surface and zeolite diffusion are described since elements of both relate to microporous gas transport. Finally, in discussing membrane transport, all of these theories are reduced into some controllable objectives which can be tested through simulation.

Figure 3 Concentration Profiles Across Membranes

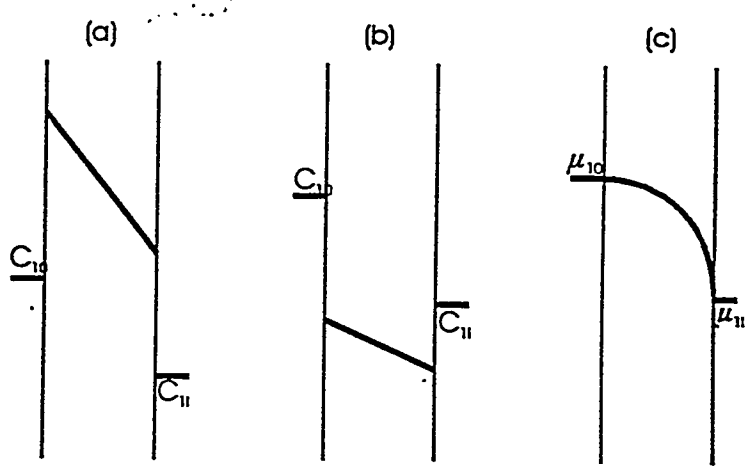

Adsorption

Since adsorption is an integral part of the overall transport of gases across a membrane, it is included in this work. In addition, N_2 adsorption is the most popular method for characterizing porous solids. Steele (1993) reviewed the molecular interactions for physical adsorption focusing on graphite surfaces but mentioning porous silica adsorption as well. He concludes that there is a need for more theoretical work, citing a great deal of computer simulation literature.

The most important contribution to membrane permeation is the adsorption of gases into the pores of the material. The Langmuir theory is the most simplified description of Type I adsorption isotherms,

$$\frac{n}{n_m} = \frac{Bp}{1+Bp}, \qquad (3)$$

where n is the amount adsorbed n_m is the monolayer capacity, p is pressure and B is an empirical constant related to the enthalpy of adsorption (Gregg and Sing, 1982). The concentration of gases in a membrane is dependent on the pressure adjacent to the membrane and the energetic interactions between the gas and the membrane material. In the dilute gas regime and for weakly interacting gases, Henry's law usually holds. That is, the concentration of gases in a membrane is directly proportional to the partial pressure. The coefficient of proportionality is termed Henry's constant. How to interpret the adsorption isotherm and determine surface area, pore size distribution and porosity is of considerable importance to many material scientists. For pore volume calculations from gas adsorption, the Gurvitsch rule is used. That is, the volume of liquid adsorbate equivalent to the gas or vapor volume taken up by the adsorbent, at ~0.4 times the saturation pressure, is the material's pore volume. The surface area of materials is often given by the monolayer number n_m, the average cross-sectional area of the adsorbate, a_m, and Avogadro's number, L,

$$S = n_m a_m L \qquad (4)$$

The cross-sectional area of many adsorbates has been studied extensively, reported by McClellen and Harnsberger (1967), and for N_2 has been determined as approximately 16.2 $Å^2$. An alternative way to determine the surface area is by using data from ^{29}Si MAS-NMR (Davis et al., 1992, 1994). That is, knowing the number of hydroxyls and other surface groups in a material (from NMR), the surface area per group gives a direct value for the surface area.

Recent developments on interpreting isotherms include a cylindrical approximation to adsorption in micropores given by Saito and Foley (1991). The relationship of pore size to relative pressure for this as well as a slit pore approximation is given. From this simple graph, the pore diameter giving adsorption for Ar in oxides (zeolite X pore structure) are: 0.46nm pore diam.($p/p_o=10^{-5}$), 0.54nm(10^{-4}), 0.65nm(10^{-3}), 0.8nm(10^{-2}), 1.3nm(0.1). Similar models may be applicable to the solids considered in this work. In general, a range of different size molecules is needed to probe the micropore size distribution of any solid. Table 1 gives the sieving diameters for several penetrants used in the zeolite literature actually taken from reference. He, H_2, Ar and CH_4 were used in permeation simulations in the present work since they can be modeled as spheres and vary considerably in size.

Molecule	He	H_2	NO	CO_2	Ar	O2	N_2	CO	CH_4	Xe	C_3H_8
Diam. (Å)	2.6	2.89	3.17	3.3	3.4	3.46	3.64	3.76	3.8	3.96	4.3

Table 1 Molecular Sieving Dimensions of Probe Gases

Bhandarkar et al. (1992) preceded their membrane permeation work with extensive adsorption experiments. Using a Dubinin-Ashtov treatment, they found empirical constants for CO_2, He, CO, H_2, and CH_4. This led Shelekhin et al. (1995) to partition the permeating gas into a surface concentration and gas concentration as shown below.

Surface Diffusion

Upon adsorption onto the surface of a porous body, surface diffusion can take place. This is described in detail by Hwang and Kammermeyer (1966a,b), Gilliland et al. (1974), Tamon, et al. (1981), Chen and Yang (1991) and Xiao and Wei (1992). Surface diffusion is most pertinent for strongly adsorbing molecules and at relatively low temperatures (< 200 K). It is not a simple matter, however, separating the gaseous from surface components of diffusion, even in simulations.

Hwang and Kammermeyer (1966 a,b) emphasize low pressure adsorption of He, which prior to their work had been assumed to have no surface diffusion component. Interaction energy in surface diffusion is first discussed by Hwang (1966). Gilliland et al. (1974) present the effect of concentration on the diffusivity of physically adsorbed gases on surfaces. That is, the differential heat of adsorption (which is used in the correlation of the surface diffusivity) varies with coverage. Sladek et al. (1974) present a correlation of surface diffusivities of adsorbed gases as a function of q/mRT, where q is the differential heat of adsorption and m is 1, 2, or 3 and characterizes the type of gas-surface bonding. The general correlation, D_s = 0.016exp(-0.45q/mRT) cm^2/s represents 11 orders of magnitude in D_s to within 1.5 orders of magnitude accuracy.

The model derived by Chen and Yang (1991) is of special interest in the present work because it also considers the concentration dependence. As a function of the fractional surface coverage θ and the degree of surface sites blocked by another molecule λ, the diffusivity is shown in Figure 4. λ is actually the ratio of the kinetic rate constants for the two processes, 1) return rate due to blockage by another adsorbate and 2) forward migration. Fitting experimental data to the curves in Figure 4, Chen and Yang found values of 0 for SO_2 on vycor glass, 0.3 for propane in zeolite 5A, 2 for benzene in ZSM-5 and 11 for triethylamine in zeolite 13 X. For a molecule hopping onto a site that is occupied, λ is the ratio of probabilities of bouncing backward over bouncing forward. Proximity of the adsorbate size and zeolite pore should result in large λ values as shown.

Figure 4 Concentration Dependence of Surface Diffusion

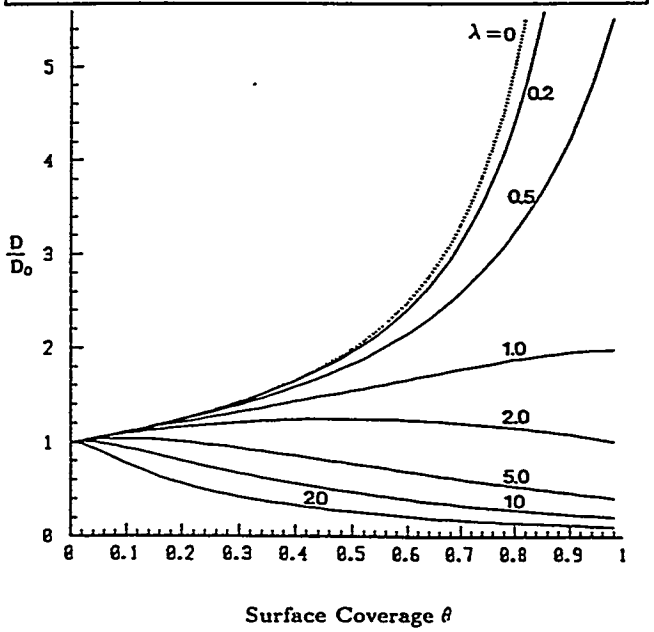

As described further below, Xiao and Wei (1992) included a surface vibrational term in their unified diffusion theory but did not apply it to their data, because the surface concentration of hydrocarbons in zeolites above room temperature was assumed negligible. This diffusivity is given by

$$D = guLe^{-E/RT} = \frac{1}{z}\nu_e \alpha^2 e^{-E/RT} \qquad (5)$$

where, ν_e is the effective vibrational frequency of the molecule inside the zeolite, related to the molecular mass and Hooke's law constant which is the curvature of the potential well at the well bottom. Since the temperature dependence is exponential as in activated micropore diffusion identifying surface diffusion is difficult.

Transport in Zeolites

Zeolites are crystalline microporous solids typified by windows separating cages, each of varying size (Figure 5). The window perimeters can have 6 Os (sodalite), 8 Os (zeolite A), 10 Os (ZSM-5), or 12 Os (zeolite X and Y). Karger and Ruthven (1992), Chen (1994), and Weisz (1995) summarize the current knowledge of gas transport in micropores focusing on zeolites. They describe all mechanisms by which materials diffuse, i.e., bulk diffusion, Knudsen diffusion, surface diffusion, and micropore diffusion, which is well described by transition state theory or an activated process. The experimental techniques used for measuring micropore diffusion are also described, such as pulse field gradient (PFG) NMR, membrane permeation and transient adsorption. Differences between the experimental results from the techniques can be huge, due in part to a surface barrier which has been theorized and discussed by many and can be tested with molecular modeling. Understanding diffusion through zeolites is a very useful starting point for molecular sieving membrane studies since the pores are of similar size.

Figure 5 Zeolite Building Blocks and Structures

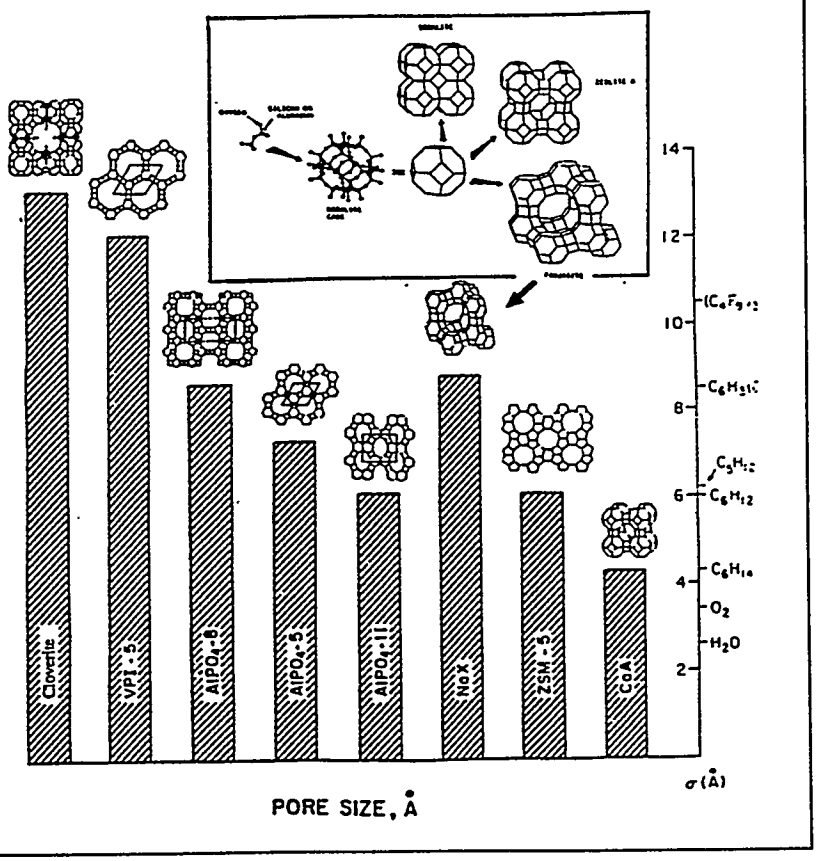

The permeation

through zeolite membranes is an excellent test of micropore membrane diffusion theories. Duval et al. (1993) present a transport mechanism through zeolite filled gas separation membranes with experimental results of CO_2/CH_4 permeation through silicalite filled polymeric membranes. The selectivity is shown to increase as the permeability of CO_2 increases from 80 to 250 Barrer as the silicalite volume fraction is increased to 0.5 while the CH_4 permeability remains the same. Two different theories were used to describe the results. Each of these included zeolite permeability as a variable in the overall permeability. From both models, the CO_2 silicalite permeability was ~1000 Barrers (1 Barrer = 10^{-10} cm^3(stp)-cm/cm^2-s-cmHg) while the average CH_4 permeability was 30 Barrers. This would give a selectivity of 33 which would place it near the edge of the envelope on a performance plot such as Figure 3-13 of Ho and Sirkar (1992) from which Figure 6 was derived.

Shah et al. (1993) report transport of C_4 hydrocarbons through a single-crystal silicalite including ideal selectivity of 2.2 for H_2 and CH_4 in these membranes. The transient analysis gives rise to diffusivities of ~ $1x10^{-8}$ cm^2s^{-1}, and the authors insist that it is accurate for pore diffusion. Similar results of ZSM-5 membranes on porous ceramic supports are described by Geus et al. (1992). Yan et al. (1995a, b) prepared polycrystalline ZSM-5 layers, approximately 10 μm thick, deposited onto a macroporous alumina support. They obtained a permeance of $9.0x10^{-5}$ cm^3/cm^2-s-cmHg for He in these membranes at 303K and 1.27atm feed pressure, and achieved notable separations with butane/isobutane.

Petropoulos and Petrou (1991) interpreted features of the observed general permeability behavior of porous adsorbents. This includes gas and surface transport components. It was noted that the distinction between 'gas phase' and 'adsorbed phase' disappears for very small pores and, due to the enhanced adsorption energy, the total concentration in the pores increases. At a relative pore size of d/r_o=2.1 (slit-shaped geometry, d=slit width and r_o is the kinetic diameter) the order of the permeation rate for a series of noble gases (He, Ne, Ar, Kr, Ze) was reversed in that the smallest molecules had the highest rate. This was not the case at d/r_o=3.5, where the order was exactly opposite, which is explained by a stronger surface diffusion component for the larger molecules. Obviously, pore size decrease leads to a transition in transport mechanism where the smallest molecules will permeate fastest. Knudsen's analysis is only significant for high temperature non adsorbing gases.

Figure 6 Permeability-Selectivity Relationships for Membrane Gas Separation

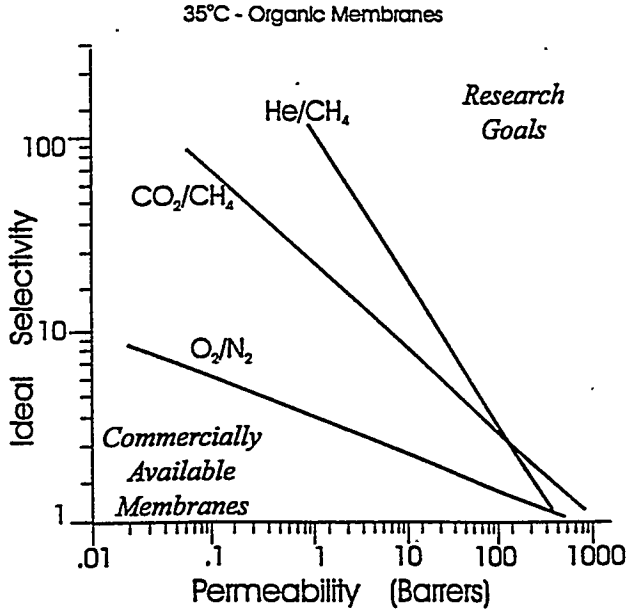

Barrer (1990) reported a mechanism for pore diffusion in porous crystal membranes. This mechanism is based on activated diffusion and is controlled by a Boltzman factor *exp(E/kT)*, where E is the activation energy, k is Boltzman constant and T is the process temperature. Figure 7 portrays the general energy profile experienced by the diffusing molecule or atom from x=0 to x=l, the inlet and outlet membrane surfaces, respectively. As can be seen, several barriers exist for diffusion. A kinetic approach to the role of surface forces in steady flow through a membrane was developed and extended to include the influence of partial blockages upon such membrane properties as permeability, diffusivity and mixture separation. Steady net flow is described as,

$$J = \frac{sk_1}{(n-1)} \exp\left(\frac{-E_1}{RT}\right)[\theta_1 - \theta_n] \qquad (6)$$

where s is the number of barriers per unit cross-section normal to flow (for zeolites between 0.3 and 0.7 per nm^2); θ is the chance that a molecule occupies each energy well, numbered 1, 2, . . . (n-1), n; and k_1 is the pre-exponential part. To find θ_1 and θ_n, the processes at the surfaces x=0 and x=l must be considered. Interfacial effects are included by considering sites of lower energy that are on the outer surface of the crystal. From here, a diffusing molecule would have to climb another barrier E_s. This gives rise to another correlation for J, which is related to the ideal maximum flow J_{id} as,

$$\frac{J_{id}}{J} = 1 + \left(\frac{1-\theta_{1eq}}{1-\theta_{0eq}} + \frac{1-\theta_{neq}}{1-\theta_{leq}}\right) \times \frac{\exp[(E_s + \Delta E - \Delta E_s - E_1)/RT]}{(n-1)} \qquad (7)$$

Figure 7 Energy Profile for Porous Crystal Membrane including Interfacial Processes

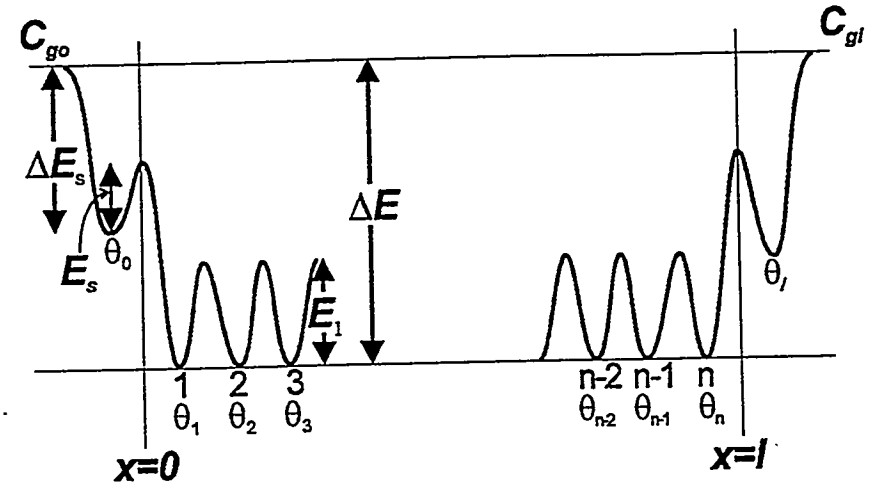

where ΔE is the difference in energy from the gas phase to the adsorbed intracrystalline phase, and ΔE_s is the difference in energy from the gas phase to the external adsorbed phase. For high temperatures and large crystal thicknesses, any role of surface processes will become less significant and vice-versa. No strong comparison with experiment was given. For optimum performance it follows by using the Langmuir isotherm that $BCo \equiv (Co/Cl)^{1/2}$, where B is the equilibrium adsorption constant, Co and Cl are the gas concentrations at the inlet and outlet sides. He extended this theory to multicomponent permeation with a nonequilibrium thermodynamic treatment (Barrer, 1992).

Xiao and Wei (1992) give a detailed analysis of the diffusion mechanisms of hydrocarbons in zeolites. This includes temperature and concentration dependence and involves a unified diffusion theory to describe gaseous diffusion, liquid diffusion, Knudsen diffusion, solid diffusion and configurational diffusion. This unified theory involves both gas transport and surface vibrational transport (given above). The gas translational diffusivity is given by

$$D = guLe^{-E/RT} = \frac{1}{z}\sqrt{\frac{8kT}{\pi m}}\alpha e^{-E/RT} \qquad (8)$$

where α is the diffusion length, E is the activation energy, m the molecular weight, and z is the number of adjacent sites to jump into, each with an equal probability of $1/z$. For example, z is four for ZSM-5, and six for zeolite 5A; α is about 10Å for ZSM-5, and 12 Å for 5A. These values result in pre-exponential terms of about 4×10^{-4} $(T/m)^{1/2}$ cm^2/s for ZSM-5, and 3×10^{-4} $(T/m)^{1/2}$ cm^2/s for 5A. Consequently, for a molecule with m=80 at room temperature, with activation energy of 10 kcal/mol, the diffusivity is about 10^{-11} cm^2/s. They conclude that diffusion of non-polar gases in zeolites above room temperature takes place in the Knudsen regime or the configurational regime and depends on the geometric properties of the molecules and the zeolite. For ZSM-5, transition from the Knudsen regime to the configurational regime may occur for roughly spherical molecules when the ratio, λ, of molecular diameter to channel diameter is greater than 0.6 at 300 K (see Figure 8) to 0.8 at 700°C. In a companion article, they confirm many assumptions by carrying out transient adsorption experiments for several hydrocarbons on ZSM-5 and zeolite 5A.

Figure 8 Transition from Knudsen to Configurational Diffusion in Zeolites

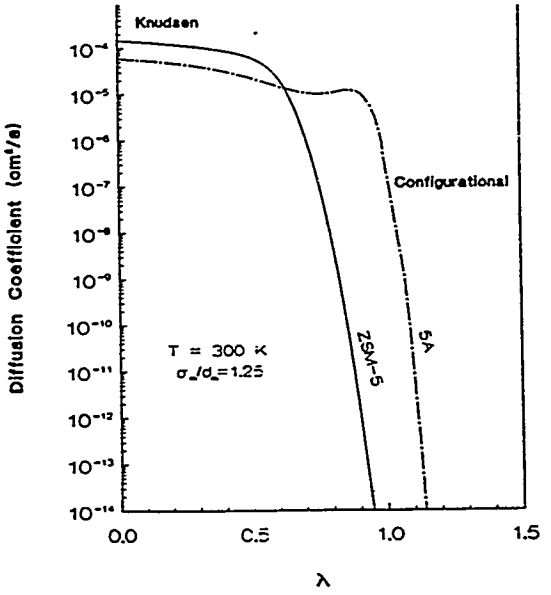

Membrane Transport

One of the earliest applications of

Maxwell-Stefan analysis to flow in porous media was given by Mason and Malinauskas (1983) in "the dusty gas model," where the solid particles were modeled as large gas molecules that are stationary. Krishna (1993) pointed out many of the pitfalls in the application of Fickian diffusivity to gas transport in porous solids, while improving the dusty gas model's predictive ability for gas diffusion in micropores. Success in predicting transient adsorption was achieved for zeolites and activated carbon. While heavy in mathematical formalism, this approach is correct from a thermodynamic point of view, using a chemical potential driving force, as pointed out by Figure 3 above. Recently, Krishna and van den Broecke (1995) have developed a theory for gas permeation through zeolite membranes. This theory requires cross-diffusion terms and assumes multicomponent adsorption is adequately described by Langmuir isotherms. Reproduction of transient permeation experimental results and steady-state mixed gas results make this methodology rather attractive.

Shelby (1979) reviewed the molecular solubility and diffusion of gases in vitreous glass. The solubility was shown to be inversely related to temperature by a number of different empirical relations, some of which showed a 1.5 power dependence. The diffusion follows a slightly modified Arrhenius law.

Fain (1991) presented selectivities as a function of pore size based on several concepts, including Knudsen diffusion, hard sphere/wall approximations, momentum accommodation, and pore plugging for mixtures. The model was for a cylindrical pore which makes comparison with imogolite ideal. In fact, Sehgal et al. (1994) did this with their composite silica/imogolite membranes. Their ideal separation factors for He/SF_6 using Fain's analysis predicted a 9 Å diameter pore, quite close to the actual tubular diameter of the aluminosilicate, shown below. The theory does not appear to be applicable to microporous silica membranes which have irregularly shaped pores.

Carbon molecular sieve membranes made by Koresh and Soffer (1986) had the following mechanism for permeation. The flux for a membrane is compared with Fick's law and the permeation result is

$$P = -D\left(\frac{dc}{dp}\right) \tag{9}$$

where c is adsorbate concentration and p is the average pressure across the membrane. Assuming a Langmuir isotherm,

$$P = DC_o \frac{B}{(1+Bp)^2} \tag{10}$$

which shows that the permeability is a decreasing function of pressure. At high temperatures and the same pressure range, the interaction parameter of the isotherm becomes exponentially smaller. Here the isotherm resides at its linear portion, i.e., dc/dp is independent of pressure;

therefore, the decrease in permeability dependence on pressure at higher temperature is as shown in Figure 9. Since the adsorption interaction parameter for light gases (H_2, He, Ar) is much less than that for CO_2, CH_4, etc, this pressure dependence is not seen at ambient temperatures.

Figure 9 Temperature Dependence of Carbon Membrane Permeability

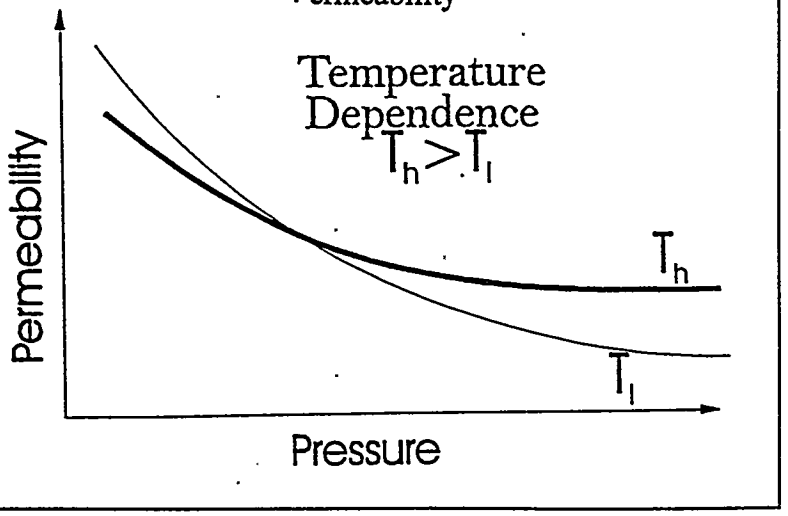

Way and Roberts (1992) have used hollow fiber membranes for gas separations. Separation factors were observed for H_2/N_2 and H_2/CO of 163 and 62, respectively. A correlation between permeability and kinetic diameter of the penetrant was noted. The molecular sieving mechanism for diffusion was presented as an activated process and described only qualitatively. Eight membered oxygen rings were mentioned and the energy barrier for molecules passing through these was addressed, a concept brought up by Shelekhin et al. (1995, 1992), in their analysis of gas separation by similar hollow fiber membranes. Using this approach, it was found that the dependence of the activation energy versus kinetic diameter calculated from the experimental data could be well fitted if the size of the pore opening lies within the range 5.5 Å to 6.1 Å for $6<n<10$ where n is the number of oxygen atoms on the pore perimeter. This concept can be tested with molecular mechanics as shown in the later chapter on Gas in Porous Solids. The permeability of permanent gases, He, H_2, O_2, N_2, Ar etc are predicted to have ideal selectivity factors,

$$\alpha = \frac{P_A}{P_B} = \left(\frac{M_B}{M_A}\right)^{\frac{1}{2}} \exp\left(-\frac{\Delta E_A - \Delta E_B}{RT}\right) \qquad (11)$$

where P is the permeability, M the molecular weight, and E the activation energy for gases A and B. The activation energy is only used for solid and configurational diffusion, and is cause for the sieving effect important in separating gases based on their molecular size. In the event that E is small, then D reduces to the Knudsen limit and the selectivity is based on molecular weights.

Hassan et al. (1995) also used the hollow fiber molecular sieving membrane and carried out mixed gas permeation studies. These showed that O_2/N_2 mixed gas separation factors are greater than ideal separation factors, while for CO_2/CH_4, there is little difference in these two selectivities. The ideal separation factors for He/CH_4 were 23,400 at 298K and 310 at 423K with a feed pressure of 21.4 atm. These values can be compared with the results presented below in the chapter on gas permeation simulation. He permeance was $1x10^6$ Barrer/cm.

De Lange (1995b) provides a detailed application of gas permeation in microporous membranes including analysis based on activated diffusion, and sequential adsorption-diffusion analysis (see Uhlhorn, 1989a,b, 1992 for preliminary work). He correctly assumes the concept of gas phase and adsorbed phase both contribute to the overall diffusion. He concludes that there was little interfacial effect, i.e., Barrer's analysis and, hence, the permeance barrier was given only by the energy barrier profile for a diffusing molecule across the membrane. Henry constants at 273K for CH_4 are 2.3×10^{-6} and 1.8×10^{-7} mol. kg^{-1} Pa^{-1}, respectively. Ideal separation factors are 20-30 for these two. Permeation of He at 200°C is 20×10^{-7} mol. m^{-2}. s^{-1}. Pa^{-1}.

To summarize, in mesopores, Knudsen diffusion and surface diffusion dominate, which both show a decreasing transport rate with increasing temperature. For smaller pores, the temperature dependency gradually changes to activated transport in micropores. De Lange, Xiao, Shelekhin, Brinker and Way have all used the approach that Karger and Ruthven (1992) did in relating the activation energy to the kinetic diameter of the diffusant. Figure 10 gives a composite graph of the results of these comparisons. Understanding this relationship in greater detail will allow optimization of the pore structure for gas separating membranes.

The best models fall into three types with the latest of these demonstrated by the theories of Shelekhin and Barrer and Krishna. In organic polymeric membranes, the solution-diffusion mechanics is adopted (Wijmans and Baker, 1995). The three theories listed all have this type of formalism with varying degrees of similarity. Shelekhin suggests that gases are either on the surface (adsorption described by empirical constants) or in the gas phase (concentration equivalent to ideal gas). Barrer uses the fraction of sites occupied, θ, at the upstream and downstream surfaces as the driving force for intracrystalline permeation, including Langmuir constants to set these coverages. Similarly, Krishna uses Langmuir constants but neglects any surface resistance and relates straight to the pore concentration based on the adsorption properties. All three theories then include a diffusivity similar to the activated diffusivity mentioned above for zeolite transport. Shelekhin gives ideal gas selectivities, while Barrer and Krishna treat the mixed gas processes with non-equilibrium thermodynamic analysis. The results of Krishna are presented as

Figure 10 Activation Energy Dependence on Kinetic Diameter of Gas

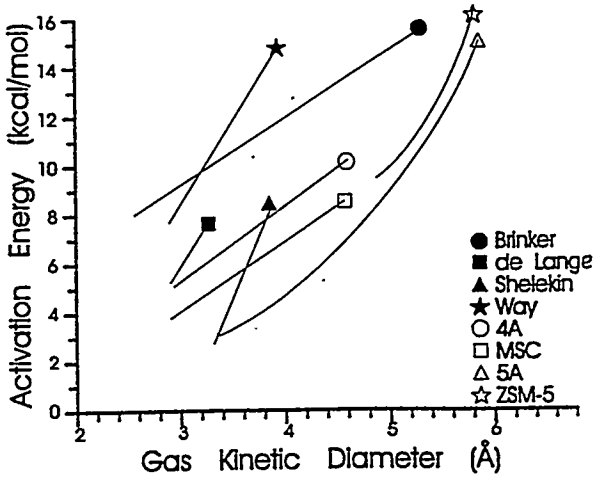

transient permeation and eventual steady-state values such as permselectivity of butane over H_2 which is counter to the ideal selectivities often reported in the membrane literature.

As shown above, it is important to grasp that there are three important aspects to gas permeation through microporous membranes. These are the concentration of gas in the pores, the diffusivity or mobility in the structure and the effects of mixed gas permeation. With molecular modeling these can be analyzed in three parts using various simulation tools or all at one time with a dual-control volume non-equilibrium simulation. Both methods are carried out in this work on three very different porous materials. Prior to describing this work, the next chapter reviews theory on molecular level computer simulations.

CHAPTER 3 - THEORY: MOLECULAR MODELING

One can simulate the movements of a large number of model particles, investigate individual particles (quantum mechanics), or analyze simulation data for the required collective phenomena (statistical mechanics). These three steps make up molecular-scale computer simulations (Haile, 1992). In the hierarchy of computational chemistry, the present work in molecular modeling fits between electronic structure calculations (*ab initio* and semi-empirical) and continuum mechanics. That is, while giving more detail and accuracy than continuum bulk phase modeling, it is limited in the size of the models that can be studied. Moreover, it lacks the quantum effects and accuracy that may be significant for some processes in micropores like catalysis and chemisorption. In this chapter the basics of the computer simulations used are given. In addition, relevant state of the art applications are reviewed to offer a proper perspective that will allow testing of the theories on gas permeation in porous solids described in the last chapter.

Molecular mechanics (MM) is the study of the potential energy of molecules. Molecular dynamics (MD) and Monte Carlo (MC) methods are similar in that they both require a model with proper intermolecular potentials to conduct simulations (Allen and Tildesley, 1987). They are equally effective for determining equilibrium properties such as pressure. They differ in that MD is deterministic, solving differential equations of motion, hence, the positions are connected in time. In MC the positions are generated stochastically. In the present work both are used, MD to simulate structures and obtain permeabilities, and MC in obtaining adsorption isotherms and Henry's law constants. Statistical mechanics is the theory in which macroscopic observables are related to the probability of the system being in particular molecular states. In addition to these simulation capabilities, commercial software such as from Biosym also offer several tools used in assessing molecular models and analyzing simulation results. These include x-ray, neutron and electron scattering, TEM, NMR, and geometric measures, and visualization methods such as animation. Faulon et al. (1994) and Kale and Brinker (1995) have each developed programs for calculating surface area, density, porosity and pore size distribution. This is discussed later.

Statistical & Molecular Mechanics

Statistical mechanics describes the relationship between the microscopic dynamics or fluctuations (as governed by quantum or classical mechanics equations) and the observed properties of a large system (such as the heat capacity or equation of state). The partition function is the integral, over the phase space of a system, of $\exp(-E/kT)$, where E is the energy of the system, k is Boltzman's constant, and T is the temperature. From this function all the thermodynamic properties of the system can be derived. In addition, the transport phenomena (diffusivity, viscosity and heat capacity) can also be derived from the radial distribution function. The constraints on the simulated system define the ensemble which is being used, and so define the relationships to the macroscopic observables.

Equations of state models and theories of dilute and dense gases have successfully been derived by Reed and Gubbins (1974). The thermodynamics text of Prausnitz et al. (1986), includes an appendix on statistical mechanics based on Reed and Gubbins work, hence,

providing a complete extension into the latest thermodynamics of fluid phase equilibria. The two ensembles used in the present work are the canonical and grand canonical. In the first, the number of atoms, N, the volume, V, and the temperature are kept constant during the simulation. Periodic boundary conditions can be imposed on the simulation box so that a diffusing particle escaping one face enters the opposite face with the same properties, hence, NVT is a popular ensemble for studying diffusion. In the grand canonical ensemble the chemical potential, μ, the volume, and the temperature are kept constant during the simulation. In this manner, the number of atoms is allowed to vary and, hence, this ensemble is appropriate for simulating adsorption where N is variable.

An example of using statistical mechanics, MD and kinetic theory is given by Thurtell and Thurtell (1988). Studying adsorption and diffusion at rough surfaces, the Maxwell-Boltzman velocity distribution is shown to break down. This is the fundamental reason why statistical mechanical theories, which generally integrate away the kinetic part of the partition function and solve only the configurational part, do not accurately predict this type of adsorption at rough surfaces. That is, when the mean free paths are long with respect to the surfaces, one should conduct simulations. This condition exists in the interaction of gases with microporous solids.

Molecular mechanics is the study of the energy between the atoms and molecules making up a system. This energy is the sum of all the individual relationships describing the different modes of interaction and is termed the configurational energy. Figure 11 depicts the relationships included in the potential functions used in Biosym's software. The cross terms (out of plane, bond-angle and angle-angle) are typically not used in simulations to speed computation time. In addition, an ionic system potential is used for silica simulations. Fueston and Garofalini (1990) have developed a program that has been used for several silica studies since.

Using molecular mechanics represents an attempt to invoke classical physics over quantum mechanics in order to have computationally workable potentials (Dykstra 1993). Obtaining the force field parameters is done in one of several ways. A promising, but very computationally intensive approach, is to use quantum mechanics. Alternatively, one can vary forcefield parameters in fitting experimental thermodynamic properties such as the Henry's law coefficient. The intermolecular interaction parameters determined from the equilibrium properties (second virial coefficient and Joule Thomson coefficient) are slightly different from those determined from non equilibrium properties (viscosity, self-diffusion). This would not be the case if an exactly correct functional form were used. However, as may be seen from the various expressions, the different properties emphasize various regions of the potential differently. Generally, the transport properties emphasize the repulsive portion of the potential function,

Figure 11 Potential Function Used in Molecular Mechanics

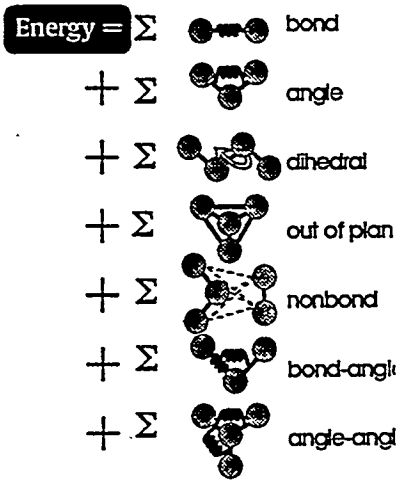

whereas the equilibrium properties stress the attractive contribution (Hirschfelder, Curtiss, and Bird, 1954).

Helium simulated gas adsorption in silicalite described by Kieslev et al. (1985) set the assumptions for most of work described below in sections *MD in Zeolites* and Monte Carlo Methods. The potential energy for Ar in silicalite (pore diam. ~ 5 Å) was derived from the polarizabilities and van der Waals diameter of the interacting atoms and was subsequently used for the adsorption calculations. A plot showing the dependence of initial isosteric heat of adsorption on the mean polarizability of the adsorbate molecules showed the closeness of the calculated and experimental values. Likewise, the dependence of the standard differential entropy of adsorption on the effective size of adsorbate was shown.

Molecular Mechanics is first utilized in the current work for energy minimization. This process takes a 3-D model of atoms and molecules and applies the above relationship to the interatomic and intermolecular distances and angles. The resulting energy is optimized (minimized) by adjusting the atomic positions, giving a more stable configuration for the model. This process is iterated until a suitably relaxed structure is attained. As described below, forces derived from the potential energy lead to movements in MD, while the configurational energy provides input for acceptance/rejection in MC.

Molecular Dynamics

MD solves the classical equation of motion $F = ma$, where F is the force, m is the mass, and a is the acceleration. The force can be computed directly from the derivative of the potential energy V,

$$\frac{dV}{dr} = m\frac{d^2r}{dt^2} \qquad (13)$$

with respect to the atomic coordinate, r. Given an adequate expression of the potential energy it should be possible to solve this differential equation for future positions in time (the trajectory). A numerical solution is used here. The concept is depicted in Figure 12 for two atoms exhibiting the popular Lennard-Jones 6-12 interaction.

In a typical MD simulation such as modeling a gas in a zeolite, several types of information are immediately obtainable. First is the trajectory or path followed by the diffusing molecule. For example, a strongly adsorbing diffusant is attracted to the framework and will move along the surface.

Figure 12 Relation Between Force for MD and Potential Energy from MM

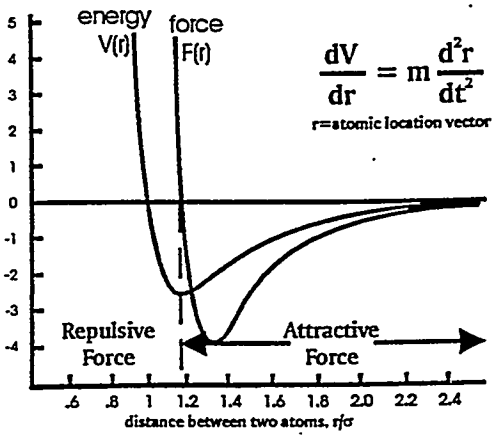

This motion is also observable from a plot of mean square displacement (MSD) versus time. Diffusivities from the MSD and Einstein diffusion equation compare well with experiment. These calculations, however, require simulation times ~ 1 ns, usually with a step of 1 fs, (i.e., ~10^6 time steps) limiting the size of the system that can be studied.

Besides the macroscopic limitations just mentioned, the microscopic limitations of MD are concerned mainly with the proper representation of the elementary processes for which the classical approximation may not always be valid (Karger and Ruthven, 1992). The equivalent wavelength is

$$\lambda = h/mv = h/(3mkT)^{1/2} \qquad (14)$$

If λ is small relative to the atomic dimensions, then, quantum effects can be neglected. It follows that, at ordinary temperatures, quantum effects will be negligible for the larger atoms but may be significant for H_2 or He. In fact, a recent determination of the quantum effects in subnanometer pores is given by Beenakker et al. (1995) which cites Brinker et al. (1994) in their use of He as a membrane gas permeant. Their calculations show that a quantum sieving barrier will arise for cases where the available diameter of the pore approaches the de Broglie wavelength, but that He seems to be the only species likely to exhibit these quantum effects for pore sizes and energetics considered in the present work.

Heffelfinger et al. (1987, 1988a,b) conducted a number of novel simulations on fluids in cylindrical pores of ca 7 molecular diameters. Besides liquid-vapor coexistence, they were able to simulate adsorption hysteresis. The results are among the first direct evidence of simulating layering transitions in capillaries. Gusev et al. (1993) simulated He and H_2 in rigid matrices of dense polymers. These are similar to the simulations made in the present work, in that small gas molecules are used and the silica matrix is amorphous. In the companion article, Gusev and Suter (1993) allowed the matrix to vibrate which was necessary for larger molecules to diffuse sufficiently to match experimental transport properties.

MD in Zeolites

Computer simulations of the molecular behavior of gases in zeolites has become popular with the advent of high-speed computers, the development of accurate zeolite structures, and appropriate software for simulating the molecular dynamics (Catlow, 1992). These studies have also required realistic potential energy relations for the diffusing gas and the material framework. MD studies have already provided a good description of the processes underlying gas diffusion in simple pores. To date, however, macroscopic gradients (driving forces such as a pressure drop across a membrane) have not been rigorously simulated on realistic models, nor have the complete porous material structure-property relationships been completely developed. The purpose of this sub-section is to point out the state of the art in simulating gases in zeolites using MD.

Most of the work reviewed in this subsection is for the zeolite ZSM-5 or its purely siliceous analog silicalite. This is probably because the unique structure has made it a commercially attractive shape selective catalyst. Nevertheless, several other systems have been studied, including Demi and Nicholson (1991), who modeled zeolite pores as a sphere-cylinder

micropore, water in ferrierite-type zeolite described by Leherte et al. (1991), Xe in ferrierite and zeolite-L given by Henson et al. (1993), benzene in faujasite by Henson et al. (1995), and Yashonath and Santikary (1992, 1993a,b) who studied faujasite and zeolite A, described more in the next section on activated diffusion because of zeolite A's very small pores.

The MD study of Xe on silicalite by Pickett et al. (1990) noted the emergence of ^{129}Xe NMR as a means of probing the internal structure of zeolites and the added value that the diameter of Xe is close to that of methane. Diffusivities were calculated from MSD plots using 10-12 fs time step and runs of 400 ps, and these compared well with Pulsed Field Gradient-NMR experiments. The activation energy was calculated at 5.5 kJ/mol. Nowak et al. (1991) followed this with a similar study of methane, ethane, and propane in EU-1, mordenite, and silicalite.

Catlow et al. (1991) presented MD studies of Methane and Ethane diffusion in ZSM-5. They used a rigid framework at 300 and 600K and loadings of 1 and 2 molecules per cell and obtained self-diffusivities within 5% of those obtained with PFG-NMR. Figure 13 shows an example of the trajectory of two diffusing methane molecules throughout the zeolite lattice. In a related work, Freeman et al. (1991) describe location and energetics of isomeric butanes in a model zeolite. A blend of MC and MD with MM energy minimization was employed. MD was performed at 1400K, ensuring excess conformational sampling during the ensuing MC study.

The analysis by Goodbody et al. (1991) of methane and butane in silicalite gives an adsorption isotherm using GCMC (see below) and diffusivities from MD simulations. At low pressures (<20bar), adsorption is predominantly at site-specific potential-energy minima in the zeolite channels while at higher pressures adsorption is determined by the total accessible

Figure 13 Trajectory of Methane Molecules in ZSM-5 at 300K

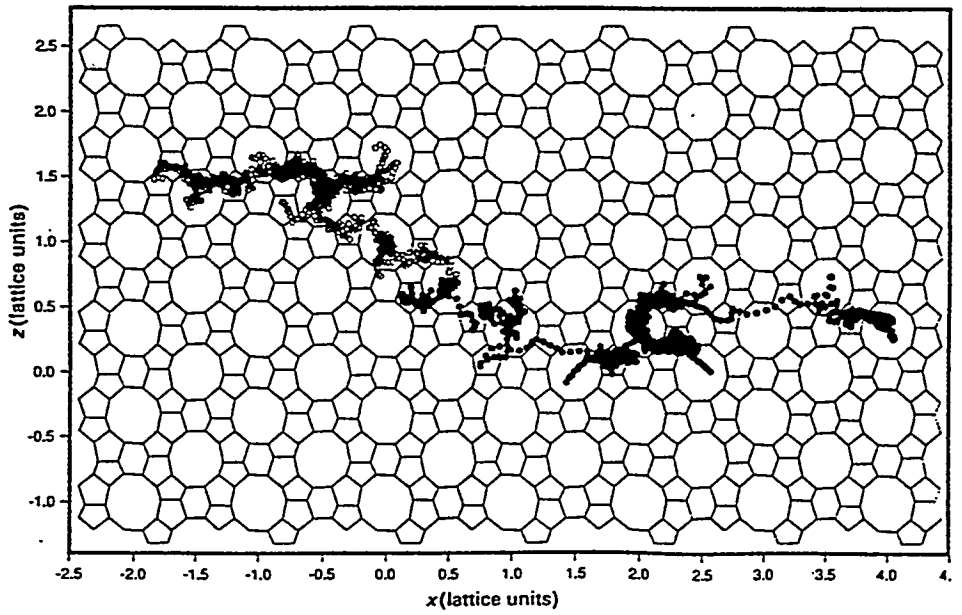

channel volume as would be expected. Diffusion is found to be highly anisotropic in this system.

Hufton's (1992) MD study of methane in silicalite was simplified by using a sphere instead of the five point methane model of June et al. (1990). Agreement of Henry's constants with experimental data was found, suggesting that assumptions like this are valid, and enabling larger systems to be studied in a more reasonable time frame.

The self-diffusion of rare gases in silicalite by MD simulations is described by el Amrani et al. (1993) using a rigid framework represented only by O atoms. The concept of supermobility is raised (this is like activated diffusion described next), and activation energies of diffusion are reported for Ne (2 kJ/mol), Ar (3 kJ/mol), Xe (6 kJ/mol at 0 atoms/unit cell to 3 kJ/mol at 9 atoms/u.c.), and methane (5 kJ/mol).

The MD study of methane in silicalite by Demontis and Suffritti (1992) at high dilution is carried out with a vibrating framework. The debate of whether to fix the framework or not is brought up often for simulations such as these. Of course, this will depend on the intended application of the simulation data and may just require adjusting a variable in the activated diffusion models. In a more recent work on Zeolite ZK4, Demontis and Suffritti (1995) showed the effect of moving lattice atoms on the pore size. This is reproduced in Figure 14. One effect of a moving lattice is to increase the MSD of diffusing molecules and, hence, predict a higher diffusivity. Fritzche et al. (1994) also studied ZK4 and found that methane diffusion follows an Arrhenius law. This diffusion increases or decreases with increased loading depending on the potential parameters used.

Figure 14 Variation of Pore Diameter in Zeolite A at 360K

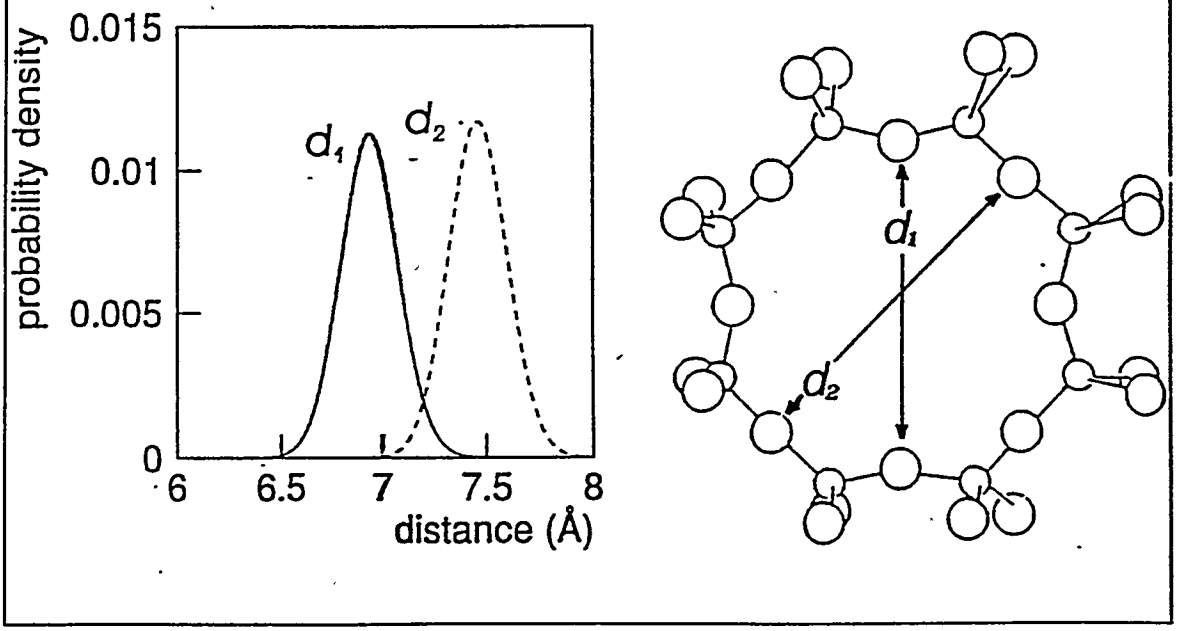

Nicolas et al. (1993) claim to have the first complete MD simulation of hydrocarbon diffusion in zeolites for which all internal degrees of freedom of the adsorbate, propane, are treated. The article looks at methane and propane in silicalite. It is studied at infinite dilution and at unit cell loadings of 2, 4, 8, 12, and 16 for methane and 4 and 12 for propane, all at 300K. The isosteric heats of adsorption of methane and propane are -5.8 and -10.3 kcal/mol, respectively. They claim excellent agreement with experimental values of the self-diffusion constants and the heats of adsorption. Silicon atoms are included in these simulations. The charges used were q(Si) = 1.2 and q(O) = -0.6, and for methane, q(H) = 0.143 and q(C) = -0.572. For understanding the energetics of interaction, if one assumes that there are an equal number of occupation sites in the intersections, zigzag, and straight channels, a simple approximation of the Boltzman probability for residence in the various sites is given by

$$P = \frac{\exp(E_i / RT)}{q_o} \tag{15}$$

$$q_o = \sum \exp(E_i / RT) \tag{16}$$

where P is the probability and q_o is a sum over the various sites of interaction energy, Ei. In the case of CH_4 in silicalite, the energy of interactions are intersections (5.9 kcal/mol), zigzag (6.71 kcal/mol) and straight (6.74kcal/mol). Based on this analysis (and the distribution of sites), one would conclude approximately equal probabilities of existence since the surface can essentially be considered energetically homogeneous. Results of simulations show more preference for the zigzag channels (13%, 53%, and 34%, respectively). They explain this as a function of the dynamics, i.e., the geometry and smaller size of the zigzag channel and its resulting slower diffusion. For propane this factor becomes more pronounced since the adsorbate is larger and requires more room to reorient. The jump diffusion model is discussed, but the smooth methane-zeolite potential energy surface does not contain the potential energy barriers normally causing jump diffusion. Finally, movement of the lattice allows energy transfer between the adsorbate and the framework, giving higher diffusivity values than if the lattice were fixed.

Activated Diffusion

Interest in this subject arose since gas phase diffusivities in zeolites measured by NMR, for example, can exceed, by 1 to 2 orders of magnitude, those expected from Knudsen diffusion or those measured by macroscopic means such as membranes (Kocirik et al., 1988). Barrer (1984) found that, contrary to the opinion of Karger and Ruthven (1992), the self-diffusion activation energy for linear alkanes approaches an asymptotic limit that is only a rather small fraction of their sorption heat. Molecular sieving effects on diffusion of molecules can be tested by calculating the energy of gas molecules placed at different locations along the diffusion path. These authors state that the Knudsen model should be entirely abandoned since its assumption of random (no memory) angular rebounding (fully inelastic collision) for each encounter does not hold. This analysis also suggests much about the adsorption energy both internal to the solid and on its external surface. The primary interactions between sorbed molecule and adsorbent are van der Waals forces. One finds two potential energy situations: "floating" molecules (activated diffusion) when the channel diameter is approximately equal to the molecular diameter, and

"creeping" molecules when the channel diameter is larger (≥ 2*molecular diameter). This is a significant consideration when designing shape selective porous materials or when enhanced diffusivities are desired (optimizing pore size).

Everett and Powl (1976) analyzed adsorption in slit-like and cylindrical micropores in the Henry's law region, originally presented as a model for carbon microporosity. The potential energy profiles for atoms in slit pores and the enhancement of the depth of the well are discussed. Smoothed potentials of the 10-4 and 9-3 type are used to represent the walls of the adsorbent. This is identical to 'floating' molecules as described by Derouane below. For cylinders, at R/r_o = 2 (R=cylinder radius, r_o =molecular collision radius), the enhancement over a flat plane is more than 50% and is still appreciable when $R/r_o = 3$.

Derouane's (1986) note describes the nest effect, one of the first accounts of the surface curvature concept and its effect on shape selectivity in zeolite catalysis. They report a maximum in the turnover frequency for n-pentane cracking at a pore size of ~6Å. Derouane et al. (1987) give the development and application of the van der Waals model for molecule-curved surface interactions in molecular sieving solids. An in-depth discussion of the surface curvature effect is given by Derouane et al. (1988). The *window* effect is also presented for explaining the n-pentane cracking maximum. The most useful derivation is the model for the van der Waals interaction of a molecule with a curved surface. R = D/a is the ratio of the distance of the molecule from the center of the cavity to the radius of the latter. This simple analysis results in *floating* or *supermobility* taking place as r approaches 1, i.e., tight fitting. This should actually take place before r=1 (Derouane, 1987) as others (Everett and Powl, 1976, and Lastoskie et al., 1993a,b) concluded.

More recently, Derycke et al. (1991) concluded that the enhancement of the physisorption energy due to surface curvature and confinement effects reaches its maximum value of 5.05, relative to the flat surface, when $D = 0.899s_e$ (~90% of the pair equilibrium distance). In addition, sorption energy remains negative down to $R = D = 0.75s_e$. This analysis is derived for spherical and slot pores which qualitatively envelop cylindrical spheres. A very accurate correlation is obtained relating the isosteric heat to the theoretically derived energy and the temperature. Its usefulness in random pore geometries is yet unclear, though the accuracy with zeolites is impressive.

Yashonath and Santikary (1992) initially described the breakdown in Arrhenius behavior of xenon diffusion in zeolite Y because of the existence of both positive and negative energy barrier heights between α-cages separated by windows of about 8Å diameter. In addition, they (1993a) showed the Arrhenius behavior, barrier height and mechanism of cage-to-cage diffuison using MD. A schematic plot of the variation of potential energy for centralized (r_p^m<3Å) and surface-mediated mode (r_p^m>3Å) is given. R_p^m is the minimum distance between the sorbate and the center of the cage. This concept is diagrammed in Figure 15. They also (1993b) described Ar in NaCaA using MD, also having negative barrier heights for cage-to-cage diffusion. This was associated with both positive and negative activation energies. Finally, they gave intracrystalline diffusion of Xe in NaY and Ar on NaCaA zeolites using MD. Rates of cage-to-

cage crossovers in the two zeolites exhibited trends contrary to that expected from geometrical considerations. This all underscores the important role of sorbate-zeolite interactions in determining the molecular sieve properties of zeolites and is explained in terms of the barrier height for cage-to-cage crossover. The barrier height can be obtained by a plot of the average potential energy of the particles during the cage-to-cage crossover. The barrier height is negative for zeolite Y and positive for zeolite A. In one computer experiment, the dispersion interactions were excluded and for Ar, there were no cage-to-cage crossovers during a 600 ps run, unambiguously demonstrating that sorbate-zeolite interactions are essential for diffusion. (Bandyopadhay and Yashonath 1994, 1995).

Figure 15 Surface Mediated and Centralized Flow

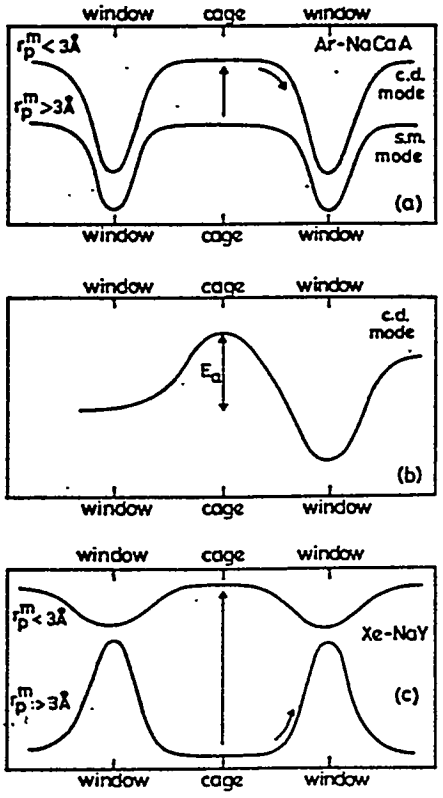

Non Equilibrium Molecular Dynamics

Determining the transport diffusivity, D_T, from equilibrium simulations or microscopic experiments depends on its the relation to the self-diffusivity, D_o, described by the "Darken equation"

$$D_t(c) = D_o(c) \left(\frac{\mathrm{d}\ln f}{\mathrm{d}\ln c}\right)_T \qquad (17)$$

where f is the sorbate fugacity in the zeolite, c is the intracrystalline sorbate concentration, and T is temperature. D_o is also called the "corrected diffusivity" and is related to molecular mobility. This is the parameter found in equilibrium NVT MD simulations. In this section, some recent attempts to simulate this relationship are reviewed.

Maginn et al. (1993) use "gradient relaxation molecular dynamics" (GRMD) by following the equilibration of a suitably chosen initial state (periodic step function in concentration) using standard equilibrium MD. The initial state was a combination of two methane-zeolite systems, each equilibrated with MD at the same temperature but different densities. By placing these two systems end to end, a step-function density profile was generated and used as the starting

configuration for a standard MD simulation. As the simulations proceeded, the step-function density profile slowly relaxed, eventually yielding a flat profile at a density halfway between the densities of the two halves of the original configuration. By following the evolution of the density profile $\rho(x,t)$ and solving Fick's second law,

$$\frac{d\rho(x,t)}{dt} = D_t \frac{d^2\rho(x,t)}{dx^2} \qquad (18)$$

the transport-diffusivity, D_t, can be obtained. However, as the authors point out, there is no way of determining if the simulation is in the linear regime where Fick's law is applicable without running many more simulations at different magnitudes of the concentration gradient. That is, GRMD is not at all applicable to systems which produce a steady-state non-linear profile.

As mentioned, and used extensively in Monte Carlo simulations described next, the grand canonical ensemble is attractive for non-equilibrium systems since it allows the chemical potential, μ, to be specified. The purpose in using the grand canonical ensemble to analyze gas diffusion in porous materials is that the diffusion is now determined in a more realistic setting as made clear by Cussler (1984). The difficulty, however, is that this restraint requires the number of particles in the study to vary depending on the other parameters in the system, hence, it is difficult to simulate in deterministic MD. Cagin and Pettitt (1991) and Jia et al. (1992) were among the first to attempt this by taking the number of particles in an NVT simulation to be a continuous variable. This, however, will destroy the dynamics that is of primary interest. Heffelfinger and van Swol (1994) developed a Dual Control Volume Grand Canonical Molecular Dynamics program for Lennard-Jones fluids (Figure 16). The method combines Grand Canonical Monte Carlo (chemical potential control in the control volumes) with MD (time dependent trajectories throughout the system) enabling steady-state phenomena to be studied (e.g., diffusion, evaporation/ condensation, adsorption, etc.). The purpose of GCMD in the present work is to simulate a pressure or concentration gradient across model porous materials. MacElroy (1994) recently used the same concept with an external field representing a mesoporous membrane within the diffusants' pathway. His results, based on a 'dusty gas model' analysis, show that slip flow, rather than viscous shear, is the predominant mechanism governing the permeation of moderately dense hard-sphere fluids in very fine pores. The pores were approximately four fluid particle diameters in size and generated by a model of random nonoverlapping spheres.

More recently, others (Ford and Glandt, 1995a,b,c; Cracknell et al., 1995a,b; and Fritzsche et al.. 1993, 1994, 1995) have simulated the gradient driven pore diffusion using a host of different assumptions demonstrating the scientific interest in this concept. Cracknell et al. (1995a,b) carry out similar simulations to the GCMD method used in the present work and compare with self diffusivities from equilibrium MD in Cracknell, et al. (1995c). Cracknell et al. and Ford and Glandt study slit pores as in graphitic carbons. Ford and Glandt look only at penetration into the pore mouth while Cracknell et al. look only at intrapore diffusion excluding entrance effects. Fritzsche et al. examine the more challenging zeolite A system, but arbitrarily maintain a concentration gradient by introducing source and sink wells at the first and last unit cells.

Figure 16 Dual Control Volume Grand Canonical Molecular Dynamics System

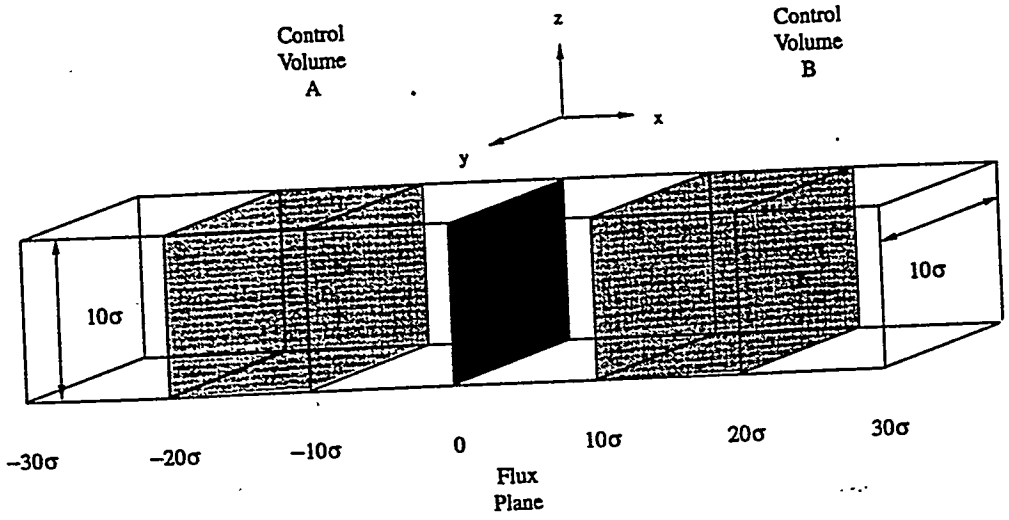

Monte Carlo Methods

In MC methods, a change in the molecular system is made at random and the total potential energy calculated. If the system becomes more stable, then, the move is taken. If not, then, the move is taken with a probability related to an exponential of the energy difference. Insertions, deletions, and particle moves are usually the changes that make up each step in the simulation. Adsorption in zeolites and graphite highlight the MC literature described (Allen and Tildesley, 1987).

Karvias and Myers (1989) first used Grand Canonical Monte Carlo (GCMC) for the adsorption of Xe, CH_4, CO_2, C_2H_4, and i-C_4H_{10} in zeolite X using a spherical approximation for the cage interaction potential and approximating the quadrupole effect of CO_2, and C_2H_4, showing that this interaction with the framework cations represents ~1/3 of the total energy of adsorption. The overall fit of isotherms from GCMC with experimental curves is very good, probably since their potential parameters were taken from second virial coefficients extracted from adsorption isotherms.

Peterson et al. (1988, 1990) carried out GCMC and Density Functional Theory simulations in a smooth cylindrical pore with strong fluid-wall interactions. The pore radius was 7 molecular diameters and the temperature below the bulk fluid triple point. The results are among the first direct evidence of simulated layering transitions in capillaries. (see Figure 17).

GCMC of Ar in VPI-5 and other ALPOs was compared with experiment by Cracknell and Gubbins (1993) and Cracknell et al. (1993). They use three models for describing the framework (with differing detail and accuracy). The computed isotherms fit qualitatively with experiment while the pore volume estimation is off slightly. The preference of adsorption was plotted as a function of position within the framework showing the Ar's preference for the corners of the pores. Cracknell and Nicholson (1994) carry out similar GCMC analysis of ethane and propane interactions with porous carbons.

Kr and Ar in zeolite ρ at high sorbate loadings is reported by Loriso et al. (1993) using GCMC computer simulations of adsorption isotherms. The adsorbates are deprived of mutual attraction on two irregular and one regular surface showing that the mean field correction makes it possible to take into account attractive interaction between adatoms. They use a model amorphous oxide with a random packing of hard spheres representing oxide ions and conclude that there are two ways to make Mean Field corrections for the interaction between adatoms in adsorption, correct adsorption and correct chemical potential. They used the latter and emphasize that it is simpler than the former.

Vernov et al. (1993) simulate Xe in zeolite, ρ. Loading is varied in order to evaluate its effect on order and to elucidate the Henry's law constant, K_H. This is related to the adsorbate-solid interaction energy $u_s(r)$ by

$$K_H = \frac{1}{kT}\int_{V_s}\left\{\exp\left[-u_s(r)/kT\right]-1\right\} \qquad (19)$$

where V_s is the sorption volume of the crystal and, thus, equal to $n_{unit}v_s$, where n_{unit} is the number of unit cells per gram of zeolite and v_s is the sorption volume per unit cell. Units of K_H are mol atm^{-1} g^{-1}, and experimental values are obtained from

$$\lim_{p\to 0}\left(\frac{N_a}{p}\right) = K_H \qquad (20)$$

Figure 17 Cylindrical Pore Meniscus Formation

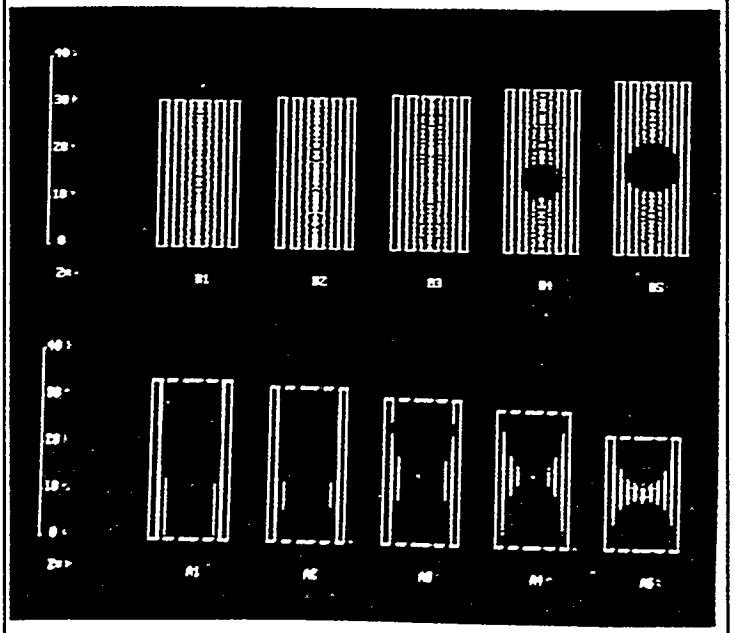

where N_a = moles sorbed per gram of zeolite. These authors are interested in the probable locations of the sorbed xenon atoms in the pore structure of this solid, the sorption energy of these atoms, and the way in which the gas-solid and gas-gas components of the total energy change with increasing amounts of sorbed xenon. The well depth, $\varepsilon_{Xe\text{-}O}/k$, which matched the slopes of the experimental and the theoretical line for K_H was found to be 151 K, which is

considerably different than some previous estimates of this parameter. For example, 237, 221 (Kiselev et al., 1985), and 127 K (June et al., 1990) have been used in calculations of Xe in X, Y, and silicalite.

Smit (1995) simulated adsorption isotherms and Henry's law constants for small hydrocarbons in silicalite. He summarizes the previous simulations and suggests optimum Lennard-Jones parameters for use in zeolites. These are not the ones used in the present simulations since we are interested in silica.

Nicholson (1994) described the GCMC adsorption simulation of N_2 in slit pore carbon, modeling N_2 as a Lennard-Jones sphere. The 10-4 potential for graphite is modified to describe corrugation of the basal plane in the rhombic unit cell by a term added describing the x,y contribution (Steele 1993). Pore widths of 1.01, 1.16 and 1.35nm (surface to surface C) are examined. All three pores show layering - the largest gives 4 layers while the two smaller slits have 3. The medium pore has relatively delocalized layers compared to the others, giving rise to slight hysteresis. The largest pore is type IV. The effect of corrugation is shown in the heat of adsorption which is less at higher coverages than the smooth surface's heat of adsorption. The adsorption quantities are given in terms of commensurate loading of molecules on a basal plane. He concludes that conventional pore analysis must be applied with caution in interpreting data. Rhykerd, et al. (1991) carried out GCMC of gases in carbon. Razmus and Hall (1991), Jameson et al. (1994), and Van Tassel et al. (1994a,b) carried out GCMC of gases in zeolite A. Each used varying degrees of accuracy in simulation detail and compared to adsorption and NMR data.

Modeling Silica and Glass

Garofalini (1990) gives an MD study of the silica surface structure and adsorption of water molecules. The potentials of Garofalini's work are used by many others, including the author of this thesis. Bulk vitreous silica using pair potentials and multibody potentials (results of the two are compared graphically in terms of RDF), as well as simulations of the interaction between H_4SiO_4-H_2O molecules are presented as background to the surface treatment. Water adsorption simulations (Webb and Garofalini, 1994) follow expected trends of dissociation of adsorbed water molecules, silanol formation, siloxane bond rupture, and preferential association of adsorbed water molecules. "Defects" such as non-bridging O, 3-coordinated Si and O, 2-, 3-, and 4-membered rings are counted as points expected to cause silanol formation. These give rise to a surface hydroxyl concentration of ~6.4/nm^2, slightly greater than the 4-6/nm^2 found experimentally. He concludes that the most reactive sites are within the top 2 to 3 Å of the surface.

More recently, the polymerization of silicic acid molecules and network formation is described by Garofalini and Martin (1994) and Martin and Garofalini (1994). Two hundered sixteen monomers were allowed to "react" over a 120 ps MD simulation, giving rise to growing clusters and, eventually, a gel-like structure. The work describes the nucleophilic reaction mechanism giving rise to a pentacoordinate transition state and formation of a siloxane bond. The NMR work initially referenced is of Assink and Kay (1991), while the actual experimental Q distribution vs. time is from Devreux (1990). The simulated Q distribution vs log(time) gave

qualitatively similar results, albeit differing in time scale by 15 orders of magnitude. For the present work, some important differences are that silicic acid is not the monomer (which would give rise to monomer-cluster aggregation) and the concentrations for making microporous membranes are low, giving rise to diffusion limited aggregation and the weakly branched polymers used in making microporous gels described below. Fueston and Higgins (1994) used the same silica simulation tools to construct models of the mesoporous material MCM-41. This model consists of amorphous silica walls and pores of variable size.

Kohler and Garofalini (1994) investigated the penetration of inert gases adsorbed onto silicate glass surfaces. Their 77K MD results show that N_2 and Ar are unable to penetrate. Individual Ne atoms were able to penetrate all of the surfaces except sodium aluminosilicate. They attribute this to the differences in glass compositions.

The most relevant computer simulation of gases in porous silica is given by MacElroy and Raghavan (1990), though the pore size is comparable to silica aerogels (see Figure 18). These are formed from colloidal suspensions by aggregation and gelation and consist of microspherical particles interlinked in a random network [see Iler (1979) or Unger (1979)]. Methods for determining the model silica system included removing spheres from random close packed assemblies as well as a MC method to generate random nonoverlapping assemblies. Five hundred sample configurations of each method were used in subsequent computation of pore fluid properties. To determine the sphere diameter σ_S using the porosity, ψ, and the internal surface area, S, they used

$$\sigma_s = \frac{6(1-\psi)}{\rho_p S} \tag{21}$$

as well as a smoothed interaction obtained using Lennard-Jones potential for nonbridging and bridging oxygens. The number of microspheres was determined subject to the requirement that the accessible void space for a classical Lennard-Jones helium atom of diameter $\sigma_{He} = 0.263$nm corresponded to the porosity of $\psi = 0.49$ measured experimentally using helium pycnometry. Results include the partitioning of adsorbed versus gaseous methane gas, comparing well with experimental measurements. MacElroy and Raghavan (1991) expand this work to model adsorbing vapors in a model silica system. Resultant isotherms showed no hysteresis. Comparison with experimental data is good for both sorption and diffusion properties. MacElroy (1993) presents GCMC simulation results for a Lennard-Jones vapor adsorbing in microporous silica which preceded the non-equilibrium work described earlier.

Figure 18 Silica Gel Model with Adsorbing Methane

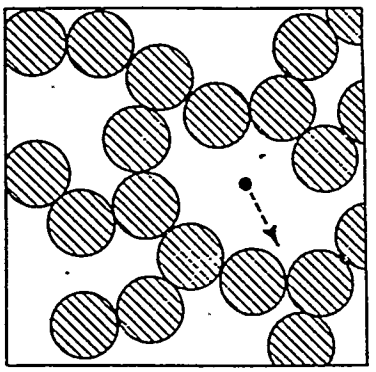

MD simulation of liquid-plastic phase transition of cyclohexane in porous silica is described by Brodka and Zerda (1992a). Two cavities of diameter ~30 and 50 Å are considered. Cyclohexane is approximated by an assembly of six Lennard-Jones potentials. MD simulation of reorientation motion of SF_6 on porous sol-gel glass is given by Brodka and Zerda (1992b). Of interest to the present work is the pore diameter of 23 Å though the intent was to better describe the Raman spectra of the probe molecules. A cube size of 58 Å containing 128 atoms was used to represent the amorphous silica. Hydroxyl groups (non-bridging oxygens) were present at 7.9 per nm^2. In order to distinguish between bridging and non-bridging oxygens, they adopted two different interaction parameters, σ, for flourine and the two oxygen types (Brodka and Zerda (1992c). Finally, Brodka (1994) simulated cyclohexane in a cylindrical pore of amorphous silica, investigating the phase as a function of loading and temperature.

Shelekhin et al. (1993) used a lattice analysis of amorphous porous silica in studying the surface area and porosity using percolation theory. Dependence of the surface area per unit volume, S_v on pore size was represented by a simple power law of the type $S_v \sim f(q) d_p^{-1}$ with $0 < f(q) < 1.23$ where d_p is the pore diameter and q is porosity. Experimental data from literature on surface area and porosity were used to verify this relationship. As a first approximation, the surface area per unit volume in porous materials with porosity $0.4 < q < 0.6$ can be estimated as $S_v = 1.23/d_p$. McElfresh and Howitt (1990) used a similar analysis to study gas accessibility into glass. Their work considered the void volume distribution in the dense material and the connectivity of these pores. A calculation of the diffusion constants for several gaseous species was made showing good correlation to experimentally determined values.

Nakano et al. (1993, 1994a,b) have constructed the largest (~41,000 atoms) simulated porous silica models to date using parallel processing and a method of expanding a glass model. A problem with this approach is that there is no way to corroborate the building process. If all the physical properties are equivalent to those of a material, then it may not matter, although their reported surface area as high as 5000 m^2/g is physically unrealistic. Another issue with this model is that the composition remains SiO_2 throughout unlike sol-gel materials which are not fully condensed silicates. Vashishta et al. (1995) evaluates these models for use as insulators. Table 2 shows a number of other simulations on various glass systems.

Table 2 Simulations of Glass Systems

Researchers	System	Property Analyzed
Abramo et al. (1993)	$(AgI)_x(Ag_2O_2B_2O_3)_{1-x}$	Medium range order
Belashenko and Fedko (1991)	B_2O_3-SiO_2	Various compositions, structure
Damodaran et al. (1990)	ZrO_2-SiO_2	Structure, edge sharing
Himmel et al. (1991)	B_2O_3	Wide angle x-ray scattering, defects
Inoue et al. (1993)	B_2O_3	Rings, diborate groups
Kawamura et al. (1993)	Na-SiO-N	Density, thermal expansion, modulus
Ogawa et al. (1980)	B_2O_3-Na_2O_2-SiO_2	x-ray diffraction, glassy state
Ochoa et al. (1991)	SiO_2	Brittle failure
Swiler et al. (1995)	SiO_2	Brittle failure
Shahand and Behrman (1991)	Several multicomponent	Perturbation theory
Soules (1990)	SiO_2	Review
Valle and Anderson (1992)	SiO_2	Temperature effects on structure
Vessal et al. (1993)	Silica	Bulk structure
Xu et al. (1988)	B_2O_3-NaO	Effects of Na composition

CHAPTER 4 - RESULTS: POROUS MATERIAL MODELS

Before conducting gas diffusion studies, the porous solid structure must be accurately modeled. To do this, one starts with material information at many length scales. At an atomic level, the elemental composition can be used. At a molecular level, the fragments that make up the structure can be pieced together. At the macroscopic level, properties such as the density or porosity can be included. This chapter presents work to date on zeolite, imogolite and silica molecular models and their pore structures. The purpose of this work is to explore the capabilities and limitations of computer simulations while developing models for investigating the effect of pore structure on gas permeation.

As mentioned, the size and complexity of the model is limited by the available computer memory. One area actively studied by atomistic computer simulations is the dynamics of gases in microporous solids as reviewed above. Micropores have pore diameters or widths less than 2 nm, (Rouquerol et al., 1994), hence, the models required are usually around a thousand atoms. Mesoporous solids such as silica aerogels are designated as having pores greater than 2 nm and less than 50 nm. Simulation of these materials must have millions of atoms to properly exhibit a statistically relevant pore structure. With regard to aerogels, a better understanding may lead to improved processing routes for producing low density aerogel-like materials at ambient pressure. That is, until recently, supercritical drying was the only proven method to minimize drying shrinkage (Schaefer, 1994). Hence, we modeled silica aerogels with available techniques.

The prediction of crystalline and amorphous structures has a few things in common, mostly at an atomic level. That is, Si prefers to be four coordinated with O. At greater length scales, the two classes of materials require differing information for structure elucidation. For crystalline materials (or paracrystalline as imogolite), short range structure determination utilizes x-ray diffraction data to uniquely specify the atomic positions, connectivity and arrangement of fragments such as tetrahedrally coordinated atoms and the regularity of bond distances and angles. For amorphous materials, the short range structure is distinguished by information such as bond length and bond angle distributions and the irregular arrangements of tetrahedral atoms. Amorphous materials have characteristics as much like liquids in terms of inter atomic positions as crystalline solids. On larger length scales, the pore structure (the primary property of interest in this work) depends on the two previous length scale descriptions. Thus, the information gathered on the atomic and molecular scales will narrow down the possible structures that will exist for a certain porous material.

Faulon et al. (1993, 1994) developed a discretized program for calculating the pore properties of molecular computer models. The method was developed for comparing various molecular models of the structure of coal. It begins (Figure 19) by forming a 3-d grid that encompasses all of the atomic coordinates of the model of interest. Next, the nature of each grid point is determined, i.e., it is defined as an atomic cell, an internal cell, or a closed cell. An atomic cell is a cell included in the Van der Waals sphere of any atom. The sum of the volume of all atomic cells defines the atomic volume. Internal cells are cells not accessible to nitrogen because

they are located between two or more atoms having an inter-atomic distance less than a critical value corresponding to N_2, (4.1 Å in our calculations). The sum of all internal cells defines the internal volume. Closed cells are determined after determining atomic and internal cells, and represent closed volumes (i.e. cells surrounded by atomic and internal cells). The sum of all closed cells defines the closed porosity volume. Next, the number of pore surface elements is determined and counted. Since atomic and internal cells are inaccessible to adsorbate molecules, the total surface area is computed by summing all the areas of cell faces between an atomic or internal cell and a non-atomic or non-internal cell (not including closed cells). The pore surface area is the surface of the micropore volume. Figure 20 gives an example of this program applied to imogolite (Carlson et al. 1993). In addition the method has been applied to bridged aryl polysilsesquioxane structures (Faulon et al. 1995).

Figure 19 Model Pore Structure Characterization

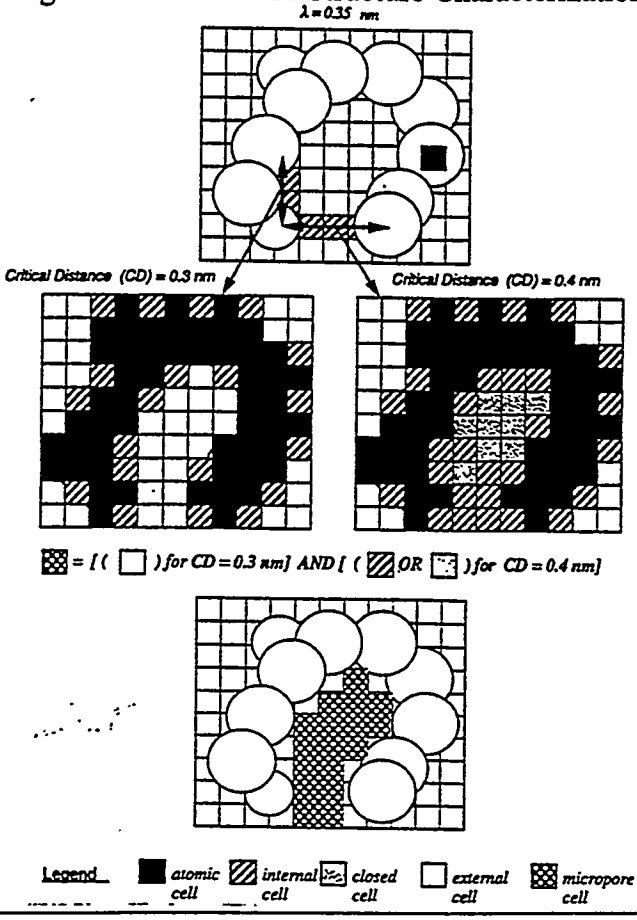

Figure 20 Imogolite Pore Structure from Pore Program

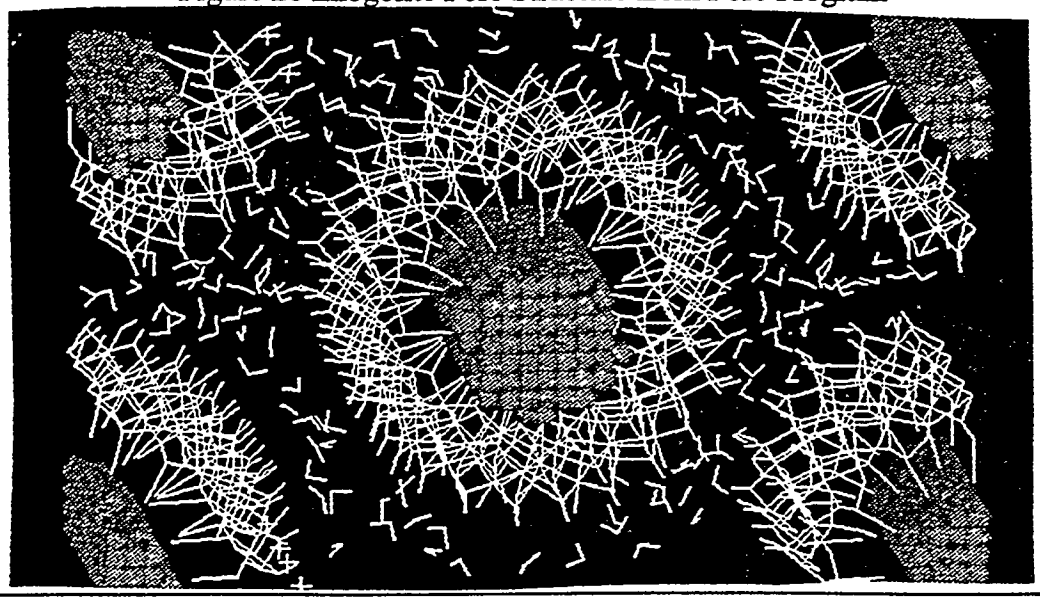

According to Dubinin (1975), however, the concept of surface area does not apply for microporous solids where the pores of the material, themselves, are very small. In essence, the adsorbate molecule is no longer interacting with a "surface" composed of many adsorbent molecules. Instead, it is interacting specifically with a surrounding pore which is of molecular dimensions. Thus, the theories which would apply to the behavior of a macroscopic surface would no longer hold good in this regime. Below, in the analysis of imogolite, this idea is revisited with a figure of N_2 adsorbed at 1 atm and 77k. In addition, Kale and Brinker (1995) have developed a percolation study method. This method determines the maximum diameter sphere that can get through a model porous material.

Zeolites

Faujasite, zeolite A, sodalite, silicalite and the aluminophosphate VPI-5 were modeled and used in the present work. This was simple because of their known structure. Success in evaluating properties with these was meant to lend validation to the modeling of more difficult structures such as silica. Gas interactions (Figure 16) with the first three were used to predict an ideal activation energy to compare permeation experiments and evaluate transport models. Silicalite was utilized in the gas permeation simulations described in the next chapter. The study on VPI-5 was to validate the finite element program of Faulon et al. (1994) just mentioned and is presented next.

As a standard for comparison of the pore volume calculation, VPI-5, a crystalline aluminophosphate with pore diameter ~1 nm, was first analyzed. Its pore volume was calculated using the scheme above and a unit cell of 37 Å x 64 Å x 16 Å and micropore entrance critical diameter for H_20 (2.65 Å). The value found (0.37 cc/g) matched within 1% of the equivalent liquid volume at $P/Po = 0.4$ for H_20 adsorption (Davis et al., 1988). This exemplifies the accuracy of the finite element method for pore volume calculations in relation to gas adsorption. The breakthrough percolating analysis of Kale and Brinker (1995) was tested on zeolite A and found 4.0 Å diameter pores as expected based on the known structure.

The zeolites used in the Grand Canonical MD permeation simulations below were silicalite and zeolite A. Silicalite has relatively straight pores approximately 5 Å diameter with periodic intersections with a sinusoidal pore. Zeolite A has a cubic symmetry and consists of cages separated by windows of 3-4 Å diameter, depending on the cation used in synthesis. Figure 21 shows the structures of these zeolites and their relative pore sizes with respect to He and CH_4. Initially, He transport in sodalite was tried, but no transport was measurable even using a vibrating

Imogolite

Imogolite, a tubular aluminosilicate (~1mm in length, ~8Å inner diameter), is perhaps the newest and most unique material for molecular sieving and for these computer simulations. Synthesis of and adsorption experiments with this material have explored many possible applications which would exploit its narrow pore size distribution and unique structure. Ackerman et al. (1993,1994) completed a study of the porosity associated with natural and synthetic imogolite which included N_2, CO_2, and CH_4 adsorption, N_2 temporal adsorption, and Xe NMR.

Figure 22 Zeolite A (top) and Silicalite Pore Shapes (He and CH_4 Spheres)

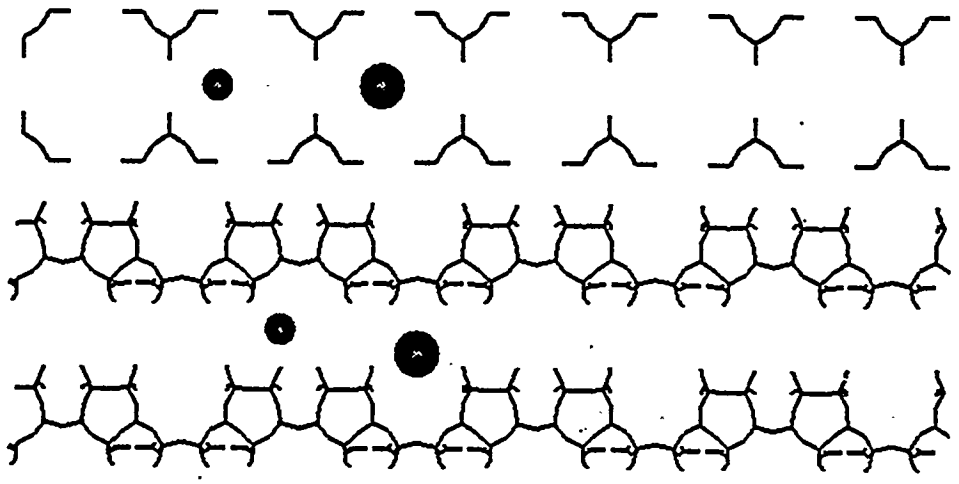

In addition, it has been embedded into dense silica membranes giving molecular sieving behavior (Sehgal et al., 1994) and has been proposed as a shape-selective catalyst (Imamura et al., 1993). The purpose of this work was to model the pore structure using various imogolite molecular models and validate the method for predicting these properties (Pohl et al., 1996).
framework at 1500 K.

Figure 21 Imogolite Atomic Structure (end view)

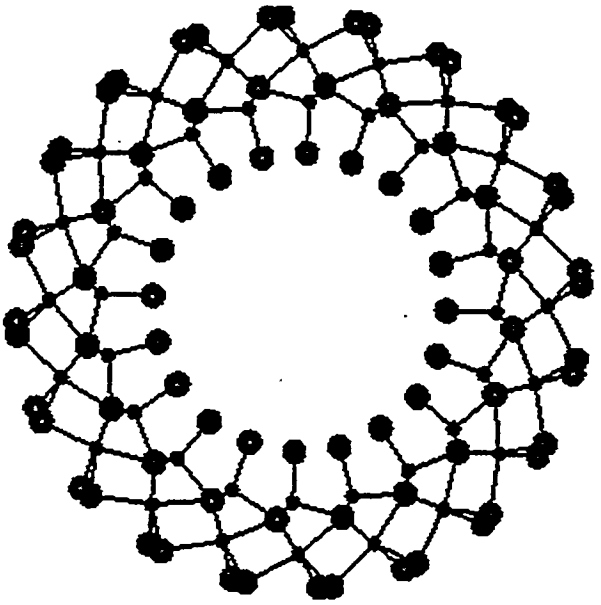

Shown end on in Figure 22, imogolite was originally reported by Yoshinaga et al. (1962). The composition, $(OH)_2Al_2O_3SiOH$, and atomic coordinates provided by XRD analysis of natural imogolite were reported by Cradwick et al. (1972), and the material was synthesized by Farmer and Frazier (1979) from dilute solutions of $Al(ClO_4)_3$ and $Si(OH)_4$. The tube diameters were enlarged by synthesis using Ge in place of Si by Wada and Wada (1982). Huling et al. (1992) developed a procedure to align the tubes into a 'fabric' of hydrated bundles. The material

thus synthesized contains little (~25%) mesoporosity associated with the random twisting of tube bundles found in all previous samples.

Based on electron diffraction measurements of the tube to tube distance, Cradwick et al. (1972) suggested that a model with 10 gibbsite units around the circumference was the most likely structure of natural imogolite. A gibbsite unit is an octahedral $Al(OH)_3$ sheet with nominal unit cell dimensions of 8.6 Å x 5.1 Å and makes up the al. layer of the material. Farmer and Fraser, on the other hand, concluded that the natural material was composed of the 12-unit structure and synthetic imogolite had a 14-unit structure. Wada and Wada concluded that for 100% Ge replacement, the tube contained up to 18 units based on an interaxial separation of ~30 Å. Our analysis below considers models with 10, 12, 14, and 16 gibbsite units.

Using imogolite (a hydrated paracrystalline material) rather than a zeolite gives some flexibility in the modeled structure providing a more challenging task for the pore property modeling procedure. For example, although the atomic positions around the circumference of the tube are known from X-ray diffraction, the center-to-center distance is known less accurately from electron diffraction or microscopy. The size of the tube also varies as per the synthesis scheme. In addition, depending upon the outgassing temperature, which drives off bound water, pores can take still different shapes (intertubular and intratubular pores) and sizes. These variables enable one to make numerous, differing structures of the same general cylindrical material.

The monolayer number for microporous solids is not equivalent to the surface area, requiring approximations to be made. In these cases, comparison with a statistical monolayer curve provides an empirical means of obtaining the surface area. In the experimental results of Ackerman et al. (1993), the BET surface area, micropore surface area, and pore volume were calculated along with approximations of the pore size distribution.

The simplest measurement is the pore size. The diameter ranges from 5-10 Å for the 10 gibbsite model, 8-13 Å for the 10 gibbsite model, 10-15 Å for the 10 gibbsite model, and 12-17 Å for the 16 gibbsite model. The pore is less cylindrical than one might first imagine, exhibiting a periodic structure along the pore axis. This heterogeneity gives rise to large pore volume and even larger surface areas for the models as described below. The experimentally determined pore diameters for synthetic imogolite were ~7 Å and ~10 Å for the 100% Si and 50% Si materials. Based on this information and model values, one might conclude that these two materials have structures consisting of 10 and 12 gibbsite units, respectively. The experimental values, however, are based on theory that has not been completely validated, so comparison must be done with caution.

The bulk models assumed hexagonal close packing with center-to-center distances of 20-30 Å. This distance depended on three things: the model size, the optimum separation based on a minima in the intertubular potential energy, and the use of intertubular water or not. This value is often obtained experimentally by electron diffraction. To remove both statistical and fractal variations, over 20 different cell sizes (from 1-4 Å) were averaged to calculate the surface area and pore volumes.

Table 3 gives the results of the pore structure analysis for the imogolite structures. The experimental surface areas are calculated from N_2 adsorption at 77K by Ackerman et al. (1993) using Harkins and Jura (1944) analysis. The models used had 10, 12, 14, and 16 gibbsite units with center-to-center distances (interaxial separation) found as the minima in the intermolecular potential energy. Based on these values and electron diffraction results ranging from 23 Å to 28 Å, we then used larger dimensions to better model water between the tubes. Water molecules were then close packed between the tube contact points. Next, we make a slight correction to the measured surface areas. The 16.2 $Å^2$ surface area per N_2 corresponds to 4 Å linear dimension, and simulated results show that the number of N_2 molecules adsorbed around the circumference is ~4 (Figure 23). Since these 4 molecules will give 16 Å linear surface and a 7 Å diameter cylinder would measure 22 Å circumference, we correct our values by the ratio 16/22 which lowers the simulated surface areas found by the pore program. These interaxial separation distances are given and the model properties are listed.

The 10-unit model would probably correspond to natural imogolite, since Cradwick et al. (1972) recorded an interaxial separation of 23 Å, Farmer and Fraser (1979) found 22.7 Å, and Imamura et al. (1993) concluded that the pore diameter must be ~6.5 Å since their natural imogolite samples refused adsorption of 1,3,5-triisopropylbenzene (diameter of 8.5 Å). The 12- and 14- unit models would correspond to synthetic materials of Ackerman et al. (1993), as these researchers reported interaxial separations of 25 Å and 26.2 Å, respectively. The 16-unit model may correspond to those materials of Wada and Wada (1982) with very high Ge content. Their method of measuring the interaxial separation was electron microscopy which is imprecise to this level of resolution, and they reported no pore volume data.

The natural form of imogolite probably has 10 units, as Cradwick et al. (1972) suggested. The model with 12 gibbsite units around the perimeter is the most likely structure of the 100% Si imogolite that was synthesized and characterized by Ackerman et al. (1993). The reason for the expanded tube size is the high temperature used in the synthesis, which stretches the Si-O bond length. The model with 14 gibbsite units is most likely representative of the 50% Si imogolite sample. In this case, the larger Ge ion caused expansion of the crystalline structure. From modeling VPI-5 and imogolite, we feel that the method described is fairly precise in predicting pore characteristics quantitative enough to evaluate and characterize differences between computer generated models based on experimental data.

The difficulty with reporting surface areas may be seen by Figure 23, where the N_2 adsorption in the 10-unit imogolite pore is given. As can be seen, the curvature of the surface and the finite size of N_2 cause the surface area to be quite different from that of a smooth surface. Using the number of N_2 molecules adsorbed and the 16.2$Å^2$ surface area per N_2 gives lower surface areas closer to experimental values. This method is not automated, however.

Table 3 Micropore Surface Area and Pore Volumes for Imogolite

Outgassing Temperature —→	275°C	250°C	225°C
synthetic(100% Si) - BET Area	398	340	259
Micropore Surface Area	324	258	177
Pore Volume	0.201	0.175	0.137
Micropore Volume (<14Å dia.)	0.16	0.11	0.09
Hydraulic Radius = r_{hyd} = 2(pv/sa)	1.01	1.03	1.06
synthetic (50% Si) - BET Area	403	332	297
Micropore Surface Area	290	267	196
Pore Volume	0.211	0.175	0.157
Micropore Volume	0.13	-	-
Hydraulic Radius	1.05	1.05	1.06

Imogolite model results

	Interaxial Separation (Å)	Pore Vol. (cc/g)	Surf. Area (m^2/g) (Corrected)	r_{hyd} (Å) 2(PV/SA) (Corrected)
10 unit internal	Internal Only			
	20.8	0.14	376(274)	0.76(1.04)
	22	0.123	338(296)	0.74(1.01)
	23	0.157	411(312)	0.76(1.04)
	24	0.192	488(356)	0.79(1.08)
12 unit internal	Internal Only			
	22.7	0.14	356(260)	0.78(1.07)
	24	0.14	354(260)	0.79(1.08)
	25	0.172	422(310)	0.81(1.11)
	26	0.201	494(360)	0.81(1.11)
14 unit internal	Internal Only			
	24.6	0.156	369(270)	0.85(1.15)
	26	0.14	336(245)	0.83(1.14)
	27	0.161	387(280)	0.83(1.14)
	28	0.194	461(340)	0.84(1.15)
16 unit internal	Internal Only			
	26.5	0.17	384(280)	0.9(1.22)
	28	0.153	343(250)	0.89(1.22)
	29	0.175	394(287)	0.89(1.22)
	30	0.20	464(380)	0.88(1.21)

Microporous Silica

Here, we summarize a report (Pohl and Faulon, 1994) on the generation of molecular models of microporous silica. With this work the objective is to predict models that mimic the silica membranes prepared by Sehgal et al. (1994). These membranes were made from sol-gel dip-coating of polymeric silica onto commercial 40 Å γ-alumina membranes and have ideal separation factors (ratio of individual gas permeabilities) for several gases, including He/N_2 of 9.

Figure 23 N_2 Adsorbed in Imogolite at 77K and 1 atm.
Left: Cutaway Side View, Right: End View

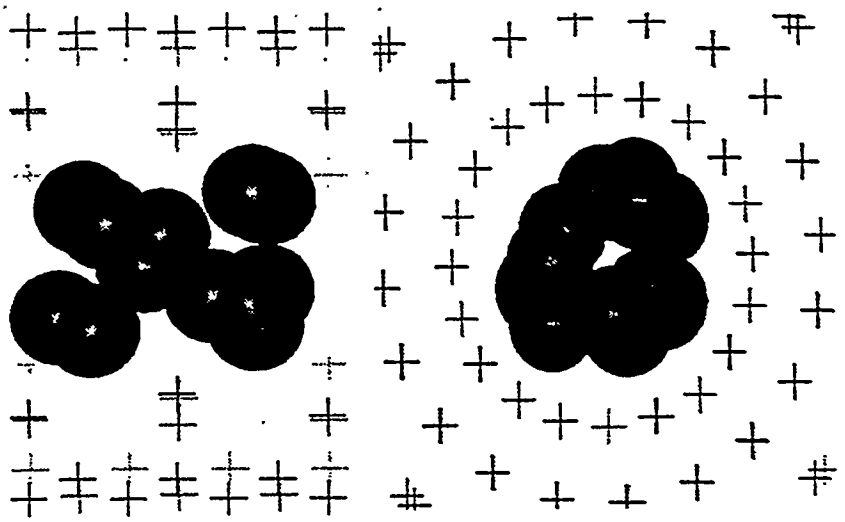

The strategy for making microporous silica relied on the theory of fractal aggregation (Mandelbrot, 1982). The density of a mass fractal object of dimension D decreases with distance from its center of mass, $\rho \propto 1/r_c^{(3-D)}$. Because density is inversely related to porosity, this relationship requires that fractal objects become more "porous" as their size increases. Hence, creating fractal silica polymers in a system with a low condensation rate was an attempt to produce a final structure which upon deposition and drying had pores of molecular dimensions. Typical analytical techniques used to follow the growth of silica polymers are ^{29}Si NMR and small angle X-ray scattering (SAXS). From NMR one can get the degree of condensation, i.e., the number of bridging SiOSi bonds for the silicon atom under consideration (Assink and Kay, 1991). From SAXS, the mass fractal dimension and Guinier radius can be obtained as described by Martin and Hurd (1987).

With these experimental data, we can make computer models of silica clusters. Here, we use the SIGNATURE program of Faulon (1994), a computer-assisted structure elucidation technique. With this program we input fragments with given bonding sites and produce a sample of randomly formed structures meeting the degree of condensation and the size desired (NMR and R_g data). The formation of a dry gel from a dilute, acidic system is best explained by a cluster-cluster aggregation mechanism (Brinker and Scherer, 1990). Computer simulations of this phenomena have been carried out on cubic lattices and reviewed by Meakin (1988). One result of this research is an understanding of the polydispersity of the sol, i.e., the aggregate size distribution. Martin (1986) concluded that this distribution must follow an exponential form, $N_X \propto X^{-\tau}$, where N_X is the number of aggregates of size X. τ is found to be 2.2 for bond percolation and assumed here to be 2.0 as determined by Meakin's simulations. We use this distribution with the SIGNATURE program to simulate the dip-coating step in membrane formation, where aggregates of different sizes collapse together.

With the theoretical understanding above and NMR and SAXS data, we did the following (in Si_X notation below, X is the number of silicon atoms in a silica polymer):

1) Generated Si_7 structures from A2 sol NMR data and SIGNATURE program.
2) Minimized Si_7 isomers to find the most energetically stable cluster.
3) Made Si_{14}, Si_{21}, . . . Si_{154} clusters by adding Si_7 randomly to preceding aggregate.
4) Computed the mass fractal dimension of each cluster.
5) Chose number of each fragment based on above size distribution and 500 Si.
6) Combined the entire ensemble of aggregates in a random manner.
7) Carried out quenched dynamics (MD for 1 ps → energy min.) for 120 ps, 300K.
8) Calculated pore volume using a finite element technique.

The size 7 was the smallest structure that could exhibit the degree of condensation given by the NMR data. The 500 Si value was chosen to give ~3000 atoms in the final model which is not a limit of MD (Nakano et al. (1994) simulated 40,000 atoms) but was selected for convenience and is probably of sufficient size to study microporous silica. Steps 5-7 were a first effort to simulate the dip-coating process which is different from gelation and drying in a bulk gel. The difference is that in dip-coating, the solid structure is deposited imposing a relatively fast consolidation of the polymers onto one another, while conventional gelation and drying relies on diffusion and reaction of the polymers until a spanning cluster exists. The structure following ~40 ps quenched dynamics (which combines molecular dynamics with intermittent energy minimization), however, maintains quite constant pore structure as shown below in Figure 24.

The Si_{154} cluster had a mass fractal dimension of 1.7 and R_g = 16Å. Figure 24 shows the results of quenched dynamics on the final silica structure. One can see the effect of simulation on the model's collapse. The average porosity of the models simulated for >40ps is 15.5%, close to the 16% found for a single layer of A2** calcined at 400°C (Sehgal et al., 1994). We "reacted" closely adjacent hydroxyls to form siloxane bonds. We found the average porosity then to be 13%, compared to 9.5% for a single layer of A2** calcined to 550°C. Fractal

Figure 24 Microporous Silica Models from Cluster Aggregation

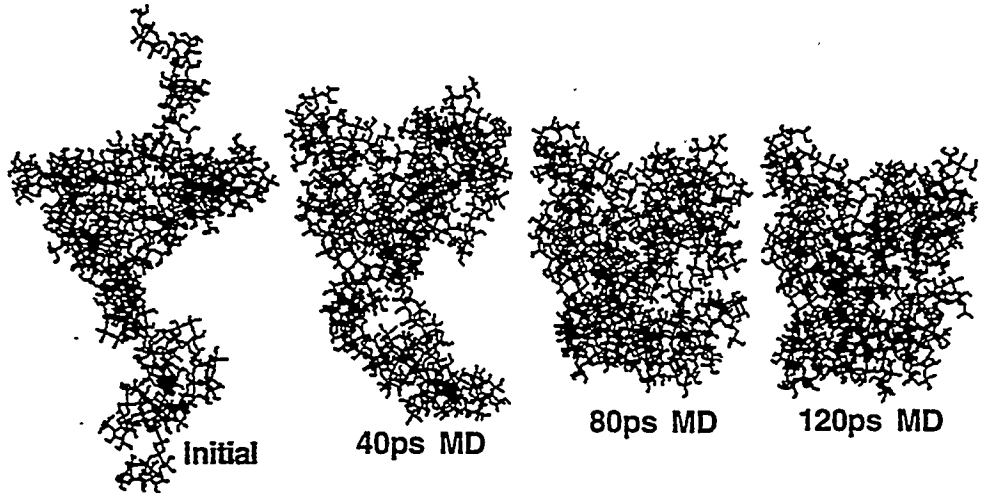

aggregation for producing microporous solids, we conclude, requires an aggregate size distribution rather than the same aggregates of low mass fractal dimension. Using the latter approach, we could not reproduce the porosity (calculated values >20%) or pore size as the model in Figure 24 has. The relative pore volumes (averaged over 5 models simulated for >100ps) for He(2.6 Å diameter)/N_2(3.6 Å)is 1.34. The experimental value for ideal He/N_2 permeance ratio of 9 corresponds qualitatively with this ratio if one considers the additional pore volume (this is accessible pore volume) to be opening up more passages through the solid for the smaller He. Without complete mapping of the accessible pathway, application of the permeation theories discussed above is not possible. Simulating gas permeation is probably the best method of studying this property.

Mesoporous Silica

The study of aerogels using molecular modeling is difficult because of model size requirements, but progress was made in identifying possibilities and limitations in this area. In this work, three approaches were taken to model the structure of silica aerogels (Pohl et al., 1995b). The first simply evaluates the surface area of different colloidal sized silica spheres based on their packing coordination number. The second, recently demonstrated on a larger scale by Nakano et al. (1994), begins with a dense silica glass and upon expanding the model and using molecular dynamics, gives rise to structures with varying density and porosity. The final method produces a distribution of silica clusters generated from a cluster-cluster aggregation approach, which upon simulating gelation, gives rise to a porous fractal structure.

To consider the effect of coordination number on the surface area, spherical SiO_2 particles were placed into a cell of various dimensions and shape. The size of the particles was varied over diameters 20 Å, 30 Å, 40 Å and 50 Å, and using coordination number N_c of 0 to 12. The size of the adsorbate was 4 or 6 Å, corresponding to N_2. The surface area of each model was then computed.

Figure 25 shows the results of the calculations for the adsorbate sizes 4 and 6Å. In addition, the theoretical curve from Kamaukhov and Kiselev (1960)

$$S_s/S_{s\text{-}geom} = 1\text{-}N_c\,(r/R)/2 \qquad (22)$$

where r is the adsorbate radius, and R, the sphere radius, is given for comparison. The porosity was related to Nc using the relation from Ouchlyama and Tanaka (1980). The S_{geom} is the surface area measured with no contacts and is greater than the ideal values for a perfect sphere. Using these S_{geom} values and the TEM size distribution from Avery and Ramsay (1973), we also computed the expected surface area of their sample and obtained exactly the same value that they measured using N_2 adsorption, 630 m^2/g.

The second method of generating aerogel models started with a cell of 5184 atoms of SiO_2 glass. This model was generated in the usual way from crystalline SiO_2 that was quenched to 300K after considerable MD at 5000K, maintaining an amorphous state. The model cell and atomic coordinates were subsequently expanded by 10% or 20%. At this point, molecular dynamics was

Figure 25 Surface Area of Microsphere Models

Lines are from equation 22, ■ 2nm dia., ▼ 3nm dia., ● 4nm dia., X 5nm dia. spheres

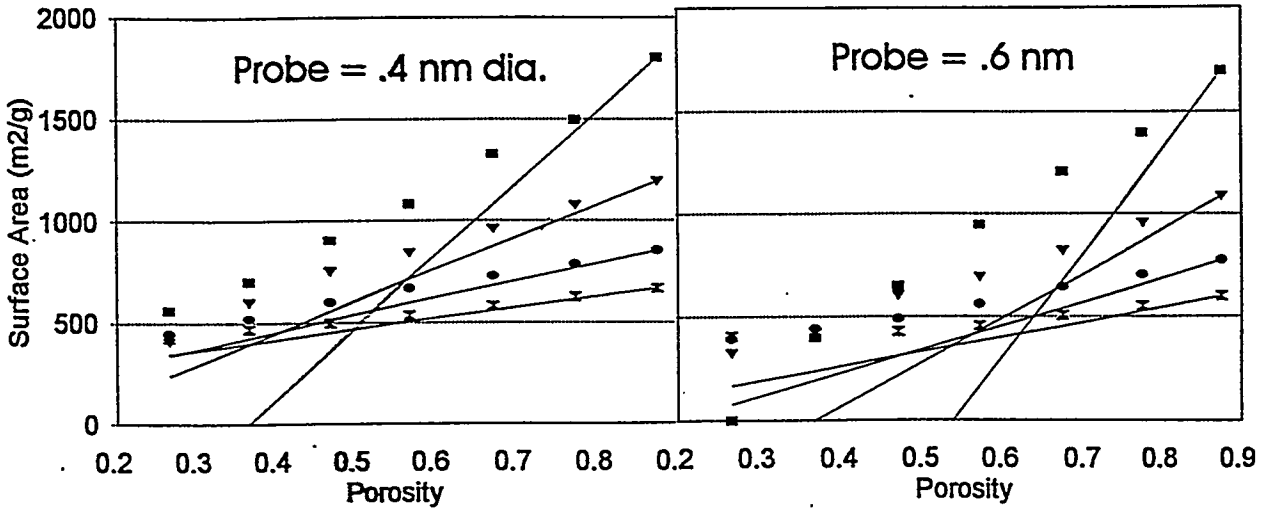

carried out on the system for 10 ps using the potentials of Fueston and Garofalini (1990). Models were saved at various densities to compute the pore properties and compare with the other methods.

The simplest measurement carried out on the expanded glass models was the pore size distribution. Figure 26 shows the pore size distribution for the expanded glass method aerogel models. The models expanded at a rate of 20% have a more narrow pore size distribution. Expanding at a 10% rate, the surface areas are 1300 m^2/g for the 1 g/cc density model, 1500 m^2/g for the 0.5 g/cc density model, and 2000 m^2/g for the 0.1 g/cc model. For the 20% rate expanded models the corresponding surface areas are 1800, 2100, and 2300 m^2/g. The values for the 10% expanded models are all in the range of experimental results reported by Davis et al. (1992) on a two-step acid-base catalyzed silica gel when placed in alcohol.

The construction of silica clusters mimicking the sol aging process was described previously for microporous silica. Briefly, the species composition was obtained from experimental ^{29}Si NMR measurements; that is, the Q distribution was determined and then used in the construction of small aggregates. In addition, the medium range order is inferred from SAXS determination of the fractal dimension and the Guinier radius. The first step in this procedure is to construct a minimum size monomer that nearly meets the degree of condensation in the final cluster. Next, clusters are pieced together randomly and further condensation carried out until the largest structure meets the experimental information. The final step is the aggregation of a distribution of the species which meets the theoretical size distribution, $\# = N^{-2}$, where N is the number of monomers in the polymer and # is the number of polymers in the system. The exponent 2 is from Martin (1986) and would equal 2.5 for a percolation model or 2.2 for the Flory model of gelation. The connectivity of each model was determined for comparison to NMR Q data and also to compare surface areas found using both techniques.

Figure 26 Expanded Mesoporous Glass Model Pore Sizes

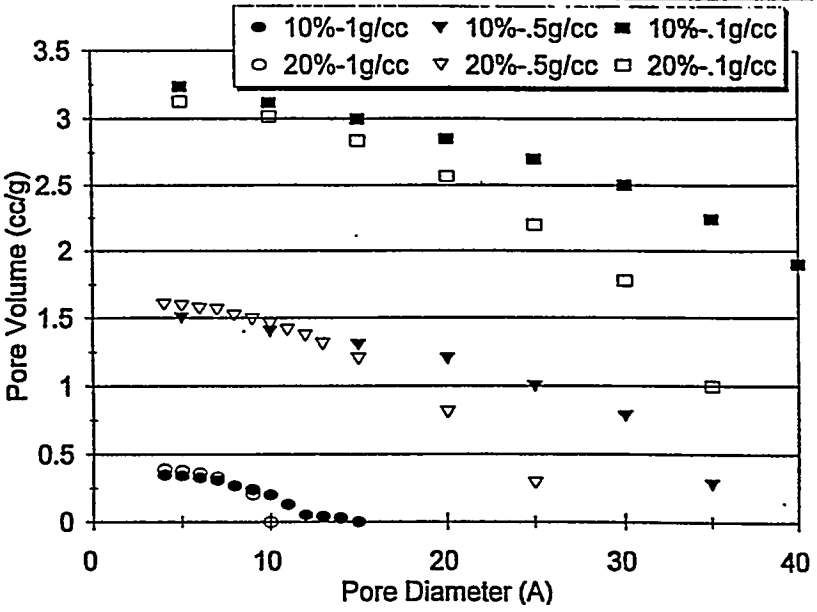

The final method of model building begins with determination of the fractal dimension of the model cluster. A plot of log (molecular weight) versus log (radius) gives a straight line with least squares slope of 2.2 ($r^2 = 0.993$). Hence, the model is characteristic of reaction-limited cluster aggregation which typically has a fractal dimension of 2.1±.2 (Brinker and Scherer, 1991). The Q distribution is from data of Brinker et al. (1994) for a two-step acid catalyzed reaction giving rise to growing silica clusters. Using the hydroxyl content of the model and the empirical surface coverage of 5 OH/nm^2, the predicted surface area is 1750 m^2/g versus 1800 m^2/g using the finite element method (Faulon et al. 1994). This agreement builds confidence for using either approach.

The surface area of the packed sphere models correlated well with the theory. Based on the above results, we feel that modeling the structure of silica aerogels can be best accomplished currently using model spheres as in the first method of this report. This is the method that MacElroy and Raghavan (1992) used in their simulations. For polymeric derived gels, the spheres used should be smaller, while for particulate gels, obviously, the model spheres can be larger.

The idea of expanding glass models to create gel models gives results that are pleasing in appearance but difficult to justify scientifically. That is, it is uncertain that even if the experimentally measured properties of the model such as pore volume, surface area, density and species distribution (from NMR) are equivalent to the model parameters, the model may still not be an accurate representation of the real material. In addition, to obtain the total pore structure over the entire range of length scales, a model of ~1 billion atoms would likely be necessary for removing statistical fluctuations in the pore properties. This is currently ~100 times the largest MD size carried out on a massively parallel supercomputer using Lennard-Jones atoms.

Finally, the use of cluster-cluster aggregation is the most highly representative means of generating silica clusters meeting the experimental composition and characteristic size. As mentioned previously, however, for the structure with 8192 Si atoms generated with the mass fractal dimension 2.2, the number of 16 Si clusters required to meet the cluster size distribution given theoretically is ~ 300,000. In this line of simulation the model size would also be huge and, currently, impossible to study.

We have demonstrated some progress in studying the mesoporous structure of silica aerogels using molecular modeling. As mentioned in the last two paragraphs, model size is the limiting factor in this work. As available computers get more powerful, this study can be continued. Based on the previous work, we chose to use the expanded glass model for simulating microporous silica membranes. In addition to these, silicate and cation free zeolite A membrane models were used to test theories of gas transport across inorganic molecular sieve membranes.

To predict the sieving pore size of the models, we used a code developed by Kale and Brinker (1995), originally designed for percolation studies of borosilicate glass. Similar to the pore program of Faulon et al. (1994), this algorithm discretizes the model into a cubic grid system and then determines the maximum sphere that can pass from one side to the other in addition to computing the total pore volume. The values found for silicalite, zeolite A and 1.5g/cc glass were 5.4, 4.0 and 3.4 Å diameter, respectively. As shown below, this causes very interesting retardation of simulated gas permeation.

CHAPTER 5 - RESULTS: GASES IN POROUS MODELS

The aim in computer simulation of gases in engineered porous solids is that varying the solid model structure should give different transport properties, thus allowing this important structure/property relationship to be resolved. This idea is based on the success to date of simulating gases in zeolites. In this chapter, gas interactions with molecular models are described along with the simulation of gas adsorption. In addition, diffusivities from canonical ensemble MD and permeation from Grand Canonical MD are determined for different models and process conditions. The results are summarized and characterized with regard to the theories discussed above.

Gas Interactions With Porous Solids

When pore size is similar to that of the diffusing molecule, the overlapping pairwise intermolecular potentials add up, giving a kinetically energetic species capable of *activated diffusion* (described theoretically above). As the porous solid walls continue to close in, the potential energy changes drastically, creating the phenomena and, at some point, giving rise to energy barriers shown in Figure 7 and resulting in the activation energies of Figure 10. Creating membranes with ability to control this property would improve their performance because, currently, reducing the pore size to create molecular sieving capabilities has come at the expense of the permeability, which can decrease dramatically as porosity decreases (moving from right to left in Figure 6, above).

The success of molecular sieve membranes is going to require a complete understanding of the energetics that the diffusing gas encounters. One bit of information that underlies this diffusion is the intermolecular energy between the two. In this first, simple experiment, model gases are moved along a path through a pore and their energy determined at various points in order to identify the energetic nature of diffusion. As shown in the equations on diffusion above, this energy barrier is vital to the application of molecular sieve materials in separations.

Figure 27 Energy Profile for Gas Diffusion (Kcal/mol)

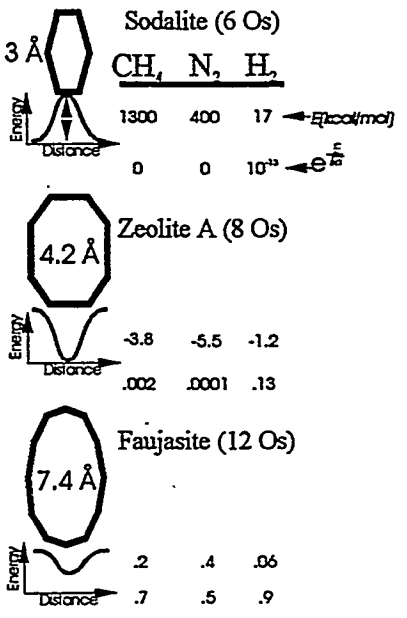

For the 6-Si ring of sodalite, 8-Si ring of zeolite A, and 12-Si ring of faujasite, the energy profile for CH_4, N_2 and H_2 are given in Figure 27 (Pohl and Smith, 1995). As can be seen, there is a barrier to diffusion for each gas through the 6-Si ring of sodalite, the barrier being greatest for methane. For the passage through zeolite A and faujasite, there is an energy well, strongest for nitrogen, which would account for the kind of "floating" described above in the section on activated diffusion. For zeolite A, based on the exponential, one would expect 0.13/0.002 = 65 ideal H_2 diffusive selectivity over CH_4, excluding adsorption. For the 8-Si ring, the results for O_2/N_2 are quite interesting, showing that the more prolate N_2 should

have a greater difficulty, in terms of energy barrier, passing through this window perpendicularly. For a 7-Si ring the activation energy for N_2 passing through parallel to the axis is 20 kcal/mol and 150 kcal/mol if perpendicular to the axis. For O_2, the corresponding energies are 3 and 50 kcal/mol.

For imogolite, on the other hand, the pore is larger and the pore imposes an enhanced energetic state for the diffusing molecule in all cases as faujasite and zeolite A did above. The reason for the differing diffusion rates as shown by dual gas canonical molecular dynamics, described below, is probably multicomponent effects or surface diffusion of the larger SF_6 molecules.

In addition to pore structure, adsorption isotherms in imogolite were simulated by GCMC for CH_4 adsorption at 273K and up to 1.2 atm (Pohl et al., 1994c). CH_4 was structureless and its interactions with an individual oxygen atom within the imogolite framework was modeled with the Lennard-Jones potential. The interaction parameters for the bridging oxygens and the surface hydroxyls were from MacElroy and Raghavan (1991, 1992). The chemical potential related to each pressure (and corresponding number of adsorbed methanes) was calculated over $1x10^5$ Monte Carlo steps. This method sampled only the inner tubular space, giving less pore volume, but corresponding to the cylindrical microporosity. GCMC CH_4 adsorption simulation results are shown in Figure 28 for the four different size models. One can see that the smaller the diameter of the tube, the greater the adsorption. Ackerman et al. had, in fact, suggested the reason that 1.6 times more gas adsorbed into the pure Si imogolite vs. the 50% Ge imogolite, was due to the smaller tube diameter. From Figure 28, the 1.6 factor is approximately the case for model 16 vs model 12 or model 14 versus model 10. Since the 10-unit model is certainly not the synthetic material from the data in Table 3, we could conclude that the 100% Si material has 12 units and the 50% Si sample has 16 units. The inexact fit with the experimental data is likely a result of the interaction parameters used.

The Henry's law constant was computed for the gases in silicalite and silica. These are 4.5 molecule/atm/unit cell for CH_4 in silicalite and 53.4 molecules/atm./unit cell for CH_4 in the silica model. Comparative values are 4.3 molecule/atm/unit cell for CH_4 in silicalite (Goodbody et al., 1991) and 23.6 molecules/atm/unit cell for CH_4 in the silica membranes (de Lange 1995b). This fit is sufficiently close to continue studies with the silica model. Figure 29 shows GCMC

Figure 28 Adsorption Isotherms for Imogolite from Simulation and Experiment

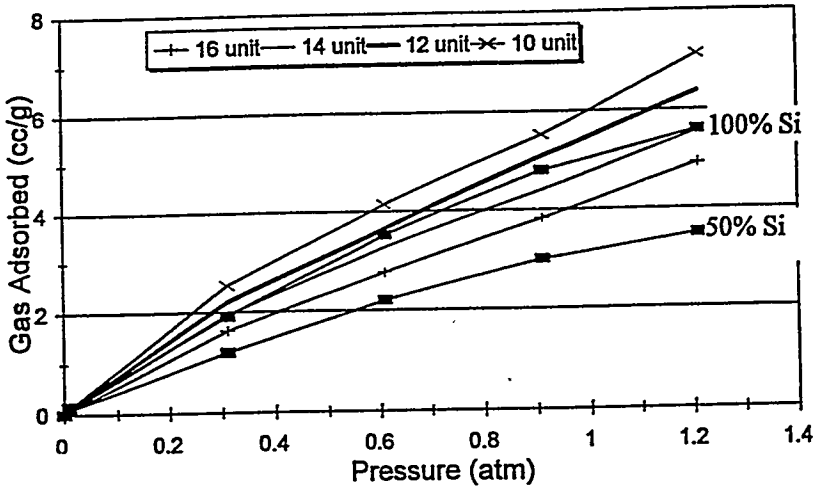

Figure 29 GCMC Adsorption Isotherms in Silicalite and Silica

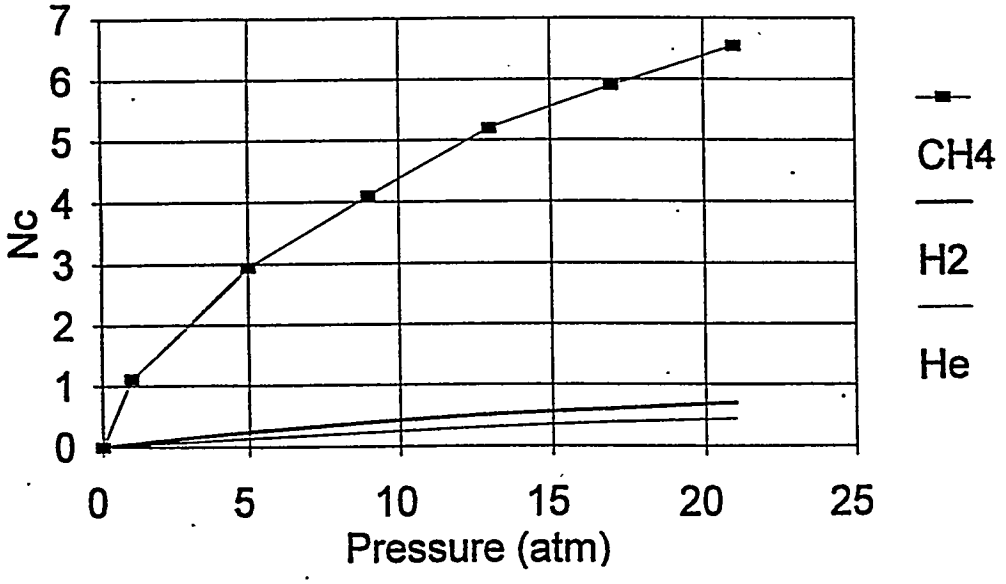

adsorption of CH_4, H_2, and He in silicalite. Figure 30 shows the interaction energies which, along with the corresponding geometry of the pores, cause differences in the adsorption properties.

Self Diffusivity from Molecular Dynamics

From a canonical ensemble (NVT) MD trajectory, the self diffusivity is determined from a

Figure 30 Interaction Potentials for He, H_2 and CH_4 with Hydroxyl groups

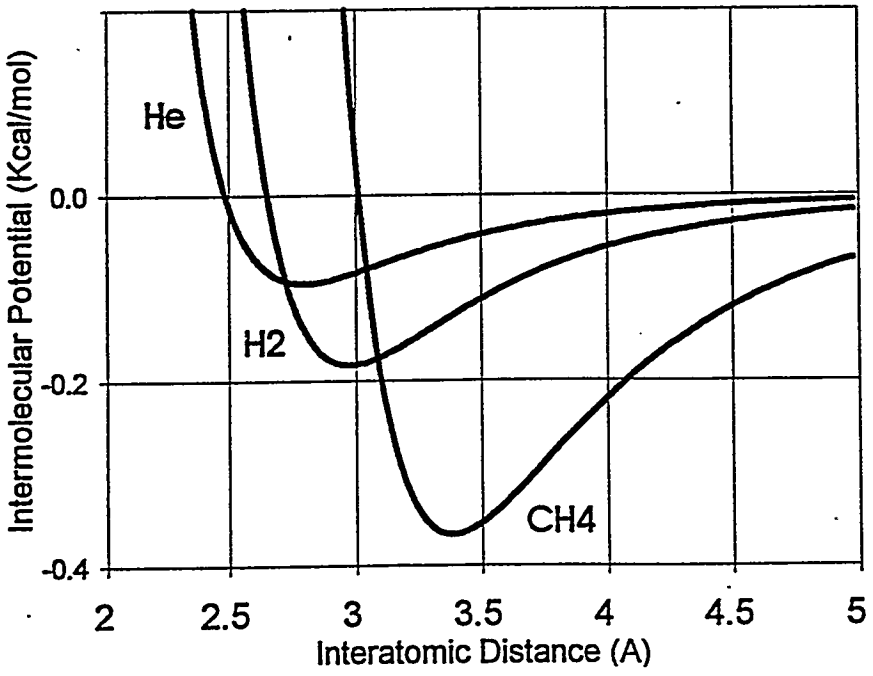

plot of the mean square displacement versus simulation time. The slope of this curve is related to the diffusivity by the Einstein equation (Allen and Tildesley, 1987),

$$D = \frac{MSD}{6t}. \tag{23}$$

This is related to the transport diffusivity via the "Darken" equation,

$$D = D_o \frac{d\ln p}{d\ln c} \tag{24}$$

where D_o is the self diffusion now and $d\ln p/d\ln c$ is the thermodynamic correction from ideality for adsorption in the pores and can be taken from the adsorption isotherm.

Diffusion in imogolite was studied using NVT MD. Recently, Seghal et al. (1994) reported the permeation of He and SF_6 using composite silica-imogolite membranes made with the 100% Si imogolite. The ideal separation (ratio of individual gas permeabilities) of these two gases ranged from 15 at 298K and with a transmembrane pressure drop of 20 psi to 33 at 298 K and 80 psi differential. To simulate this experiment, Lennard-Jones spheres were placed in the tubular region of each model using a cell 33Å long with periodic boundary conditions and encompassing the cylindrical imogolite walls. The Lennard-Jones interaction parameters for imogolite oxygens were the same as above for GCMC, and those for He and SF_6 were (ε=10e/k, σ=2.6Å) and (ε=200e/k, σ=5.51Å), respectively, from Hirshfelder et al. (1954). For the simulations, only the oxygens in the imogolite structure were used and were fixed. Ten atoms each of He and SF_6 were then allowed to diffuse for ~50ps using time steps of 1 fs. The trajectories were recorded every 10 steps and later used to predict the self-diffusivity based on equation (22), the slope of the mean square displacement vs. time plots. The ratio of these self-diffusivity values are reported below.

The diffusivity ratios for He/SF_6 were: 7 for the 16-unit model, 20 for the 14-unit model, 50 for the 12-unit model and 80 for the 10-unit model (Pohl et al., 1996). The ideal separation of this gas mixture based on Knudsen diffusion (which is based on different molecular velocities) is 6.6; therefore, the value of 7 for the largest pore material was somewhat of a surprise. Based on this result in addition to the measured pore properties above, one could assume that the 12-unit imogolite was that which Sehgal, et al. had embedded in their membranes. If they were able to isolate or synthesize the smaller tubed material, then higher separation factors could be possible.

Permeability by Grand Canonical Molecular Dynamics

Grand Canonical Molecular Dynamics (GCMD) enables calculations in an ensemble specifying chemical potential, temperature, and volume as independent variables, coupled with MD. Doing so allows spatial control of the chemical potential in a dynamical system, which is equivalent to specifying a density, composition, or pressure gradient. This approach is ideal for diffusion and adsorption process simulation, the two phenomena which make up permeation. To completely investigate membrane pore diffusion, we have simulated gas movement driven by a

pressure gradient in silicalite, zeolite A, and 1.5g/cc silica using a newly developed dual control volume grand canonical molecular dynamics method of Heffelfinger and van Swol (1994).

To test the assumptions used in arriving at equation 9 above, we recently employed a number of simulation techniques including molecular mechanics to predict E ($e^{-E/RT} = 0.13$ for He in zeolite A at 300K) (Figure 27), grand canonical Monte Carlo (GCMC) to simulate the concentration in model pores (Figure 28), and analysis of available pore space for different size molecules to evaluate porosity/tortuosity effects (Figure 26). The focus of the present section is an alternative to this three pronged approach. That is, simulate pressure driven gas permeation through a porous membrane model, which is more like the actual experiments carried out in testing molecular sieving zeolite (Yan et al., 1995) or silica (Sehgal et al., 1995) membranes.

Recently, the structures (only O atoms) of a cylindrical pore were placed between the dual control volumes (Heffelfinger et al., 1995). Using GCMD, the flux was determined by counting the gas molecules that pass a given point per unit time or by recording the number of insertions and deletions and finding the difference between the two concentration points. Figure 31 shows the axial density profile obtained with this model. This first simulation was primarily to test and demonstrate the concept.

The Dual Control Volume Grand Canonical Molecular Dynamics (DCV-GCMD) method employs molecular dynamics (MD) moves throughout the system, each MD move being followed by a series of GCMC-like insertions and deletions of fluid molecules in each of the two control volumes in order to maintain the chemical potential in the control volumes constant at a desired value. By measuring the flux and the drop in pressure, the permeability of each fluid component, i, can be determined from equation 1. DCV-GCMD was initially demonstrated for binary color diffusion by Heffelfinger and van Swol (1994). In the present work we have extended the method to model a fluid experiencing a pressure gradient across a porous wall, as

Figure 31 Simulated Density Gradients Using GCMD in a Cylindrical Pore

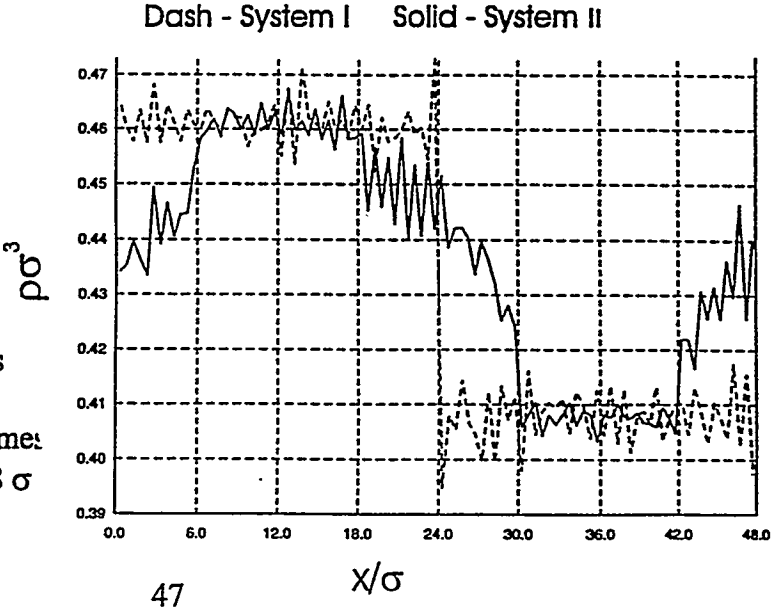

In System I, each half of the simulation system was used as a control volume.
In System II, the control volumes were placed between 6 and 18 σ and between 30 and 43 σ.

well as running the code on a massively parallel computer. The pressure gradient is achieved for a pure component fluid simply by choosing chemical potentials in the two control volumes which produce two different fluid densities, which we relate to a bulk pressure using the van der Waals equation of state. Gradient driven gas diffusion simulations in pores is being tried by several others, as mentioned above.

The fluid-fluid and fluid-wall interactions were modeled with the cut and shifted Lennard-Jones potential, the cut-off distance taken to be 2.5σ for all interactions,

$$V(r) = V(r) - V(2.5\sigma) \cdots r < 2.5\sigma$$
$$V(r) = 0 \cdots\cdots\cdots\cdots\cdots r \geq 2.5\sigma \qquad (25)$$

The parameters were taken as those for silica hydroxyl oxygens (MacElroy and Raghavan, 1992) (σ_O=3.0 Å, ε_O/k=230K) since we are eventually interested in modeling silica membranes. The gas parameters were from kinetic theory (Hirshfelder et al., 1954) (σ_{He}=2.6 Å, ε_{He}/k=10K; σ_{H2}=2.9 Å, ε_{H2}/k=38K; σ_{CH4}=3.8 Å, ε_{CH4}/k=148K), and Lorentz-Bertholot combining rules used for the cross-terms. The Si atoms in the zeolite model were neglected as they are effectively shielded by the oxygens making up the tetrahedral framework. The densities in the system were initially set only to give ample flux for study but can be controlled to the desired bulk pressure, the temperatures were 300K and 450K and the MD time step 2.9 fs for He and H_2 and 6 fs for CH_4.

We calculated the flux via two different methods (Heffelfinger and Van Swol, 1994), the flux plane method and the control volume flux method (J^x and ζ^x), respectively:

$$J^x = \frac{j^{LTR} - j^{RTL}}{\Delta t A_{yz} N_{planes}} \qquad (26)$$

$$\xi^x = \frac{M(B) - M(A)}{4\Delta t A_{yz} N_{steps}} \qquad (27)$$

where j^{LTR} and j^{RTL} represent the net number of fluid molecules which move through each flux plane (two planes were used in this work, one at x = 10nm and another at the periodic boundary, x = 0 and 20nm) and N_{planes} is the number of flux planes (2 for this work). *M(B)* and *M(A)* are the net number of insertions (accepted insertions - accepted deletions) in control volumes A and B, respectively; Δt is the MD timestep; A_{yz} is the cross sectional area of the model, and N_{steps} is the number of MD timesteps. The permeabilities from equation (1) above are given in Barrers, where 1 Barrer = 10^{-10} cm^3(stp)-cm/cm^2-s-cmHg.

The algorithm employed in this work is a massively parallel version of the DCV-GCMD (Heffelfinger, 1996). Briefly, this parallel algorithm employs a superposition of two different

parallel algorithms: spatial GCMC and spatial MD. With this parallel DCV-GCMD algorithm, simultaneous insertions/deletions can be attempted in each control volume, thus, for this work, 64 insertions and/or deletions were attempted in each control volume after each MD step. Because the parallel spatial GCMC and spatial MD algorithms scale with system size and are most efficient for large systems (tens of thousands of atoms), the primary application of the parallel DCV-GCMD algorithm is to simulate such systems.

Silicalite Membranes

In this section we simulate the permeation of Lennard-Jones gases across a silicalite model membrane. Using the GCMD technique, we create a steady-state pressure gradient across the membrane. The results from the simulation compare very favorably with recent experimental results of He, H_2, and CH_4 permeation through ZSM-5 polycrystalline membranes. This work is used to validate the procedure of simulating gases across microporous membranes. The next two sub-sections are different in that no zeolite A membranes have yet been made, and the structure of silica membranes is not known exactly.

The membrane atoms, which did not move, were positioned at the coordinates of silicalite oxygen atoms, the purely siliceous analogue of ZSM-5. The pore structure of silicalite is well known and consists of straight and zig-zag channels, approximately 5-6Å in diameter. In the present work, the He, H_2, and CH_4 (modeled as Lennard-Jones particles at 300K and 450K) permeabilities are determined for a thin (4nm) silicalite membrane arranged so that the straight pores are aligned in the direction of flow. These values are then compared to those of Yan et al. (1995).

The system was 20nm long, thus the x coordinate stretched from 0.0 to 20nm. Periodic boundary conditions were employed along all planes and at x = 0.0 and x = 20 nm. Each control volume encompassed the entire pore cross section (Figure 32). While we have positioned the control volumes for both systems outside the pore, they could just as easily have been positioned inside the pore, enabling one to exclude entrance effects and focus on pore diffusion (Heffelfinger et al., 1995). After starting with no gas molecules in each control volume, the

Figure 32 Schematic of Silicalite DCV-GCMD Membrane Simulation System

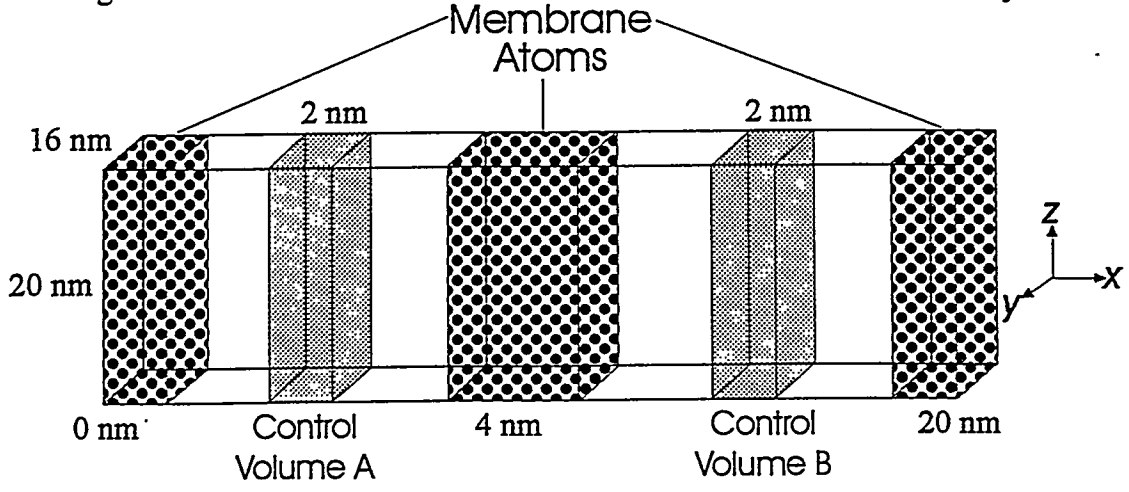

system was equilibrated for greater than 50,000 steps until a constant number of gas atoms was achieved. A configuration was saved and used as the starting point for the simulation where averages were accumulated for up to 100,000 steps.

While the systems studied by Heffelfinger et al. (1995) were relatively small (Figure 31), here, a model of approximately 9,000 CH_4 atoms and 90,000 static oxygen atoms constituted one run (CH_4 being the strongest adsorbing gas of the three and, hence, most plentiful in the system). For this simulation, carried out on 800 processors of Sandia's Intel Paragon, each MD timestep and its associated 64 attempted insertions/deletions in each control volume took 0.8 cpu seconds. Since the system is large and the flux relatively high, a good approximation of the steady state flux is obtained in 10,000 to 20,000 time steps. Carrying the simulation further (42,000 steps) gave a very precise determination of the flux and, hence, the permeability.

The axial density was determined by averaging over time the number of fluid molecules in a bin 2Å wide and across the entire y-z plane. The axial density profile ($\rho(x)$) is shown in Figure 33. From this figure we can see that the density in control volumes A and B are $\rho\sigma^3$ = 0.01 and 0.001, which correspond to bulk pressures of 20 and 1.5 atm, respectively. The axial density profile in Figure 33 shows several extraordinary features never before simulated, namely the relative gas densities across the membrane and the difference in gas adsorption on the outside of the membrane models. Methane fills the pores as it is the gas which is nearest to its critical point. Pellenq and Nicholson (1995) show similar profiles from GCMC of Ar at high loading with no gradient. The fluxes, calculated via both methods, and the permeabilities, calculated via equation 2 and the known pressure drop, are shown in Table 4. The experimental values are assuming a 10μm thick membrane as Yan et al. (1995) approximated their membranes to be.

Figure 33 Axial Density Profiles in Silicalite Membrane

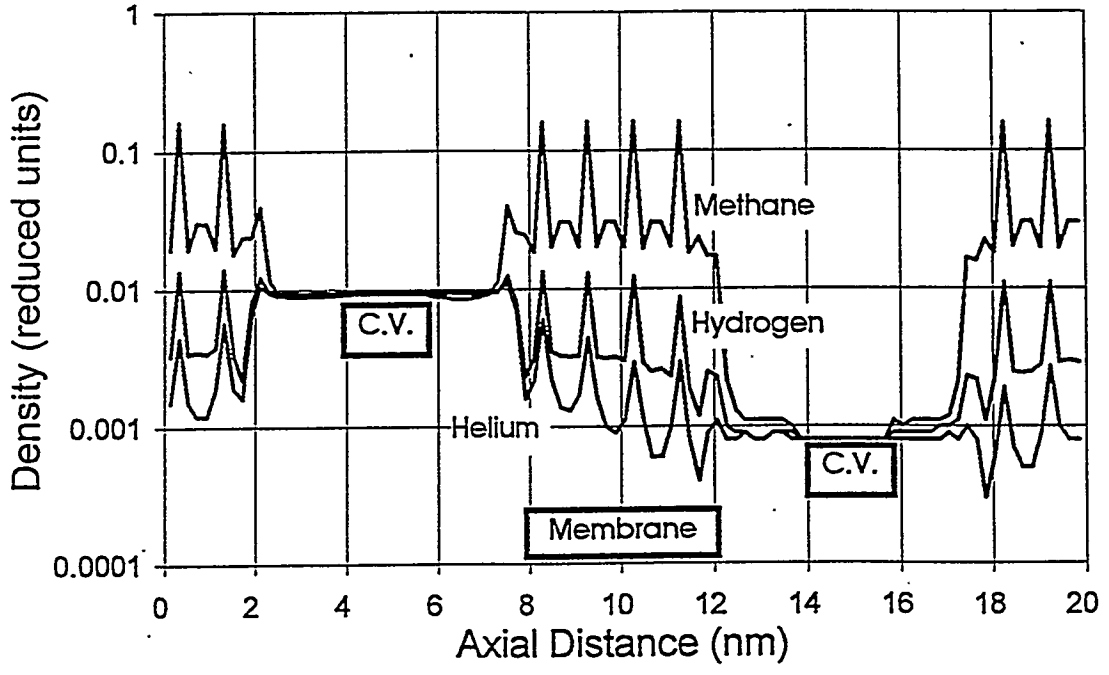

From Table 4 we see that the fluxes calculated via the two methods agree well with each other and yield values for the permeabilities which are approximately 40 times greater than the experimental values of Yan et al. (1995), if we assume their membranes to be 10 μm thick. In the experimental system, the membrane crystals are oriented randomly, the active surface area is less than the entire membrane surface and some of the pores are likely to be plugged. All of these tend to reduce the flux, making the absolute value of our predicted values quite good. With regard to the relative fluxes, one must consider the various mechanisms which describe the pore diffusion to appreciate the results. First, if the controlling mechanism is molecular sieving, then He would permeate faster than H_2, which neither simulation or experiment demonstrate. Further, if Knudsen diffusion was dominant, then He should permeate faster than CH_4, which is also not seen. This simulation has thus captured a great deal of reality in terms of light gases diffusing across zeolite membranes. Insofar as the temperature dependence is concerned, we show a decrease in permeability with increasing temperature. This is opposite to what Yan et al. (1995) found, but agrees qualitatively with Vroon (1995) and Jia et al. (1993).

Table 4. Fluxes and Permeabilities (Barrers) for Silicalite

	J^*(Plane)	ξ^* (C.V.)	permeability	Ref. 3	(sim./exp.)
He(450)	3.5e-4	3.5e-4	32,500	1,480	22
He(300)	5.1e-4	5.0e-4	42,000	890	47
H_2(450)	6.0e-4	6.0e-4	53,000	3,000	18
H_2(300)	9.6e-4	9.7e-4	79,000	1,800	44
CH_4(450)	3.1e-4	3.1e-4	27,700	2,200	13
CH_4(300)	4.9e-4	4.7e-4	47,000	1,100	43
CH_4(300)LP	5.0e-5	3.0e-5	28,000	2,200	25

Zeolite A Membranes

The wall atoms for simulations described in this section, which also did not move, were positioned according to the coordinates of zeolite ZK4, the siliceous analogue of Linde Type A zeolite; thus, the two are used interchangeably throughout this discussion. The cubic pore structure of zeolite A is well known and consists of cavities separated by windows approximately 4Å in diameter. In the present work, the He, H_2, and CH_4 permeance is determined for zeolite ZK4 membranes. In addition, mixed gas He/H_2 permeation is simulated. Yurcel and Ruthven (1980) found diffusivities of 2.5×10^{-11} cm^2/s for CH_4 in zeolite 4A at 273K. In addition, Henry's constants at 273K and 323K, respectively, were 4.61 and 1.33 molecule/cavity/mTorr.

While the systems studied by Heffelfinger et al. (1995) were relatively small, these simulations were quite the opposite. Approximately 2,000 H_2 atoms and 82,000 static wall atoms constituted one run. For this simulation, carried out on 1728 processors of an Intel Paragon, each MD timestep and its associated 64 attempted insertions/deletions in each control volume took 0.37 cpu second. The He/H_2 simulations described herein took ~10 CPU hours.

Figure 34 Schematic of ZK4 DCV-GCMD Pore System

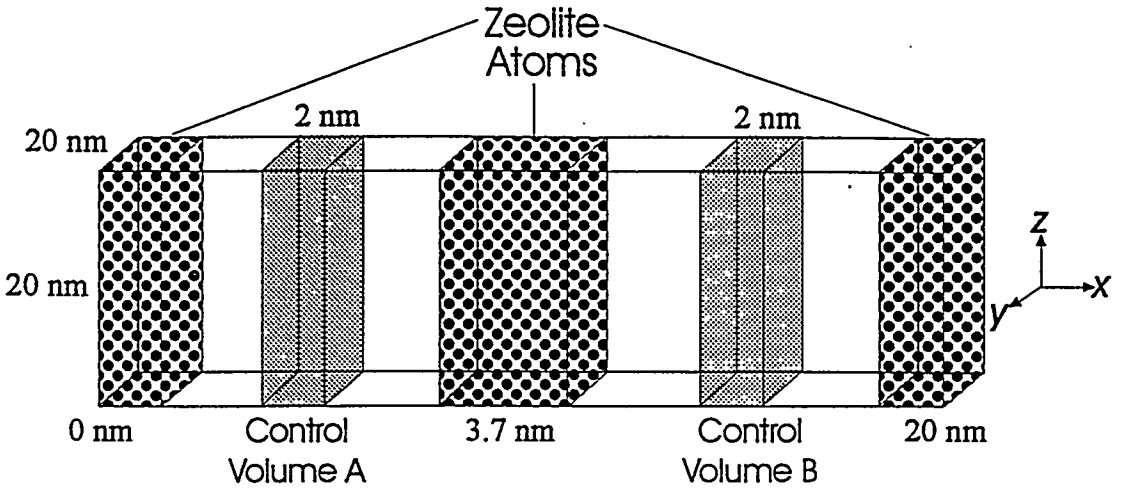

Figure 34 shows the setup of the zeolite A/ZK4 simulation system. Gas-solid interactions are as described above. Based on the size of the system in the y-z plane, the number of entry ports into the membrane wall was 264. Comparatively, for silicalite above, there were 160, and for silica, described next, there were only 4 for large molecules such as CH_4, but many more for small molecules such as He which can find these passageways.

Table 5 gives the simulated permeabilities for the systems studied. Figures 35-37 give various density profiles across the system. From Figure 35, the He mixed gas has higher concentrations than for a single gas simulation. The results show that the H_2 gas is the more strongly adsorbing one as indicated by Figure 36. In Figure 37 the temperature dependence of H_2 adsorption is clearly indicated by the reduced density of gas in the system.

Table 5 Fluxes and Permeabilities for ZK4 from GCMD

Gas (temp/K)	*Flux* (J^*)	*Flux* (ζ^*)	*permeability* (Barrers)
He (300)	0.00018	0.00022	15,500
He (450)	0.00011	0.00013	10,300
H_2 (300)	0.00028	0.00027	21,000
H_2 (450)	0.00018	0.00018	14,900
He (mixed-300)	0.00020	0.00024	17,000
H_2 (mixed-300)	0.00031	0.00033	24,400
CH_4 (300)	0.00001	0.00001	900

Figure 35 Single Gas Profiles: He across ZK4, single gas (dashed), mixed gas (solid)

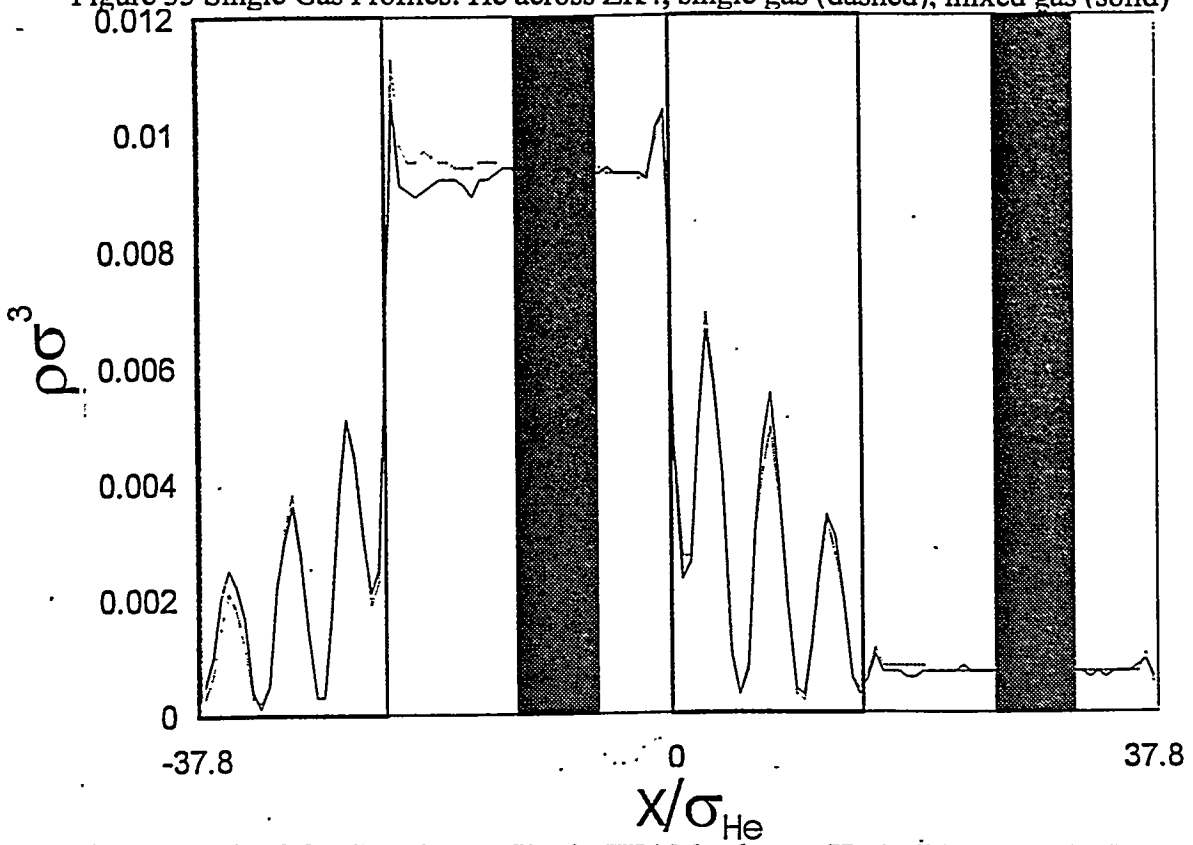

Figure 36 Mixed Gas Density Profiles in ZK4 Membrane, He (solid), H_2 (dashed)

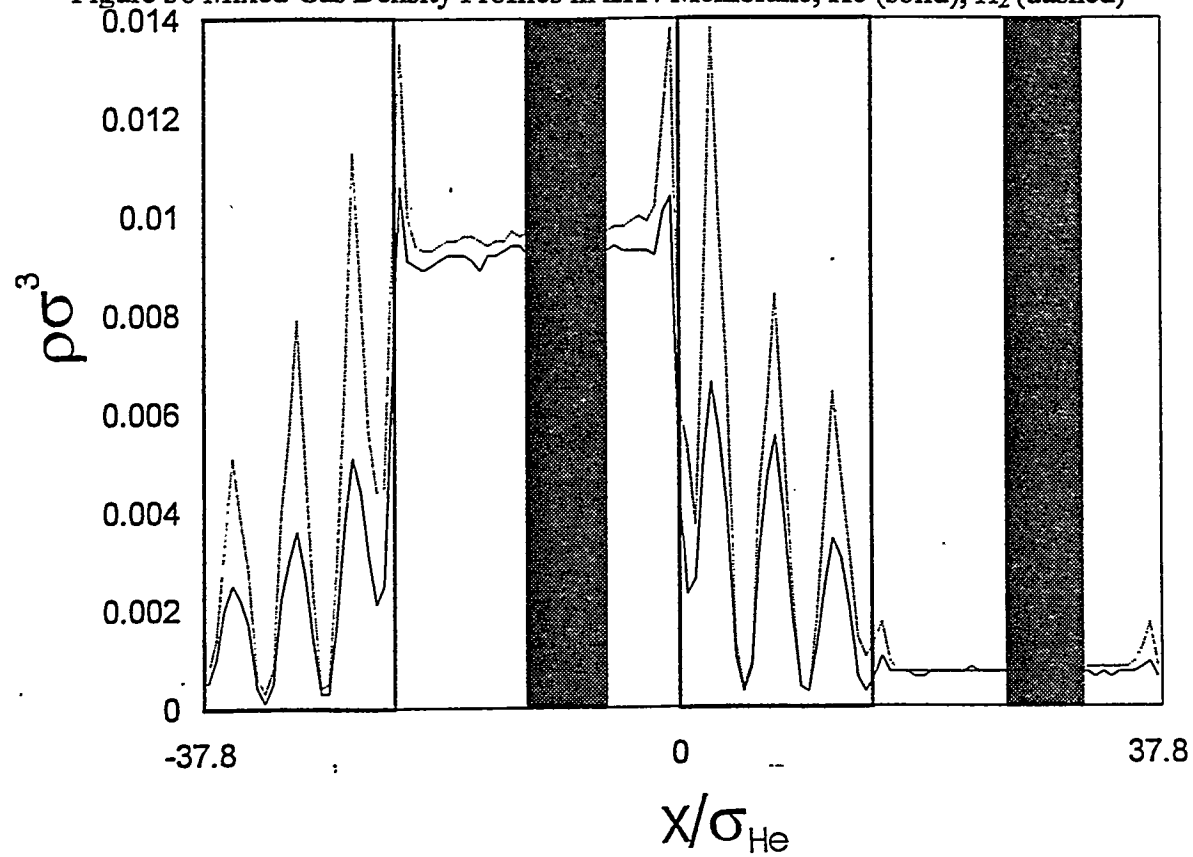

Figure 37 Gas Profiles in ZK4 Membrane H_2 (300K) solid, H_2 (450K) dashed

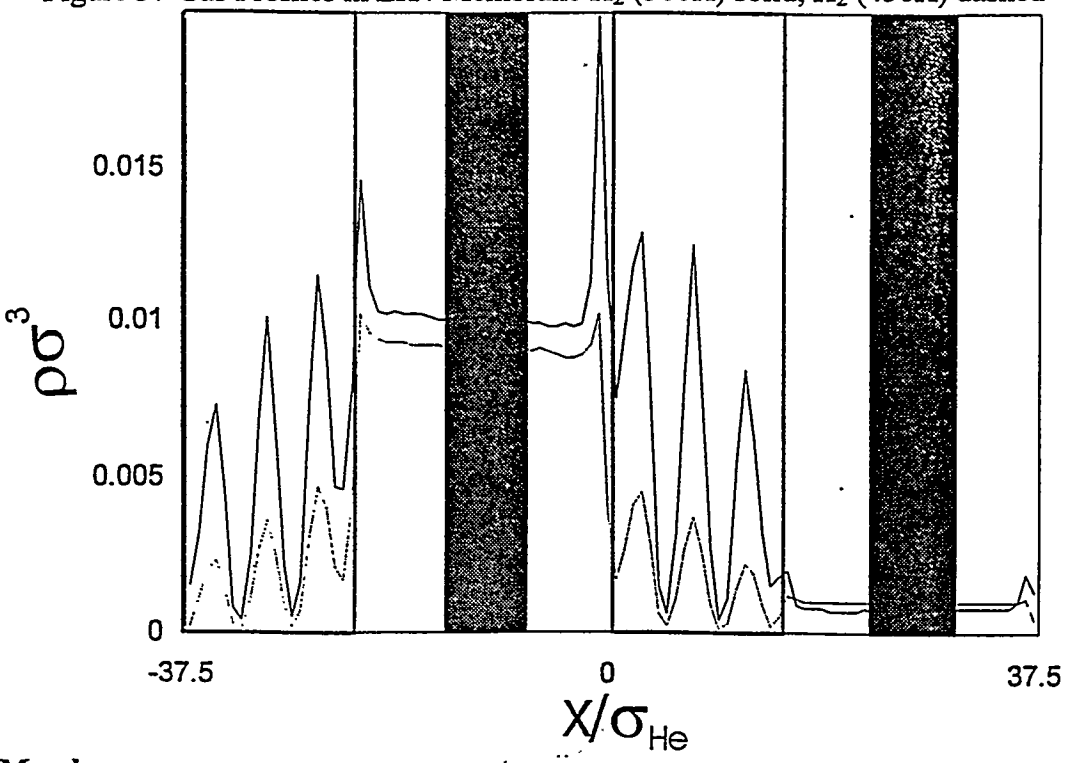

Silica Membranes

In this section, a model from earlier studies on porous silica was used to test the permeation of gases through a disordered material. The pore size of current generation sol-gel derived silica membranes consists of a distribution, and all indications suggest that it may be similar to that of our model. That is, Brinker and Seghal (4) have been able to demonstrate molecular sieving by preparing membranes that exclude CH_4 at detectable levels, but allow He to permeate at a rate of 2.25×10^{-5} cm^3/cm^2-s-cmHg at 313K. The bulk density of the model used here was 1.5g/cc and the pore size distribution (using Kale and Brinker's (1995) method)is shown in Figure 38. A breakthrough pore size analysis was carried out and the maximum sized sphere able to pass through the model is approximately 3.4Å diameter. Based on this value, no CH_4 is expected to pass through, while He and H_2 should pass easily. For this reason, Ar was tested (σ = 3.4 Å, ε=140K) and its permeability also tabulated. The simulations were carried out on 250 nodes of the Intel Paragon and the results, as found previously, are given in Table 6, while the density profiles along the direction of permeation are given for He, H_2, Ar and CH_4 in Figure 39. Also given in Table 6 is the ratio of simulation to experiment based on the results of Brinker and Sehgal (1995), assuming a membrane thickness of 1μm.

In contrast to the zeolite simulations, these permeation experiments were very slow. For example, He at 300K took ~110 CPU hours and the net insertions/deletions for computing the control volume flux were 130 in each. This gives a good first approximation but a longer simulation would give a more accurate permeability. The interaction potential cut-off value of 2.5 used in equation 25 increases the computation time considerably but allows adsorption to take place more realistically. Heffelfinger et al. (1995) used a much shorter (~1.2σ) cutoff which allowed a quicker analysis of the model system.

Figure 38 Silica Model Pore Size Distribution

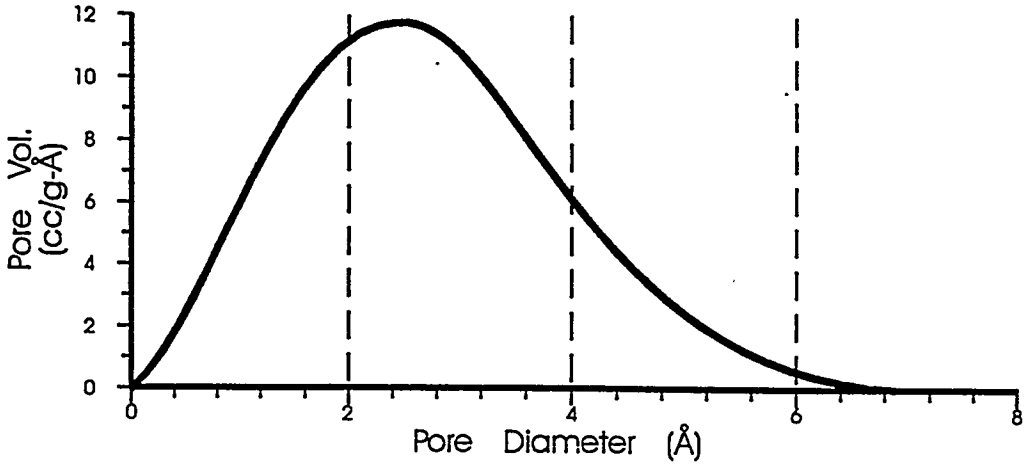

From Figure 39, one can see the huge adsorption of Ar and CH_4 on the surface of the silica model membrane. This adsorption gives rise to a large concentration in the pores but still does not give a flux due to the size of the constricting pores described in Figure 38 and the breakthrough analysis which calculated a 3.4 Å cutoff (CH_4 σ=3.8 Å). What this means is that the model is molecular sieving for CH_4, but not for the other smaller gas molecules such as Ar.

Table 6 Model Permeabilities (Barrers) in 1.5 g/cc Silica Model

	$J_i^x \sigma^3 \sqrt{\frac{m}{\varepsilon}}$	$\zeta_i^x \sigma^3 \sqrt{\frac{m}{\varepsilon}}$	*permeability*	*simulation/exp*
H_2 (300K)	3.3e-5	3.2e-5	3,000	340
H_2 (450K)	2.4e-5	1.9e-5	2,300	15
He(300K)	3.5e-5	3.8e-5	3,500	150
He(450K)	3.6e-5	3.7e-5	3,300	24
Ar (300K)	3.2e-6	1.4e-6	230	-
CH_4 (300K)	7.0e-7	0.0e-6	<10	-
CH_4 (450K)	0.0e-5	2.2e-6	<100	-
He (Mixed - 450K)	1.4e-5	1.3e-5	2,700	-
CH_4 (Mixed - 450K)	6.0e-6	7.0e-6	1000	-

The mixed gas results show a very interesting phenomena taking place. From Figures 40 and 41, one can see that the adsorption of CH_4 is only slightly less in the mixed gas simulations due to its lower vapor pressure. For He, on the other hand, there is virtually no surface

Figure 39 Axial Single Gas Density Profiles in Silica Model Membrane, H_2, He, Ar, CH_4

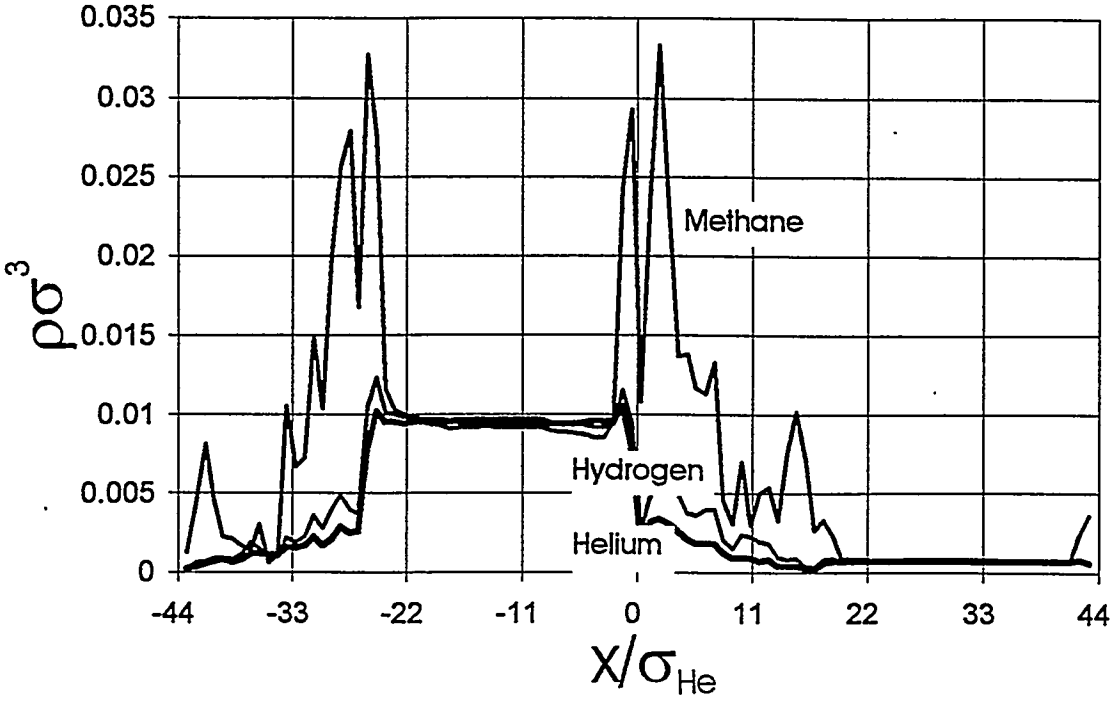

Figure 40 Pure He and Mixed (CH4) He Gas Density Profiles in Silica Model

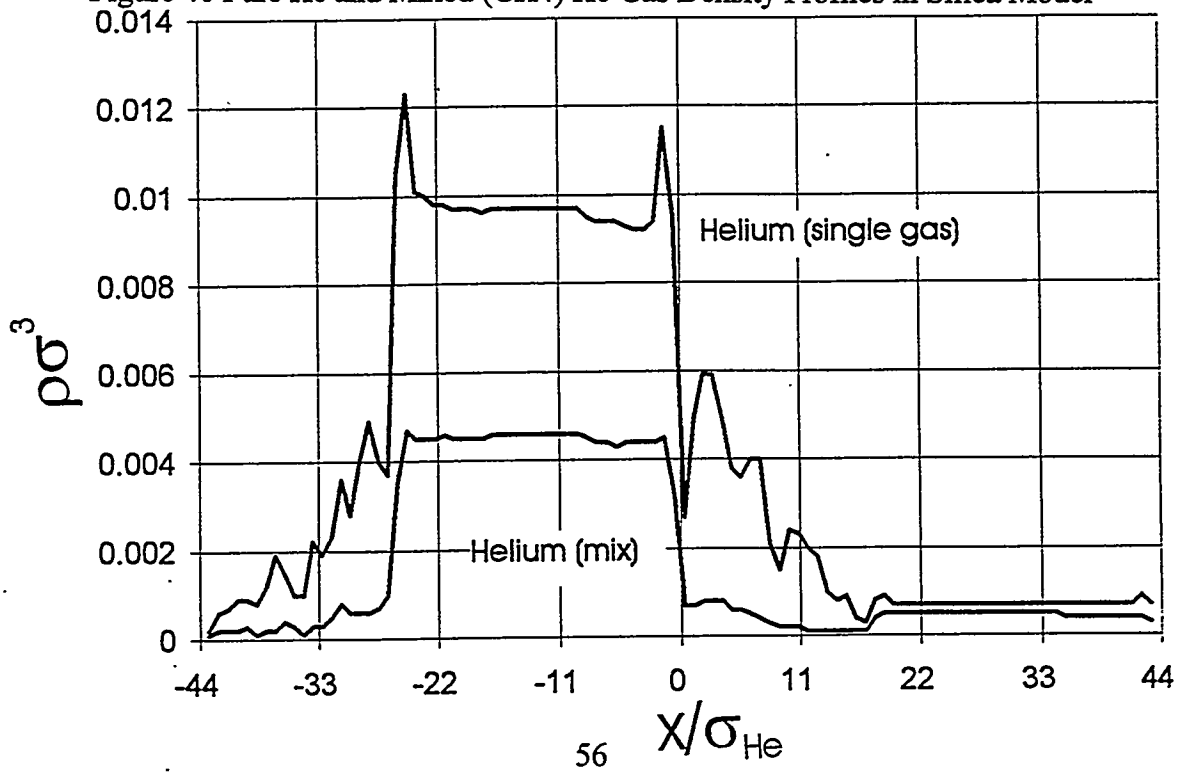

Figure 41 Pure CH_4 and Mixed CH_4 (with He) Gas Density Profiles in Silica Model

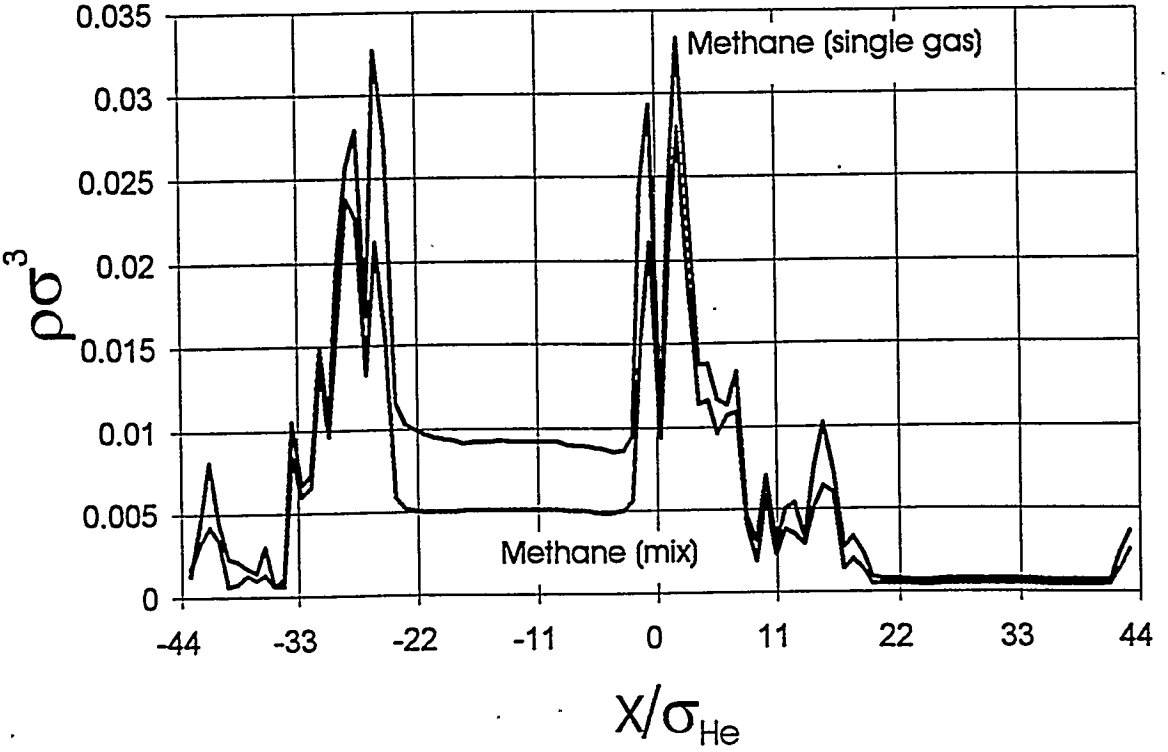

adsorption and the pore concentration is very much lower than in the pure gas case. Hence, in separations using porous silica membranes, the stronger adsorbing gas will have a much higher pore concentration and exclude the lesser adsorbing gas. This is also apparent by the reduced He permeability seen in Table 6.

Discussion

The purpose of this section is to focus the important features of the results given in the last two chapters and provide a solid basis for conclusions and recommended future work. The preceding computer "experiments" give ample data to compare with the theories presented in the second chapter.

The activation energies presented in Figure 27 allow tests of all the relevant temperature dependencies described in Chapter 2 and are a good screening method for selecting crystalline materials for gas separation. Using molecular dynamics simulation as presented in the previous section gave a brief simulation of the activated permeation of gases in membranes. For the silica membrane, CH_4 was the only gas that had an increasing permeation with temperature, while He and H2 decreased with temperature as predicted by Knudsen diffusion.

The theories of Shelekin, Barrer and Krishna all speak towards adsoption being important for gases only at low temperatures. This adsorption is seen for Ar and CH_4 and to a lesser extent for He and H_2 on all the model membrane gas density profiles. The fact is, adsoption is an important phenomena for all gases at all temperatures as demonstrated by the silicalite results.

The models of Krishna and Barrer allow tests of the non-ideality of the sorption process in a mixed gas system. The methane adsorption is greatest as seen in Figure 39. At this point in mixed gas simulations, the membrane looks much more dense to a smaller molecule, hence, it will experience a more tortuous pathway giving a smaller permeability. This is not born out in single gas permeation experiments as Krishna (1995) has shown. Hence, it is important to test membranes for gas separations with dual gas experiments.

The impact of the results above, and as predicted by most of the theories in Chapter 2, is to grasp that there are three important aspects to gas permeation through microporous membranes. These are the diffusivity or mobility of the gas in the structure, the concentration of gas in the pores, and the effects these have on mixed gas permeation.

CHAPTER 6 - CONCLUSIONS AND RECOMMENDATIONS

The initial part of the work was constructing porous material models. Properties of the pore structure were computed. The gas diffusion through these models was then determined. Since slight changes in reaction conditions of silica solutions give marked difference in the final membrane's separation ability, this was a good test of our ability to model the sol-gel process. Specifically, the items in Table 7, described in detail in this thesis, were accomplished. The fundamental success of this effort was in finding the permeance of gases in microporous models approximately equal to experimentally found membrane values.

Table 7 Gas Permeation (Barrers) in Silicate Model Membranes

Gas	He	H_2	CH4	He	H_2	CH_4
Temp(K)	300	300	300	450	450	450
			Silica			
Permeability	3,500	3,000	<10	3,300	2,300	100
			Zeolite A			
Permeability	15,500	21,000	<100	10,300	14,000	
			Silicalite			
Permeability	42,300	79,500	46,900	32,500	53,600	28,000

Microporous Silica Molecular Models

We have demonstrated the ability to model microporous dip-coated silica from sol-gel chemistry. The SIGNATURE program was used to generate precursor polymeric aggregates and also to collapse a distribution of these into a final silica structure. MD and energy minimization were then applied, simulating the shrinkage which occurs during deposition. The porosity is similar to the molecular sieving membranes of Sehgal et al. (1994). The pore size distribution may be similar, but the experimental values have not yet been determined with high confidence.

Microporous silica and zeolite membrane models were constructed. The purpose of this effort is to produce more accurate and reproducible microporous silica models than before. The silica method begins with a glass model and systematically expands and equilibrates the model, creating a porous structure. The variables in this process are the density, the rate of expansion, and the degree of dynamics carried out to relax the structure. The final model used had density of 1.5 g/cc. The sample used is only a portion of the whole system, so if the fractal nature of the gel is taken into account, it is difficult to relate such a small model to the entire material.

The properties of a porous solid that are measurable and which should be comparable with experimental data are the porosity, pore volume, surface area, pore size distribution, closed porosity, extent of condensation, and pair correlation function. These were measured for the models and compared with experimental values.

The purpose of this effort was to validate the construction methods used and lend credibility to the entire molecular modeling concept. In addition, the membrane physical properties used in the gas permeation theories above will now be available for testing of these theories.

Gas Dynamics in Porous Silica Models

The material's pore structure/diffusion property relationships should be well understood since essentially all the structural properties will be known. Simulating gas permeation in porous models was done in the grand canonical ensemble. The gases studied were He, H_2, Ar, and CH_4. These can be accurately modeled as Lennard-Jones gases and are used in membrane research because of their significant difference in size and weight.

The purpose of this effort was to provide researchers with a better understanding of gas diffusion through model pores and, hopefully, real membranes. It should complete the cycle of information needed to strongly validate/invalidate assumption in the models above.

Discussion

The structure of greatest interest in this work is porous silica. Imogolite and zeolites are novel materials but used only as a tool with known structure to calibrate the methods involving pore structure and membrane permeation. Porous silica can be microporous or mesoporous. For membranes, the passable molecular sieving constricting pores is one aspect that will govern their overall performance.

Modeling silica has been challenging since the structure is amorphous. It is apparent that five methods exist for building such models:

1. Building from scratch, atom by atom, fragment by fragment, the sol precursors and then combining them in some fashion.
2. Taking models of glass monoliths and removing portions creating the desired pore structure.
3. Packing spheres of small size giving microporous particulate solids.
4. Using a structure generator and predict sol precursor compounds based on analytic data and, again, combining them.
5. Taking models of monolithic glass and expanding the model and relaxing the structure.

The present work explored all of these. Using larger fragments such as cyclic tetramers, pentamers and dense clusters make method 4 somewhat like method 3. Minimizing the predicted structures during building forced the sample of clusters to be most favorable at least from a thermodynamic point of view. This may not always be preferable since kinetic phenomena have been shown to play an important role in sol formation. Modeling microporous membranes will require a better understanding of the chemistry of the sol precursors and the ensuing gel network formation as well

as collapse during drying. Results presented show that molecular models for imogolite and silica are reasonably precise, so success in permeation experiments was expected.

To study gas permeation through micropores, one should assume that diffusion through micropores is currently described best as an activated process. Empirical constants are used in most studies. On the other hand, molecular scale models include more material properties but have been slow to predict the actual permeation data that is being accumulated for both crystal or amorphous molecular sieving membranes. The successful permeation theory will probably be a combination of these two ideas in that it must include some empiricism, yet rely on sound model parameters in assessing the interaction energy. It must also somehow account for the size distribution of pore throats and mouths. Using GCMD has been a key simulation tool in testing these theories.

Recommendations

The molecular modeling of microporous solids and the direct computer simulation of gas permeation through these are described in this thesis. In this final section, an evaluation will be given of two main questions: what are the prospects for inorganic molecular sieving membranes in gas separations, and what do computer simulations have to offer material scientists.

First, molecular sieving inorganic membranes depend on defect free thin inorganic layers with molecular size pores. The size of the pores will control the selectivity while the number of pores will affect the net flux. Both of these are complex interrelated phenomena described best by the theories of Shelekhin et al. (1995) in a first approximation and by Krishna and van den Broecke (1995) in a more rigorous way. The results of simulations on zeolites were at least an order of magnitude higher than experimental values. For our silica model they were two orders of magnitude greater than experiment. A compromise structure between silica and zeolite membranes is needed. That is, a membrane is needed with more pores than silica membranes, but thinner than current zeolite membranes. The silica model used in the present simulations was much lower density than state of the art silica membranes because there are large pockets of the sol-gel material that is so dense it is not even permeable.

As far as computer simulations are concerned, from Figure 2 and the myriad of examples presented in the bulk of this thesis, one can be very optimistic about applying computer techniques to material science related issues. The primary issues here are which problems to attack and in which way. There are limitations, presently, in computer simulations which will make some results impossible to attain. There are other subjects which have yet to be explored in any way to date. Simulation of gas permeation through current generation silica membranes is presently too slow to study completely with classical molecular dynamics.

Based on the work results and discussion provided, prospects for further understanding of gas permeation in molecular sieving membranes are, however, very good. The intention of this last part of this dissertation is to clearly provide guidance for future research on the subject of discerning the pore permeation properties of molecular sieving membranes. Four recommendations are made below which would be reasonably simple extensions of the present

work. Two methods are proposed to test, with simulations, different hypotheses for the extraordinary temperature dependence of gas permeability that Seghal and Brinker (1995) have seen experimentally. Following these, two ideas are suggested to enhance the accuracy of the computed permeabilities that the present work generated.

RECOMMENDATION 1: The first hypothesis supposes that the movement of the membrane atoms increases with temperature and that the pores experience a breathing effect, allowing a temperature dependent tortuosity. To test this, simulate the temperature dependent movement of atoms in the porous structure. This can be done in a couple of ways. The simplest way in simulations would be to take 5, 6, or 7 membered rings of SiO_n and simulate, using MD, the structure for a long enough period to sample all of the configurational space. Following this, measure the distribution of distances between atoms and study this as a function of temperature. Alternatively, one could take a porous model of ~1000 SiO_2 atoms and simulate this at different temperatures for a sufficient period. With each movement of the porous structure, the breakthrough diameter, described above, could be computed. This would give a more meaningful parameter describing the temperature dependent permeation behavior, but is much more computationally demanding. In either approach, one should arrive at a histogram plot of the distribution of pore dimensions at each temperature studied. If the diameter gets significantly larger with temperature, then one could further hypothesize that this is causing the extraordinary temperature dependence that Seghal and Brinker (1995) have seen experimentally.

RECOMMENDATION 2: The second hypothesis assumes that adsorbed solvent molecules are blocking the pathway of the permeating gas molecules. This idea suggests that as the temperature is raised, these blockers are removed and the permeation rises. To investigate this, one could simulate the adsorption/desorption of solvents (H_20) in the porous region. Doing this at different temperatures would show if solvents adsorbed in the smallest pores could be removed over a very small temperature range giving rise to pores that permit larger molecules to pass (Ar, N_2, ...). To test this, a conical shaped model pore could be packed with solvent molecules. Then, MD simulation at several different increasing temperatures could be carried out to look at the equilibrium position of the adsorbed molecules as a function of temperature. Eventually, at some high temperature, the solvent molecules will all escape to the adjacent vacuum region. Precise determination of the approach to this empty pore situation would give tremendous insight into this hypothetical reason for the strong temperature dependent permeation seen experimentally.

RECOMMENDATION 3: To improve the accuracy of the present work, one could carry out mean field theory (MFT) investigations. While detailed accuracy in computer simulations is essential to permeation studies, the limited number of variables results in serious shortcomings. Analytic calculations, blended carefully with simulations, elude this shortcoming. We'll make simple models of various sieves, construct an MFT using initial simulations, use the MFT to take into account the variables simulations neglect, feed the results back into the simulations, and repeat. This iterative procedure, successful in ferromagnetic phase transition phenomena, will achieve for molecular sieving more than what simulations alone can. That is, by looking at a small model using more degrees of freedom, one can sample a conformational space that is more scientifically accurate.

RECOMMENDATION 4: Finally, quantum sieving studies would address the validity of the "classical" simulations used in the present work. Since the de Broglie wavelength can be comparable to the pore size even at room temperature, quantum effects can be nonnegligible. One could study this poorly understood but important aspect of sieving by studying quantum effects of molecular motion on wall potentials. That is, with a simple model pore (zeolite or disordered silica) and various gas molecules (N_2, CH_4, He) compute the total energy using Hartree-Fock or other suitable quantum mechanics computations. With the total energy computed, move the molecules through the pores and at several other geometric positions, determining a more exact energy profile as in Figures 7, 10, and 27. Next, comparing this energy profile against that profile from Lennard-Jones potentials used in the present simulations, better parameters may be suggested or an improved form of the energy equation developed.

NOMENCLATURE

		page(s) used
A	cross sectional area	1
A_{yz}	cross sectional area of the model	48
B	empirical Langmuir constant	4,10
C_k	Knudsen diffusion constant	1
Cl	gas concentration at the outlet side	8
Co	gas concentration at the inlet side	8
C_p	Poiseuille flow constant	1
C_s	surface diffusion constant	1
D	diffusivity	6,10,46
D_o	self-diffusivity	22,46
D_t	transport diffusivity	22,23
E	activation energy	6,8,9,11
Ei	interaction energy	20
F	force	16
J^x	flux determined from plane method	48,51,52,55
K	the equilibrium adsorption constant	8
K_H	Henry's law constant	26
L	Avogadro's number	4
N	molar flow rate	1
N_a	moles sorbed per gram of zeolite	26
N_c	coordination number of sphere models	39
N_{planes}	number of flux planes	48
N_{steps}	number of MD timesteps	48
P	gas permeability	1,10
P	probability	20
R	sphere radius	39
S	internal surface area	4,28,39
S_{geom}	surface area of a sphere	39
T	temperature	5
V_s	sorption volume of the crystal	26

a	acceleration	16
a_m	average cross-sectional area of an adsorbate	4
c	adsorbate concentration	10,46
d_m	minimum molecular dimension	9
dp/dl	pressure gradient	1
j	net number of fluid molecules moving through each flux plane	48
k_1	pre-exponential constant	8
m	gas surface bonding strength parameter	5
m	mass	16

m	molecular weight	9
n	amount adsorbed	4
n_m	monolayer capacity	4
n_{unit}	number of unit cells per gram of zeolite	26
p	pressure	1,4,10,26,46
q	heat of adsorption	5
q_o	a sum over the various sites of interaction energy	20
r	adsorbate radius	39
r	mean pore radius	1
s	number of barriers per unit cross-section normal to flow	8
v_e	effective vibrational frequency	6
v_s	sorption volume per unit cell	26
z	number of adjacent sites	6,9

α	diffusion length	6,9
λ	equivalent wavelength	17
ξ^x	flux from control volume method	48,51,52,55
ψ	porosity	28
f	sorbate fugacity	20
θ	the chance that a molecule occupies each energy well	8
ΔE	the difference in energy from the gas phase to the external adsorbed phase	8
σ, σ_m	molecular diameter	9,48
σ_s	sphere diameter	28
Δt	MD timestep	48

REFERENCES

1. Abramo, C. M., Caccamo C., and Pizzimenti, **1993**, *J. Phys*, 397-406.
2. Ackerman, W. C.; Hua, D. W.; Kim, Y-W.; Huling, J. C; Smith, D. M.; **1994**, *Characterization of Porous Solids III*, J. Roquerel, F. Rodriguez-Reinoso, K. S. W. Sing, and K. K. Unger, eds, 735, Elsevier.
3. Ackerman, W. C.;Smith, D. M.; Huling, J. C.; Kim, Y-W.; Bailey, J. K.; and C. J. Brinker, *Langmuir*, **1993**, 9, 1051-1057.
4. Allen, M. P. and D. J. Tildesley, *Computer Simulations of Liquids*, (Oxford University Press, New York, **1987**).
5. Assink, R. A., and B. D. Kay, *Ann. Rev. Mater. Sci.*, **1991**, 21, 491-513.
6. Avery, R. G., and Ramsay, J. D. F., **1973**, *J. Colloid and Interface Sci.*, 42(3), 597.
7. Bandyopadhyay, S., and Yashonath, S., **1994**, *Chemical Physics Letters* 363-368.
8. Bandyopadhyay, S., and Yashonath, S., *J. Phys. Chem.* Vol. 99 No. 12, **1995**.
9. Barrer, R. M. *J. Chem. Soc. Faraday Trans.*, **1990**, 86(7), 1123-1130.
10. Barrer, R. M., "Single Porous Crystal Membranes: Mixtures in Steady Flow", *J. Chem. Soc Faraday Trans.* **1992** 88(10), 1463-1471.
11. Barrer, R. M., **1984**,(p 227 & 261 of NATO ASI Series E No. 80).
12. Beenakker, J. J. M., Borman V. D., and Krylov S. Yu., **1995**, *Chemical Physics Letters* 232, 379-382.
13. Belashchenko D. K., and Fed'ko, A. D., Neorganicheskie Materialy, Vol. 28(8),1628-1689, **1991**.
14. Bhandarkar, M. Shelekhin A. B., Dixon A. G., and Y. Ma, *J. Memb. Sci.*, 75, **1992**, , 221-231.
15. Bhave, R., *Inorganic Membranes*, **1991**, Van Nostrand Reinhold, New York.
16. Breck, D. W., Zeolite Molecular Sieves, (J. Wiley and Sons, New York, **1974**)
17. Brinker, C J., and R. Seghal, U.S. Patent Application, **1995**.
18. Brinker, C J., T. L. Ward, R. Sehgal, N. K. Raman, S. L. Hietala, D. M. Smith, D.W. Hua, Headley, T, *J. Memb. Sci.*, **1993**, 66, 271.
19. Brinker, C. J., and G. W. Scherer, *Sol-Gel Science,* (Academic Press, San Diego, **1990**)
20. Brodka, A. *Molecular Physics*, **1994**, Vol. 83, No. 4, 803-813.
21. Brodka, A. and T. W. Zerda, *J. Chem. Phys.*, **1992a**, 97(8), 5676.
22. Brodka, A. and T. W. Zerda, *J. Non-Cryst. Solids.*, **1992b**, 139, 215-221.
23. Brodka,, A. and Zerda T. W., *Materials Research Society Symposium*, Vol. 278, **1992c**.
24. Burggraaf , A. J, P1, 3rd lat. cont. on Inorganic Membranes, Y. Ma, ed., Worcester, MA, **1995**.
25. Cagin, Tahir, and Pettitt, Montgomery, B., *Molecular Physics*, **1991**, Vol. 72, No. 1, 169-175.
26. Carlson, G. A, J. L. Faulon, P.I. Pohl, and J. A. Shelnutt, **1993**, Proc. of the '93 Science and Technology Materials Conference, October 27-29, Greensboro, North Carolina.
27. Catlow, C. R. A., C. M. Freeman, B. Vessal, S. M. Tomlinson, and M. Leslie, , *J. Chem. Soc. Faraday Trans.*, **1991**, 87(13), 1947-1950.

28. Catlow, C. R. A., ed, *Modeling of Structure and Reactivity in Zeolites*, (Academic Press, **1992**).
29. Chapman, S., and T. G. Cowling, *The Mathematical Theory of Non-Uniform Gases*, , (Cambridge University Press, Cambridge, UK **1970**).
30. Chen, N. Y., *Molecular Transport and Reaction in Zeolites: Design and Application of Shape Selective Catalysts*; **1994**, VCH Publish, NY.
31. Chen, Y. D., and R. T. Yang, **1991**, *AIChE J.*, 37(10), 1579.
32. Cracknell R. F., and Nicholson, D., *J. Chem Soc Faraday Trans.*, **1994**, 90(11), 1487-1493.
33. Cracknell R. F., Gubbins, K. E., Maddox, M., and Nicholson, D., *Accounts of Chemical Research* Vol. 28. No. 7, **1995a**.
34. Cracknell R. F., Koh, C. A., Thompson, S. M., Gubbins, K. E., *Materials Research Society* Vol. 290, **1993a**.
35. Cracknell R. F., Nicholson, D., Gubbins, K. E., *J. Chem Soc. Faraday Trans.*, **1995c**, 91(9), 1377-1383.
36. Cracknell, R. F., and K. E. Gubbins, *Langmuir*, **1993b**, 9, 824-830.
37. Cracknell, R. F., D. Nicholson, and N. Quirke, *Phys. Rev. Let.*, 74(13), 2463-2466, **1995b**.
38. Cradwick, P.D.G.; Farmer, V. C.; Russell, J. D.; Masson, C. R.; Wada, K.; Yoshinaga, N. *Nature, Phys. Sci.*,**1972**, 240, 187.
39. Cussler, E., *Diffusion*, (Cambridge **1994**).
40. Damodaran, K. V., Nagarajan V. S., and Rao, K. J., *J. Non-Cryst. Solids*, **1990**, 124, 233-241.
41. Davis, M. E., and Lobo, R. F., *Chem Mater*. **1992**, 4, 756-768.
42. Davis, M. E.; Saldarriage, C.; Montes, C.; Garces, J.; Crowder, C., *Zeolites*, **1988**, 8, 362.
43. Davis, P. J.; Brinker, C. J.; Smith, D. M.; Assink, R. A., *J. Non-Cryst. Solids*, **1992**, 142, 197.
44. Davis, P. J.; Deshpande, R.; Smith, D. M.; Brinker, C. J.; Assink, R. A., *J. Non-Cryst. Solids*, **1994**, 167, 295.
45. de Lange, R. S. A., Hekkink, J. H. A., Keizer K., Burggraaf, A. J., *Journal of Membrane Science*, 99, **1995a**, 57-75.
46. de Lange, R. S. A., K. Keizer, and A. J. Burggraaf, *J. Memb. Sci*, 104, 81-100, **1995b**.
47. Demi, T. and D. Nicholson, *J. Chem Soc. Faraday Trans*, **1991**, 87(23), 3791-3791.
48. Demontis, P. and Suffritti G. B., **1994**, *Zeolites and Related Microporous Materials, Studies in Surface Science Catalysis, V84, p 2107, Elsevier.*
49. Demontis, P., and G. B. Suffritti, *Chem. Phys. Lett.*, **1992**, 191 (6), 553.
50. Demontis, P., and Suffritti, G. B., *Chemical Physics Letters*, 223, **1994**, 355-362.
51. Derouane, E. G., J. Andre, and A. A. Lucas *J. Catal.*, **1988**, 110, 58-73.
52. Derouane, E. G., *J. Catal.*, **1986**, 100, 541-544.
53. Derouane, E. G., J. Lucas, and A. A. Lucas, *Chem. Phys. Lett.*, **1987**, 137(4), 336.
54. Derycke, I., J. P. Vigneron, Ph. Lambin, A. A. Lucas and E. G. Derouane, **1991**, *J. Chem. Phys.*, 94(6), 4620.
55. Devreux, *Phys. Rev. A*, **1990**, 41, 6901.
56. Dubinin, M. M., **1975** *Progress in Surface & Membranes Science*, V. 9, D. A. Cadenhead, J. F. Danielli, and M. D. Rosenberg, eds., Academic Press, New York.
57. Duval, J. M., B. Folkers, M. H. V. Mulder, and C. A. Smolders, *J. Memb. Sci.*, **1993**.
58. Dykstra, C. E., *Chem. Rev.*, **1993**, 93, 2339-2353.

59. el Amrani, F. Vigne-Maeder, and B. Bigot, *J. Phys. Chem.*, **1993**, 96, 9417-9421.
60. Everett, D. H., and J. C. Powl, *J. Chem. Soc. Faraday Trans I*, **1976**, 72, 619-636.
61. Fain, D. E., *Key Engr. Mat.*, **1991**, V. 61-62, 327-336.
62. Farmer, V. C.; Fraser, A. R. In *International Clay Conference,* Mortland, M. M., Farmer, V. C., Eds.; Elsevier Science Publishers: Amsterdam, **1979**; p. 547-553.
63. Faulon, J., G. A. Carlson, and P. G. Hatcher, *Energy & Fuels*, **1993**, 7, 1062.
64. Faulon, J., *J. Chem. Inf. Comput. Sci.*, **1994b**, 34, 1204.
65. Faulon, J., J. P. Mathews, G. A. Carlson, P. G. Hatcher, *Energy & Fuels*, **1994**, 8, 408.
66. Faulon, J., Loy, D. A., Carlson, G. A., and Shea, K. J., *Computational Materials Science,* 3, **1995**, 334-346.
67. Feuston, B. P. and J. B. Higgins, *J. Phys. Chem*, **1994**, 98, 4459-4462.
68. Feuston, B. P.; and Garofalini, S. H.; J. Phys. Chem., **1990**, 94, 5351.
69. Ford, D. M. and E. D. Glandt, *J. Chem. Phys.*, 99, 11543-11549, **1995a**.
70. Ford, D. M. and Glandt, E. D., *J. of Memb. Sci.* 107, **1995b**, 47-57.
71. Ford, D. M., and Glandt, E. D., *Access in Nanoporous Materials*, T. J. Pinnavaia and M. F., Thorpe, eds, Plenum, **1995c**.
72. Forslund, David, W., Slocomb, Charles, A., and Agins, Ira, A., Los Alamos Science, Number 22, **1994**.
73. Freeman, C. M., C. R. Catlow, and J. M. Thomas, *Chem. Phys. Lett.*, **1991**, 186 (2,3), 137.
74. Fritzsche, S. Haberlandt, R. Karger, *Zeitschrift fur Physikalische Chemie*, Bd. 189, **1995**, 211-220.
75. Fritzsche, S. Haberlandt, R. Karger, FJ. Pfeifer, H. and Waldherr-Teschner, M., *Zeolites and Related Microporous Materials, Studies in Surface Sciences, and Catalysis*, Vol. 84, 2130, **1994**.
76. Fritzsche, S. Haberlandt, R. Karger, J. Pfeifer, H, and Heinzinger, K., *Chemical Physics* 174, **1993**, 229-236.
77. Garofalini, S. H. *J. of Non-Cryst. Solids.*, **1990**, 120, 1-12.
78. Garofalini, S. H., and G. Martin, *J. Phys. Chem.*, **1994**, 98, 1311-1316.
79. Geus, E. R., M. J. den Exter, and H. van Bekkum, , *J. Chem. Soc. Faraday Trans.*, **1992**, 88(20), 3101-3109.
80. Gilliland, E. R., R. F. Baddour, G. P. Perkinson, and K. J. Sladek, *Ind. Eng. Chem. Fundam.*, **1974**, 13(2), 95.
81. Goodbody, S. J., K. Watanabe, D. MacGowan, J. P. R. B. Walton, and N. Quirke, *J. Chem. Soc. Faraday Trans.*, **1991**, 87(13), 1951-1958.
82. Gregg, S. J., and K. S. W. Sing, *Adsorption, Surface Area and Porosity* (Academic Press, London, **1982**).
83. Gusev, A., and Suter, U. W., *J. Chem Phys.*, 99,(3), **1993**, 2228.
84. Gusev, A., Arizzi, S., Suter, U. W., and D. Moll, *J. Chem Phys.*, 99,(3), **1993**, 2221.
85. Haile, J. M., *Molecular Dynamics Simulations Elementary Methods*, (John Wiley & Sons, New York, **1992**.
86. Harkins, W. D., and Jura, G., *The Laboratory of Surface Chemistry*, Vol. 66, **1944**, 1362-1373.
87. Hassan, M. H., Way, J. D., Thoen, P. M., and Dillon, A. C., *J. Memb. Sci*, 104, **1995**, 27-42.

88. Heffelfinger, G. S., ***in preparation,* 1996.**
89. Heffelfinger, G. S., and F. van Swol, *J. Chem Phys.*, **1994**, 100(10), 7548.
90. Heffelfinger, G. S., and van Swol, F., *Molecular Physics*, **1987**, Vol., 61, No. 6, 1381-1390.
91. Heffelfinger, G. S., Tan, Z., Gubbins, K. E., Marconi, U. M. B., and van Swol, F., *International Journal of Thermophysics,* Vol. 9, No. 6, **1988.**
92. Heffelfinger, G. S., van Swol, F., Gubbins, K. E., *J. Chem. Phys.*, 89 (8), **1988.**
93. Heffelfinger, G.S., P.I. Pohl, and L.J.D. Frink, *Dynamics in Small Confining Systems II*, MRS Vol 366, 225-*230*, **1995.**
94. Henson, N. J., A. K. Cheetham, B. K. Peterson, S. D. Pickett, and J. M. Thomas, *J. Computer-Aided Material Design*, **1993**, 1, 41-54.
95. Henson, N. J., Cheetham, A. K., Redondo, A., Levine, S. M., and Newsam, J. M., **1995.**
96. Himmel B., Weighelt, J., Gerber, Th., Nofz, M., *J. Non-Cryst. Solids*, 136, **1991**, 27-36.
97. Hirschfelder, J. O., C. F. Curtiss, and R. B. Bird, *Molecular Theory of Gases and Liquids*, (John Wiley & Sons, New York, **1954**)
98. Ho, W. S. W. and K. K. Sirkar, eds., *Membrane Handbook*, **1992**, Van Nostrand Reinhold, New York.
99. Hufton, J. R., *J. Phys. Chem.*, **1992**, 95, 8836-8839.
100. Huling, J. C.; Bailey, J. K; Smith, D. M.; Brinker, C. J; *Better Ceramics through Chemistry V*; edited by M. J. Hampden-Smith, W. G. Klemperer, C. J. Brinker, (Materials Research Society: Pittsburgh, PA, **1992**) 271, p 511.
101. Hwang, S.-T., *AIChE J.*, **1966**, 14(5), 800.
102. Hwang, S.-T., and K. Kammermeyer, *Can. J. Chem. Engr.*, **1966a**, 44, 82.
103. Hwang, S.-T., and K. Kammermeyer, *Sep. Sci.*, **1966b**, 1(5), 629-639.
104. Iler, R. K., *The Chemistry of Silica*, **1979**, Wiley, N.Y.
105. Imamura, S.; Hayashi, Y; Kajiwara, K; Hoshino, H; Kaito, C, *Ind. Eng. Chem. Res.*, **1993**, 32, 600.
106. Inoue, H., Aoki, N., and Yasui, I., *J. Am. Cerem. Soc.*, 70, **1987**, 622-27.
107. Jameson, C. J., Jameson, A. K., Baello, B. I., and Lim, H., *J. Chem Phys.*, 100 (8), **1994**, 5965.
108. Ji, Jie, Cagin, Tahir, and Pettit, Montgomery, B., *J. Chem. Phys.*, 96 (2), **1992**, 1333-1342.
109. Jia, M., Peinemann, K. V., and Behling R. D., *J. Memb, Sci*, 82, **1993**, 15-26.
110. June, R. L., A. T. Bell, D. N. Theodorou, **1990**, *J. Phys. Chem.*, 94, 8232.
111. June, R. L., Bell, A. T., and Theodorou, D, N., *J. Phys. Chem*, **1991**, 95, 8866-8878.
112. Kale, R. P. and C. J. Brinker, MRS Symposium, Vol 371, 351-356, **1995**
113. Kapoor, A. and R. T. Yang, **1989**, *Catal. Rev.-Sci. & Eng.*, 45, 3261.
114. Karavias, F. and A. L. Myers, *Mol. Sim.*, **1989**, 8, 23-50.
115. Karger, J., and D. M. Ruthven, *Diffusion in Zeolites and Other Microporous Solids*, (John Wiley & Sons, New York, **1992**).
116. Karnaukhov, A. P.; Kiselev, A. V., *Russian J. Phys. Chem.*, **1960**, 34(10), 1019.
117. Kawamura, K. Sawaguchi, N., Maekawa, H., Yokokawa, T., *J. Am. Ceram. Soc.*, 76 (5), **1993**, 1308-12.
118. Keizer, K.; R. J. R. Uhlhorn, R. J. van Vuren, and A. J. Burggraaf, *J. Memb. Sci.*, **1988**, 39, 285.
119. Kiselev, A. V., A. A. Lopatkin, and A. A. Shulga, *Zeolites*, **1985**, 5, 261.

120. Kocirik, M., Struve, P. Fiedler, K. and Bulow, M., *J. Chem., Soc. Faraday Trans.*, 84 (9), **1988**, 3001-3013.
121. Kohler, A. E., Garofalini, S. H., *Langmuir*, **1994**, 10, 4664-4669.
122. Koresh, J. E., and A. Soffer, *J. Chem. Soc. Faraday Trans.*, **1986**, 82, 2057-2063.
123. Koros, William J., *Chemical Engineering Progress*, **1995**, 68-81.
124. Krishna, R., *Chem. Eng. Sci.*, **1993**, 48(5), 845.
125. Krishna, R., van den Broeke, L. J. P., *The Chemical Engineering Journal*, 57, **1995**, 155-162.
126. Lastoskie, C. M., N. Quirke and K. E. Gubbins, **1993a**, *Langmuir*, 9, 2693-2702.
127. Lastoskie, C., Gubbins, K. E., and Quirke, N., *J. of Phys. Chem.* Vol. 97, No. 18, **1993b**.
128. Leherte, L., J. Andre, E. G. Derouane, and D. P. Vercauteren, *J. Chem. Soc. Faraday Trans.*, **1991**, 87(13), 1959.
129. Loriso, A., M. J. Bojan, A. Vernov, and W. A. Steele, *J. Phys. Chem.*, **1993**, 97, 7665.
130. Lupkowski, Mark, and van Swol, Frank, *J. Chem. Phys.*, 95 (3), **1991**, 1995-19998.
131. MacElroy, J. M. D., *J. Chem. Phys.*, 101(6), 5274-5280, **1994**.
132. MacElroy, J. M. D., and K. Raghavan, *J. Chem. Phys.*, 93(3), 2068-2079, **1992**.
133. MacElroy, J. M. D., and K. Raghavan, *J. Chem. Soc. Faraday Trans.*, **1991**, 87(13) 1971.
134. MacElroy, J. M. D., *Langmuir*, **1993**, 9, 2682-2692.
135. Maginn, E. J., A. T. Bell, and D. N. Theodorou, *J. Phys. Chem.*, **1993**, 97, 4173-4181.
136. Mandelbrot, B., *The Fractal Geometry of Nature*, **1982**, Freeman, San Francisco.
137. Martin, G. E., and Garofalini, S. H., *J. Non-Cryst. Solids*, 171, **1994**, 68-79.
138. Martin, J. E., and A. J. Hurd, *J. Appl. Cryst.*, **1987**, 20, 61-78.
139. Martin, J. E., *J. Appl. Cryst.*, **1986**, 19, 25-27.
140. Mason, E. A., A. P. Malinauskas, **1983**, *Gas Transport in Porous Media: The Dusty Gas Model*, Elsevier, Amsterdam.
141. McClellen, A. L.; Harnsberger, H. F. *J. Coll. Interface. Sci.*, **1967**, 23, 577-599.
142. McElfresh, D. K., and Howitt, D. G., *J. Non-Cryst. Solids*, 124, **1990**, 174-180.
143. Meakin, P., *Ann. Rev. Phys. Chem.*, **1988**, 39, 237-67.
144. Nakano, A. Bi, L., Kalia, K., and Vashishta P., *Physical Review Letters*, Vol. 71, No. 1, **1993**., 85-88.
145. Nakano, A., Kalia, R. K., and Vashishta, P., *J. Non-Cryst. Solids*, 171, **1994b**, 157-163.
146. Nakano, A., L. Bi, R.K. Kalia, P. Vashishta, *Phys. Rev. B*, **1994a**, 49(14), 9441.
147. Nicholson, D., *J. Chem. Soc. Faraday Trans.*, **1994**, 90(1), 181-185.
148. Nicolas, J. B., F. R. Trouw, J. E. Mertz, L. E. Iton, and A. J. Hopfinger, *J. Phys. Chem.*, **1993**, 97, 4149-4163.
149. Nowak, A. K. Den Ouden, C. J., Pickett, S. D. Smit, B., Cheetham, A. K., Post, M. F. M., and Thomas J. M., *J. of Phys. Chem.* Vol. 95, No. 2, **1991**.
150. Ochoa, R. Swiler, T. P., and Simmons, J. H., *J. Non-Cryst. Solids*, 128, **1991**, 57-68.
151. Ogawa, H., *J. Non-Cryst. Solids*, 143, **1992**, 201-206.
152. Ouchlyama, Norlo, and Tanaka, Tatsuo, *Ind. Eng. Chem. Fundam.*, **1980**, 19, 338-340.
153. Pellenq, Roland J., and Nicholson, David, *Langmuir*, **1995**, 11, 1626-1635.
154. Peterson, B. K., G. S. Heffelfinger, K. E. Gubbins, and F. van Swol, *J. Chem. Phys.* , **1990**, 93(1), 679.

155. Peterson, Brian K., Gubbins, Keith E., Heffelfinger, Grant S, Marconi, Umberto Marini Bettolo, and van Swol, Frank, *J. Chem Phys.* 88 (10), **1988**, 6487-6499.
156. Petropoulos, J. H., and J. K. Petrou, *J. Chem Soc. Faraday Trans*, **1991**, 87(13), 2017.
157. Pickett, S. D., A. K. Nowak, J. M. Thomas, B. K. Peterson, J. F. P. Swift, A. K. Cheetham, C. J. J. den Ouden, B. Smit, and M. F. M. Post, *J. Phys. Chem.*, **1990**, 94, 1233-1236.
158. Pohl, P. I. and D.M. Smith, *Advances in Porous Materials*, MRS Vol 371, 27-33, **1995**.
159. Pohl, P. I., and J. L. Faulon, **1994**, *Proceedings of Third International Conference on Inorganic Membranes*, Worcester, Y. Ma editor.
160. Pohl, P. I., *Commercial and Research Status Report on Inorganic Membranes*, **1993**, SAND92-1777, Sandia National Laboratories, Albuquerque, NM.
161. Pohl, P. I., G. S. Heffelfinger and D. M. Smith, **1996** "Molecular Dynamics Computer Simulation at Gas Permeation Through Thin Silicalite Membranes", Submitted to *Mol. Phys.*
162. Pohl, P. I., J. L. Faulon, and D. M. Smith, **1995b**, *J. Non Cryst. Solids,* 186, 349.
163. Pohl, P. I., J. L. Faulon, and D. M. Smith, **1996**, "A Computer Study of the Pore Structure of Imogolite", Submitted to *Langmuir.*
164. Prausnitz, J. M., R. N. Lichtenthaler, and E. G. Azevedo, *Molecular Thermodynamics of Fluid-Phase Equilibria*, (Prentice-Hall, Englewood Cliffs NJ, **1986**).
165. Razmus, David M. and Hall, Carol K., *AIChE Journal*, Vol. 37, No. 5, **1991**, 769-779.
166. Reed, T. M., and K. E. Gubbins, **1974**, *Applied Statistical Mechanics*, (McGraw Hill).
167. Rhykerd, Charles, Tan, Ziming, Pozhar Liudmila A. and Gubbins, Keith E., *J. Chem Soc, Faraday Trans.*, **1991**, 87 (13), 2011-2016.
168. Rouquerol, J.; Avnir, D.; Fairbridge, C.W.; Everett, D. H.; Haynes, J. H.; Pernicone, N.; Ramsay, J. D. F.; Sing, K. S. W.; Unger, K. K., **1994**, *Pure Appl. Chem.*, 66, 1739.
169. Saito, A. and H. C. Foley, *AIChE J.*, **1991**, 37(3), 429.
170. Schaefer, D. W., *MRS Bulletin*, **1994**, xix(4), 49.
171. Scherer, G. W., **1994**, *J. Sol-Gel Sci. Tech.*, 1(3), 76.
172. Sehgal, R; Huling, J. C.; Brinker, C. J., *Proceedings of the Third International Conference on Inorganic Membranes*, Y.Y. Ma, ed. Worcester, MA, **1994**, p. 85.
173. Shah, D. B., Chockchalacha, S., and Hayhurst, D. T., *J. Chem. Soc. Faraday Trans.*, **1993**, 89 (16), 3161-3167.
174. Shah, Ritesh P., Behrman, E. C., *J. Am. Ceram. Soc.*, 74 (10), **1991** 2599-2602.
175. Shelby, J. E., *Treatise on Materials Science and Technology*. Vol. 17, **1979**.
176. Shelekhin, A. B., Dixon, A. G., and Ma, Y. H., *J. of Memb. Sci*, 75, **1992**, 233-244.
177. Shelekhin, A. B., Dixon, A. G., and Ma, Y. H., *AIChE Journal*, Vol. 41, No. 1, **1995**.
178. Shelekhin, A. B., Dixon, A. G., and Y. H. Ma, *J. Memb. Sci.*, **1993**, 83, 181.
179. Sladek, K. J., E. R. Gilliland, and R. F. Baddour, *Ind. Eng. Chem., Fund.***1974**, 13(2), 100.
180. Smite, **1995b**, *J. Phys. Chem*, 99, 5597..
181. Soules, Thomas F., *J. of Non-Cryst. Solids* 123, **1990**, 48-70.
182. Steele, W., *Chem. Rev.*, **1993**, 93, 2355-2378.
183. Swiler, Thomas P., Simmons, Joseph H., and Wright, Adrian C., *J. Non-Crys. Solids* 182, **1995**, 68-77.
184. Tamon, Hajme, Kyotani, Susumu, Wada, Hiroyuki, Okazaki, Morio, and Toei, Ryozo, *J. of Chemical Eng. of Japan*, Vol. 14, No. 2, **1981**.

185. Thurtell, J. H., and G. W. Thurtell, *J. Chem. Phys.*, **1988**, 88(10), 6641.
186. Uhlhorn, R. J. R., Huis In't Veld, M. H. B., Keizer, K. and Burggraaf, A. J., *J. of Materials Science Letters*, 8, **1989**, 1135-1138.
187. Uhlhorn, R. J. R., Keizer, K., and Burggraaf, A. J, *J. of Memb. Sci.*, 46, **1989**, 225-241.
188. Uhlhorn, R. J. R., Keizer, K., and Burggraaf, A. J., *J. of Memb. Sci*, 66, **1992**, 271-287.
189. Unger, K. K., *Porous Silica*, V16-J. Chromatography Library, Elsevier, **1979**.
190. Valle, R. G. D., and Andersen, Hans C., *J. Chem. Phys.*, 97 (4), **1992**, 2682-2689.
191. Van Tassel, P. R., Davis, H. Ted, and McCormick, Alon, V., *Langmuir*, **1994**, 10, 1257-1267.
192. Van Tassel, P. R., Davis, H. Ted, and McCormick, Alon, V., *AIChE Journal*, Vol. 40, No. 6, **1994**, 925-934.
193. Vashishta, Priya, Nakano, Aiichirok, Kalia, Rajiv K., and Ebbsjo, Ingvar, *J. Non-Cryst. Solids*, 182, **1995**, 59-67.
194. Vernov, A. V., W. A. Steele, and L. Abrams, *J. Phys. Chem.*, **1993**, 97, 7660-7664.
195. Vessel, B., Amini, M., and Catlow, C. R. A., *J. of Non-Cryst. Solids*, 159, **1993**, 184-186.
196. Vroon, Z.A.E.P. Doctoral Thesis, University of Twente, Netherlands, **1994**.
197. Wada, S.; Wada, K. *Clays Clay Minera.* **1982**, 30, 123.
198. Wada, Shin-Ichiro, *Clays and Clay Minerals*, Vol. 35, No. 5, 379-384.
199. Way, J. D., and D. L. Roberts, *Sep. Sci. and Tech.*, **1992**, 27(1), 29-41.
200. Webb, Edmund B., and Garofalini, Stephen H., *J. Chem. Phys.*, 101 (11), **1994**.
201. Weisz, Paul B., *Ind. Eng. Chem. Res.*, **1995**, 34, 2692-2699.
202. Wijmans, J. G., and Baker, R. W, *J. of Memb. Sci.*, 107, **1995**, 1-21.
203. Xiao, J., and J. Wei, Chem. Engr. Sci., **1992**, 47(5), 1123.
204. Xu, Qiang, Kawamura, Katsuyuki, and Yokokawa, Toshio, *J. of Non-Cryst. Solids*, 104, **1988**, 261-272.
205. Yan, Y., M. E. Davis, and G.R. Gavalas, *Ind. Eng.Chem. Res.*", 34, 1652-1661, **1995a**.
206. Yan, Yushan, Tsapatsis, Michael, Gavalas, George R. and Davis, Mark E., *J. Chem.Soc., Chem, Commun.*, **1995**, 227b.
207. Yashonath, S., and P. Santikary, *J. Phys. Chem.*, **1993a**, 97, 13778-13787.
208. Yashonath, S., and P. Santikary, *Mol. Phys.*, **1993b**, 78(1), 1.
209. Yashonath, S., and P. Santikary, *Phys. Rev. B*, **1992**, 45(17), 10095.
210. Yoshinaga, N.; Aomine, S, *Soil Sci. and Plant Nutrition*, **1962**, 8, 6 and 14. [Abstr. *Am. Mineral.*] 48, 434, 196.
211. Yucel, Hayrettin, and Ruthven, Douglas, J. C. S., Faraday I, **1980**, 76, 60-70.

Appendix - LDRD Project Information

Awards: No awards were obtained as a result of this LDRD

Publications:

1. Carlson, G.A., J.L. Faulon, P.I. Pohl, and J.A. Shelnutt, "Applications of Molecular Modeling to the Design and Characterization of Materials", *Proc. '93 Science and Technology Materials Conference*, Greensboro, NC.

2. Pohl, P.I., J.L. Faulon, and D.M. Smith, "Molecular Dynamics Computer Simulation of Silica Aerogels", *J. Non-Cryst. Solids*, 186, 349-355, 1995.

3. Pohl, P.I. and D.M. Smith, "Molecular Simulation of Porous Silicates", *Advances in Porous Materials*, Mater. Res. Soc. Symp Proc., Vol 371, 27-33, 1995.

4. Heffelfinger, G.S., P.I. Pohl, and L.J.D. Frink, "Molecular Dynamics Computer Simulation of Diffusion in Porous Silicates", *Dynamics in Small Confining Systems II*, Mater. Res. Soc. Symp Proc., Vol 366, 225-230, 1995.

5. Pohl, P.I. and J.L. Faulon, "Computer Simulation of Microporous Silica", *Proc. Third International Conference on Inorganic Membranes,* 1994, Y. Ma, ed., Worcester, MA, 617-620.

6. Pohl, P.I., J. L. Faulon, and D. M. Smith, "The Pore Strucuture of Imogolite Computer Models", *Langmuir*, In Press

7. Pohl, P.I., G. S. Heffelfinger, and D. M. Smith, "Molecular Dynamics Computer Simulation of Gas Permeation in Thin Silicalite Membranes", *Mol. Phys.*, In Press

8. Pohl, P.I, "Computer Simulation of Gases in Microporous Solids: Zeolites, Imogolite and Silica", PhD Dissertation, University of New Mexico, July, 1996.

Presentations:

1. "Computer Aided Molecular Analysis of Imogolite", Pohl, P., J. Huling, J. Brinker, D. Smith and G. Carlson, 1993 American Ceramic Society Meeting, Cincinnati, OH.

2. "Molecular Dynamics Computer Simulations of Porous Silicate Membranes", Pohl, P., J.L. Faulon, D.A. Loy, N.K. Raman and D.M. Smith, 5th Joint Meeting of the NM Sections of the American Ceramic Society and Materials Research Society, Albuquerque, 1993.

3. "Molecular Dynamics Computer Simulations of Porous Silica Membranes", Pohl, P., J. L. Faulon, N. K. Raman, D. M. Smith, 1994 Spring Materials Research Society Meeting, San Francisco.

4. "Computer Simulations of Gases in Microporous Membranes", Pohl, P., N. K. Raman, D. M. Smith, North American Membrane Society Sixth Annual Meeting, Breckenridge, CO, 1994.

5. "Computer Simulation of Microporous Silica", Pohl, P., J.L. Faulon, Third International Conference on Inorganic Membranes, Worcester, MA, 1994.

6. "Computer Aided Molecular Analysis of Imogolite", Pohl, P., D. M. Smith and J. L. Faulon, 1994 American Chemical Society Summer Meeting, Washington D.C..

7. "Molecular Dynamics Computer Simulation of Silica Aerogels", Pohl, P., J.L. Faulon, and D.M. Smith at the Fourth International Symposium on Aerogels, Berkeley CA, 1994.

8. "Molecular Simulation of Porous Silicates", Pohl, P., D.M. Smith, at the Advances in Porous Materials Symposium at the Fall 1994 Materials Research Society Meeting, Boston, MA.

9. "Molecular Dynamics Computer Simulations of Diffusion in Porous Silicates", Pohl, P., G. S. Heffelfinger and L.J.D. Frink, in Dynamics in Small Confining Systems Symposium at the Fall 1994 Materials Research Society Meeting, Boston, MA.

10. "Simulation of Gases in Molecular Sieving Silica" Pohl, P., S. Hietala, S. Wallace, G. Heffelfinger, J. Brinker and D. Smith, in Access in Nanoporous Materials Symposium, 7-9 June, 1995, Lansing, MI.

11. "Simulation of Gases in Molecular Sieving Silicate Membranes" P. Pohl, G. Heffelfinger, and D. Smith, in Access in Nanoporous Materials Symposium, 7-9 Nov, 1995, Miami, FL.

Patents: No patents were associated with this project.

Copyrights: No copyrights were associated with this project.

Employee recruitment: During this LDRD project, one permenant staff member was hired to contribute partially to its completion.

Student involvement: During this LDRD project, three students were used at least for the summer to develop portions of the results.

Follow-on work: Significant involvement in the Advanced Supercomputing Initiative (ASCI) project resulted partly because of this LDRD project's collaborations. An other LDRD project was initiated that involved molecualar modeling and three others were being pursued in June 1996.

Distribution

Internal

1	MS 0710 J. L. Faulon, 6211
1	MS 0720 K. B. Sorenson, 6626
10	MS 0720 P. I. Pohl, 6626
1	MS 1111 G. S. Heffelfinger, 9221
1	MS1436, LDRD Office, 4523
5	MS 0899 Technical Library, 4414
1	MS 9018 Central Technical Files, 8523-2
2	MS 0619 Review and Approval Desk, 12630 for DOE/OST I